Title

Human Entorhinal-Hippocampal Structure in Aging & Stimulation Mediated Episodic Memory Enhancement

Permalink

https://escholarship.org/uc/item/9723394v

Author

Wishard, Tyler J

Publication Date

2022

Peer reviewed|Thesis/dissertation

UNIVERSITY OF CALIFORNIA

Los Angeles

Human Entorhinal–Hippocampal Structure in Aging

& Stimulation Mediated Episodic Memory Enhancement

A dissertation submitted in partial satisfaction of the

requirements for the degree Doctor of Philosophy

in Neuroscience

by

Tyler James Wishard

2022

ABSTRACT OF THE DISSERTATION

Human Entorhinal-Hippocampal Structure in Aging

& Stimulation Mediated Episodic Memory Enhancement

by

Tyler James Wishard

Doctor of Philosophy in Neuroscience

University of California, Los Angeles, 2022

Professor Nanthia A. Suthana, Co-Chair

Professor Susan Y. Bookheimer, Co-Chair

Decades of accumulated scientific evidence has demonstrated that vital factors (*e.g.*, amyloid-β (Aβ) and the gene apolipoprotein E (APOE) ε4) contribute to the neuropathological changes and memory deficits observed in Alzheimer's disease (AD) and related dementias. Identifying these factors prior to disease onset could facilitate earlier access to disease-modifying treatments or promote healthy lifestyle modifications that might reduce neuropathology or cognitive deficits. However, the relationship between plasma-derived Aβ, APOE ε4, and brain atrophy in older adults before the manifestation of clinically relevant memory loss remains unclear. Furthermore, brain stimulation has emerged as a powerful approach for developing novel neuromodulatory therapies for those with deficits in cognition. Thus, these techniques may be used as potential treatments for those at risk for AD and other severe memory impairments.

The studies from this dissertation investigated the neural correlates and causal outcomes of cognitive and memory-related systems in the aging human brain. The first study examined the relationship between plasma-derived Aβ, APOE ε4, and brain atrophy in a large sample of 160 healthy older adults (ages 50+). The second and third studies showed promising effects on memory using invasive and non-invasive brain stimulation in cognitively healthy adults without memory impairments. Together these findings suggest that genetic, biological, and neural determinants could be combined with neuroimaging-guided brain stimulation to better identify individuals at risk for AD and improve their hippocampal-related memory.

Future studies of brain aging in healthy and memory-impaired older adults should monitor the molecular and neurobiological markers indicative of cognitive function and study novel methods like brain stimulation therapies. Since cognition is detrimentally influenced by these factors ensuring memory-enhancing therapies are effective despite indicators of impairment is necessary for the development of clinically viable treatments of benign senescence or more advanced impairment. Using different MRI modalities, the structural and microstructural properties of the brain can be used to predict treatment response or optimize hippocampal network targeting to restore aberrant function and alleviate the deficits associated with progressive memory loss.

The dissertation of Tyler James Wishard is approved.

Nader Pouratian

Jesse A. Rissman

Andrew F. Leuchter

Nanthia A. Suthana, Committee Co-Chair

Susan Y. Bookheimer, Committee Co-Chair

University of California, Los Angeles

2022

To

Joaquín Alexander Wishard

Table of Contents

Tyler James Wishard

Department of Psychiatry & Biobehavioral Sciences

Jane & Terry Semel Institute for Neuroscience & Human Behavior

University of California Los Angeles, Los Angeles, CA 90095

Education

2010 – 2015	B.S., Physiology & Neuroscience, University of California, San Diego Developing an *in vivo* Disease Model to Study Fragile X Syndrome in *Xenopus laevis* *Cum Laude* with honors in Biological Sciences

Research Positions

2018 – 2022	Graduate Student Researcher, UCLA
2018 – 2021	MRI Analyst, Longeveron: Cell-Based Therapies, Miami, Florida
2015 – 2016	Technician, Dorris Neuroscience Center, The Scripps Research Institute
2014	Summer Research Assistant, Department of Neuroscience, Brown University
2010 – 2015	Research Assistant, Dorris Neuroscience Center, The Scripps Research Institute
2010	Trainee, Southern California Biotechnology Center, San Diego Miramar College

Teaching Positions

UCLA Teaching Fellow & Reader

2021 – 2022	Anatomy of Central Nervous System (M 203), Winter quarter Molecular & Developmental Neuroscience (M 101B), Winter quarter Cellular & Systems Neuroscience (M 101A), Fall quarter
2018 – 2019	Project Brainstorm: Neuroscience K–12 Outreach (NS 192B), Spring quarter Project Brainstorm: Neuroscience K–12 Outreach (NS 192B), Winter quarter Neuroscience for 21st Century (NS 10), Fall quarter Functional Anatomy of Central Nervous System (NS 102), Fall quarter
2017 – 2018	Project Brainstorm: Neuroscience K–12 Outreach (NS 192B), Spring quarter Skills for Improving Productivity & Wellbeing (PSYCTRY 79), Spring quarter Project Brainstorm: Neuroscience K–12 Outreach (NS 192B), Winter quarter Skill for Improving Productivity & Wellbeing (PSYCTRY 79), Fall quarter Neuroscience for 21st Century (NS 10), Fall quarter

<u>UCSD Tutor & Instructional Apprentice</u>

2014 – 2015	Healthy & Diseased Brain (BIPN 152), Spring quarter
	Cellular Neurobiology (BIPN 140), Winter quarter
	Organismic & Evolutionary Biology (BILD 3), Fall quarter
2013 – 2014	Healthy & Diseased Brain (BIPN 152), Spring quarter

<u>Brown University Pre-College</u>

Summer '14	Introduction to Physiology in the Human Body (Physiology II)
Summer '14	Secret Life of the Brain from Shrimps to Humans (Laboratory Assistant)

Training & Fellowships

2022	Neuromatch Academy: Deep Learning course
2022	Human Brain Mapping Brainhack, University of Glasgow, Scotland, UK
2021	Science Communication Training, Alan Alda Center, Stony Brook University
2021	Decision Neuroscience & Aging, Duke Institute for Brain Sciences
2020	University of California Office of the President Dissertation Year Fellowship
2020	Laurie & Steven Gordon Commitment to Cure Parkinson's Disease, UCLA
2019	FSL course: structural, functional, and diffusion image analysis
2018 – 2020	Achievement Rewards for College Scientists (ARCS) Foundation, Los Angeles
2016 – 2018	Eugene V. Cota Robles Graduate Research Fellowship, UCLA
2016	Competitive Edge: Summer Transition to the Doctorate
2014	Ledell Family Summer Undergraduate Research Scholarship, Brown University
2014	Carl Storm Underrepresented Minority Fellowship, GRC-Fragile X
2013 – 2015	NIH-MARC U*STAR T34 Undergraduate Research Training Program
2012	Calit2 Summer Undergraduate Research Scholarship, Qualcomm Institute

Honors & Awards

2018	Outreach & Community Service Award, Brain Research Institute, UCLA
2015	Tracee Parsons LGBT Scholar in Math & Science, UCSD

I

AGING–RELATED COGNITIVE DECLINE: ENTORHINAL–HIPPOCAMPAL STRUCTURE,

AMYLOID–β & APOLIPOPROTEIN E BIOMARKERS.

1.1 Introduction

The Administration on Aging, U.S. Department of Health and Human Services, released a report in 2020 summarizing the present and projected U.S. population statistics for people aged 65 years and older. The total U.S. population is currently around 330 million people, with 54 million people aged 65 and older—approximately 16% of the total—which over the next two decades will increase by 6% [ACL, 2020]. By 2034, adults over 65 will outnumber children under 18 for the first time in U.S. history, and by 2040, the number of working-age adults will decrease from 4.5 to 2.5 for every person 65 and older [Iriondo & Jordan, 2018].

At present, the most common neurological disease affecting this age group is dementia which impacts 5% of the world's older population—approximately 55 million people—significantly contributing to physical, emotional, and economic pressures on individuals, families, world governments, and health agencies [WHO, 2017]. By 2050, people with dementia will triple worldwide [WHO, 2021]. These reports forecast urgent complexities regarding social and public health services and further emphasize the need to understand lifestyle factors that mitigate disease, maintain a high quality of life with age, and sustain a healthy republic and thriving democracy for future generations.

Recent demographic surveys of people over 65 show about 125 women for every 100 men, approximately 55% and 45% of the older U.S. population. These proportions increase to 178 women for every 100 men aged 85 and above. The total number of older adults that are members of a racial or ethnic minority group is 1 in 4 people and will increase in the next two to three decades. Regarding educational attainment, 89% of older adults completed High

school, with around 33% having attained a bachelor's degree, compared to 1970 when only 28% had completed High school education. While there are limitations to these estimates, current efforts are being made to improve the methodology for U.S. census collection [Mervis, 2022]. Importantly, these figures highlight the dynamics of demographic features necessary for accurate population-based statistics that describe age-related cognitive and memory abilities and reflect the current and future U.S. population aged 65 and older. Therefore, we provide national and study sample demographic averages (**Table 1.1**). Still, much work is needed to improve the equitable assessment and fundamental access to public services for older adults, especially for women and minority groups; we hope the findings presented herein represent progress towards a healthier and more lively tomorrow for all people.

	Study sample (%)	National avg. 65+ (%)
Sex		
Female	54.80%	55.00%
Race		
Asian American	3.75%	5.00%
Black or African American	10.50%	9.00%
Native American/Alaskan Native	–	0.60%
Native Hawaiian or Pacific Islander	–	0.10%
White	81.20%	–
More than one race	3.00%	0.80%
Unknown or not reported	1.50%	–
Ethnicity		
Hispanic or Latino	9.02%	9.00%
Not Hispanic or Latino	91.70%	–
Unknown or not reported	–	–
Total Members of Minority Groups	26.30%	25.00%

Table 1.1 U.S. population aged 65+ and HCP-A study sample demographics.

The Aging Brain in Health & Disease

Recent efforts in normative aging research mapped the course of human brain growth across the lifespan [Bethlehem *et al.*, 2022; Marek *et al.*, 2022]. This study measured several

features of brain development; each phenotype had a different temporal trajectory across an individual's life and age at which the brain measure reached its maximum value assessed using magnetic resonance imaging (MRI). They divided the brain into broadly distinct areas based on structural features, such as the cortical and subcortical regions, referring to the location, density, and neuronal cell layers present. Another structural category of brain tissue is whether areas appear gray or white in contrast on MRI scans [Nolte, 2013]. The gray matter regions are densely packed with neuronal cell bodies, dendrites, unmyelinated axons, and various types of glia. The white matter primarily consists of bundled axon fibers insulated by a fatty substance called myelin that facilitates signal fidelity between distantly connected regions forming networks throughout the brain [Campbell *et al.*, 2009]. There are also specialized cavities that run in series along the brain's midline called ventricles, which are important for proper maintenance of intracranial pressure and disposal of cellular respiratory waste from neural activity via the glymphatic and venous circulatory systems [Silverthorn *et al.*, 2006].

On average, the brain reaches its maximum cortical and subcortical gray matter volume between 6-12 years old. Yet, the cortical white matter volume continues to develop and increase in size until the thirties [Baum *et al.*, 2022; Paquola *et al.*, 2019], then gradually declines with age, related to measures of cognitive decline [Dhana *et al.*, 2022]. Ventricular volume increases until the age of 2, stabilizing into adulthood, then gradually increases until about the age of 60, then increases exponentially, becoming more variable, towards the end of the life course [Bethlehem *et al.*, 2022; Kozlov, 2022].

Pioneering studies on memory function have shown that reductions in the size of key brain regions located within the medial temporal lobe (MTL) are associated with alterations or

impairments in brain function [Penfield & Milner, 1958; Scoville & Milner, 1957; Milner, 1954]. The hippocampus, a vital brain region in the MTL, plays an integral role in episodic memory, consolidating the experiences and events of life into a coherent and recallable framework (**Figure 1.1**). The hippocampus is a core hub in the memory network, working with different brain regions to accomplish extraordinary neural phenomena, specifically associative, episodic, and semantic qualities of intellectual function [Battaglia *et al.*, 2011]. The hippocampus forms local connections with adjacent MTL regions, collectively referred to as the parahippocampal gyrus, including the perirhinal, entorhinal, and parahippocampal cortical areas [Patel *et al.*, 2022].

Figure 1.1 Sagittal view of hippocampal subfields and amygdala nuclei.

In the absence of disease, even subtle changes in brain structure can affect cognition and the ability to remember experiences essential for supporting independence and wellbeing with age (**Figure 1.2**) [Gullett *et al.*, 2020; Arfanakis *et al.*, 2016; O'Shea *et al.*, 2016; Fleischman *et*

al., 2013; Jagust *et al.*, 2007; Wu *et al.*, 2002]. Currently, there are no effective treatments for modifying the degenerative effects of aging on physical and mental capabilities highlighting the need to identify brain-protective and risk health factors that reduce age-related decline.

A   **B**   **C**
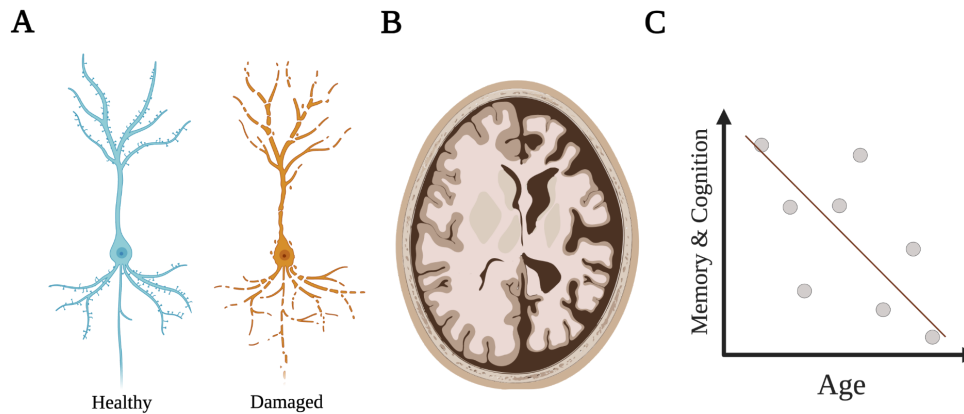
Figure 1.2 The (**A**) neuronal, (**B**) brain structural, and (**C**) intellectual changes

in healthy and diseased aging.

Biomarkers of Brain & Cognitive Decline

The most common form of dementia, Alzheimer's disease (AD), has an early and late-onset presentation characterized by Amyloid-β (Aβ) plaques and neurofibrillary tangles; approximately 90-95% of cases are late-onset, meaning the diagnosis occurs after age 65 [Chernecky & Berger, 2012]. Nearly two decades of scientific evidence have demonstrated that the deposition of the Aβ protein in human brain tissue contributes to the pathogenesis of AD.

The traditional methods for measuring Aβ *in vivo* are Positron Emission Tomography (PET) to reveal the location of plaques in the brain or Mass Spectroscopy to measure cerebrospinal fluid (CSF) metabolites typically collected by a spinal tap or lumbar puncture. While both of these approaches are technically feasible and have advanced our understanding

of the contributions of the Aβ burden in cognitive decline [Bourgeat *et al.*, 2022; Morar *et al.*, 2022; Sala *et al.*, 2021], these measures can be challenging to obtain and may be further complicated by age-related susceptibility, particularly with comorbid diseases.

A novel assay for detecting Aβ using plasma collected from whole blood samples would simplify this procedure, improve the availability of diagnostic assessment for dementia, and potentially promote peoples' willingness to participate in Aβ-focused research studies. Therefore, a blood-based assessment of Aβ 40,42 plasma concentrations tightly correlated with amyloid plaques in the brain would provide appreciable utility in the clinic [Kirmess *et al.*, 2021; West *et al.*, 2021]. In the U.S., a first-in-class test was certified by the Clinical Laboratory Improvement Amendments program, and, in the E.U., it received the CE Mark of approval for *in vitro* medical diagnostics [Alzforum, 2020; Shapiro *et al.*, 2020]. Currently, plasma-derived measurements of amyloid pathology are collected in the AD prevention (AHEAD) study evaluating a monoclonal antibody treatment designed to reduce soluble Aβ in early and pre-clinical cases [Eisai Inc., 2020]. Similar measures will also be used as trial outcomes in the Longitudinal Early-Onset Alzheimer's Disease Study (LEADS), developing sensitive biomarker standards for clinical and research use [Apostolova *et al.*, 2018]. Moreover, several studies have already confirmed the applicability of plasma-derived Aβ in AD diagnosis [Hu *et al.*, 2022; Janelidze *et al.*, 2021; Tosun *et al.*, 2021].

The collection procedure for the test involves a blood draw, typical healthcare practice for older adults, and only requires a minimal (4 mL) sample for analysis. In addition, the projected cost to implement this diagnostic measure in the clinic is $500 USD, compared to an average PET brain scan cost of $5000 - $8000 or CSF measurement costs of $1,000 [Everding, 2022].

Limitations of this technique include the fidelity of peripheral (*i.e.*, non-brain-based) biomarkers for measuring changes in neuropathological hallmarks affecting cognition [Zetterberg & Karikari, 2021]. Studies using PET and CSF biomarkers reveal that Aβ in AD patients provides a good marker of early disease state and memory impairment severity; however, other biological determinants are closely associated with cognition and accurately predict disease stage [Brier *et al.*, 2016; Lucey, 2016; Vlassenko *et al.*, 2016]. These biomarkers share an inverse relationship where lower CSF concentrations of Aβ 42 are associated with greater amyloid positivity on PET using a marker of cortical deposition [Fagan *et al.*, 2014].

Similar to CSF, studies using blood-based measures of Aβ report that lower plasma concentrations correlate with greater amyloid plaque neuropathology, smaller MTL regions, and memory deficits [Li *et al.*, 2022; Risacher *et al.*, 2019; Gabelle *et al.*, 2014; Graff-Radford *et al.*, 2007; Pomara *et al.*, 2005; Mayeux *et al.*, 2003], although variable findings suggest future studies are needed [Cantero *et al.*, 2016; Blennow *et al.*, 2010; van Oijen *et al.*, 2006], potentially the result of analytical and statistical differences [Chen *et al.*, 2016]. Several studies comparing these biomarker detection methods, specifically the method used in this report, have reliably linked peripheral biomarkers acquired from blood plasma with direct brain-based measurements using either PET or CSF measurements in patients with cognitive impairments [Zicha *et al.*, 2022; Schindler *et al.*, 2019; Ovod *et al.*, 2017]. More recent studies of brain changes in typically aging older adults with unimpaired cognition are beginning to shed light on the age-dependent mechanisms of cognitive decline, suggesting a more common etiology between Aβ deposition and brain atrophy in older adults before the manifestation of clinically relevant

memory loss. However, additional research on the early detection of these blood-based biomarkers and their role in cognitive senescence is needed [Hansson *et al.*, 2022].

Furthermore, the most significant risk factors for the development of AD are age and apolipoprotein E (APOE) ε4 carrier status [Veldsman *et al.*, 2021], with a higher frequency in women, accounting for longevity and demographic variables [Nebel *et al.*, 2018]. The APOE gene codes for a lipid transport protein (ApoE) involved in lipoprotein, triglyceride, and cholesterol metabolism [Sienski *et al.*, 2021]. ApoE helps repair cell membranes throughout the brain and body [Lanfranco *et al.*, 2020; Yin & Wang, 2018; Huang & Mahley, 2014]. APOE has three genetic variations, one of which is the ε4 allele [Yamazaki *et al.*, 2019]. Studies in single carriers with one ε4 allele are twice as likely to develop late-onset AD, whereas double carriers are 12-15 fold more likely [Chernecky & Berger, 2012]; however, other studies suggest that a single ε4 allele only confers a 20% risk [Bookheimer & Burggren, 2009], further highlighting the need to identify additional early detection factors contributing to memory deficits.

The copy number of the ε4 variant is considered to contribute to volume reductions, Aβ plaques, and neurofibrillary tangles [Lim *et al.*, 2017; Corder *et al.*, 1993; Strittmatter *et al.*, 1993]; exactly how APOE contributes to AD is unknown. However, mounting evidence suggests the degree to which APOE influences AD prognosis may not be ubiquitous across racial, ethnic, and genetic admixture groups [Miyashita *et al.*, 2022; Sepulveda-Falla *et al.*, 2022; Llibre-Guerra *et al.*, 2022; Suchy-Dicey *et al.*, 2022; Griswold *et al.*, 2021; Kunkle *et al.*, 2021; Marca-Ysabel *et al.*, 2021; Shigemizu *et al.*, 2021; Reiman *et al.*, 2020; Blue *et al.*, 2019; Arboleda-Velasquez *et al.*, 2019; Barnes & Bennett, 2015; Kaup *et al.*, 2015; Chung *et al.*, 2013; Logue *et al.*, 2011; Tang *et al.*, 1998; Farrer *et al.*, 1997].

Part I – Study Aims & Objectives

Our study used data collected from the Lifespan Human Connectome Project in Aging (HCP-A) study [Bookheimer *et al.*, 2019], including a sample of cognitively typical older adults (ages 50-89) collected across four U.S. academic health centers. We aimed to characterize age-related cognitive decline in mid-to-late life, investigating the relationships between cognition, Aβ, APOE ε4, and brain structure. We begin by exploring whether subcortical, cortical, or specific MTL brain regions show age, Aβ, or APOE-dependent changes in volume. We postulated that reduced regional volumes would be associated with age, pathologic levels of Aβ, and carriers of at least one ε4 allele.

Then, we used linear models to demonstrate the relationship between domain-specific cognition function, age, and biomarkers (Aβ, APOE ε4). We hypothesized that memory scores for late-life adults would be lower compared to mid-life adults and relate strongly to biomarker phenotype. We show that total cognition and fluid intelligence scores are related to age and Aβ compared to crystalized intelligence, evaluating vocabulary, and reading ability, which is age-invariant. Here, we assess the relative fit of each cognition model.

Finally, we show that blood-based biomarkers are sensitive to detecting memory performance variability in typically aging adults. We discuss future avenues of research (*e.g.*, neuroinflammation) and address nuanced areas of study requiring further examination.

1.2 Methods
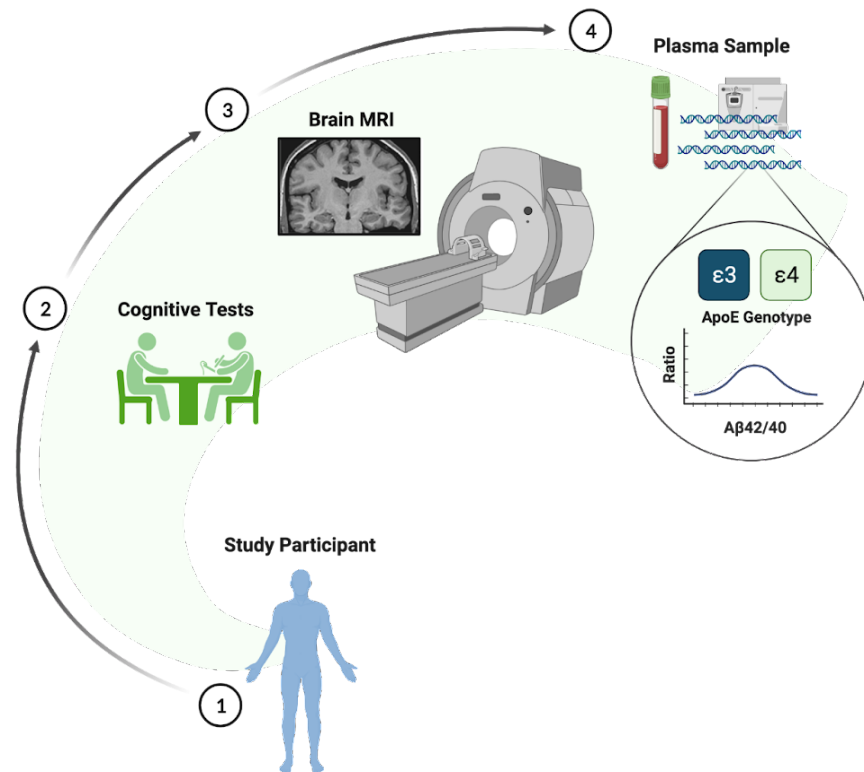
Figure 1.3 Study design for the Human Connectome Project in Aging. (**1**) Participants aged 36 and older enrolled in the HCP-A study following an interview that screened for neurological diseases, psychiatric illnesses, and other health-related concerns. (**2**) Participants completed neuropsychological assessments to evaluate domain-specific cognition and other behavioral elements of typical psychological and physiological function. (**3**) Brain scans were collected, including structural MRIs processed through standard neuroimaging pipelines to obtain volumetric measurements of the brain. (**4**) Blood samples were measured for Aβ 40,42 plasma concentrations and screened for APOE variation by C_2N Diagnostics.

Participants

This study includes a sample from the Lifespan Human Connectome Project in Aging (HCP-A; **Figure 1.3**). Participants were well-screened, cognitively unimpaired older adults (mean age ± S.D. = 73.5 ± 11.9 years; median = 75.2 years; Female n = 73; mean education ± S.D. = 17.7 ± 2.22 years; median = 18 years) with at least one sample of blood analyzed for plasma Aβ across two study visits. Study sample demographics are detailed (**Table 1.1**).

A total of 133 participants were included in our analyses. They completed behavioral assessments, brain MRI scans, and blood draws. Data were removed from the study analyses if behavioral assessment scores were not available from the same visit as the collection of blood samples (n = 10) or if an APOE ε2 variant was detected (n = 17).

The Lifespan HCP-A study was comprehensively reviewed [Bookheimer *et al.*, 2019] and received NIH Neuroscience Blueprint funding [Grant U01AG52564]. The Institutional Review Board (IRB) at each study site approved research protocols [UCLA IRB#16-001922].

Plasma & Genetic Biomarker Detection

Whole blood samples analyzed by C2N Diagnostics (St. Louis, MO, 2020) quantified Aβ 40,42 concentrations (pg/mL) derived from blood plasma. The Aβ ratio was determined by the total concentration of Aβ 42:40, with a value of less than 0.089 indicating protein deposition in brain tissue associated with PET Aβ positivity [Ovod *et al.*, 2017]. In addition, the apolipoprotein E (ApoE) proteotype was determined via trypsin-mediated chromatographic separation to produce isoform-specific peptides detectable using mass spectroscopy. For each of the six APOE genotypes (ε2/ε2, ε2/ε3, ε2/ε4, ε3/ε3, ε3/ε4, ε4/ε4), ApoE proteotyping quantified the

presence/absence of the four isoform-specific peptides [Kirmess *et al.*, 2021]. The APOE ε3 and ε4 variants were included in the study analyses since ε4 carriers have a greater genetic risk of developing AD compared to ε3 carriers, considered the standard 'baseline' allele occurring in approximately 78% of the general population, and the ε2 variants were removed due to low subgroup samples needed to differentiate between protective effects [Phillips, 2014].

Behavioral Measures

Neuropsychological assessments included the Montreal Cognitive Assessment (MoCA), the Rey Auditory Verbal Learning Test (RAVLT), and the Cognition Battery of the NIH Toolbox. This study used the RAVLT delayed-recall assessment and the NIH Toolbox composite scores to investigate age-related cognitive decline.

The MoCA is a cognitive screening test for clinicians and researchers to evaluate problems [Nasreddine *et al.*, 2005]. The test has a total of 30 items with a maximum score of 30-points assessing language, memory, visual and spatial thinking, reasoning, and orientation skills. MoCA score cut-offs were used to screen for low performance based on age-adjusted norms. Participants with a MoCA score below 19 (for ages 22-79), 17 (ages 80-89), and 16 (aged 90+) were not enrolled in the HCP-A study.

The RAVLT was administered to participants using an iPad that presented a list of 15 unrelated words while participants listened [Rey, 1941; Corwin & Bylsma *et al.*, 1993]. Participants were instructed to repeat as many words as possible after the presentation, repeated over five learning trials using the same word list. Then, a second interference word list of the same length was verbally administered. This cognitive distractor promotes task

dependence on hippocampal-mediated memory for subsequent recall of the initial word list. Finally, participants were asked to repeat as many words as remembered from the first list only. The short-delay performance was measured as the total words recalled during the trial following the interference trial. Trials had a maximum score of 15-points, with 1-point assigned for each correctly recalled word from the proceeding list.

The NIH Toolbox[©], administered using an iPad, evaluated five domain-specific cognitive abilities across a total of seven assessments: (1) executive function and attention (dimensional change card sort & flanker), (2) episodic memory (picture sequence memory), (3) working memory (list sorting), (4) processing speed (pattern comparison), and (5) language abilities (picture vocabulary and oral reading recognition) [Weintraub *et al.*, 2014; Gershon *et al.*, 2014; Gershon *et al.*, 2013]. Three composite scores, measuring total cognition, fluid intelligence, and crystallized intelligence, were averaged across all assessments (total), domains 1-4 (fluid), or domain 5 (crystallized). A higher score represents better cognitive performance and relates to a percentile group based on a standard distribution of national averages, where a score of 70 or below represents very low (2%), 85 below-average (16%), 100 average (50%), 115 above-average (84%), and 130 or above superior cognitive ability (98%) [NIH & Northwestern University, 2021].

Neuroimage Acquisition

Images of the brain were collected at four academic health centers on five 3-Tesla Siemens MRI systems. These centers included the Washington University in St. Louis, the University of Minnesota Twin Cities, Massachusetts General Hospital with Harvard University, and the University of California Los Angeles.

The imaging centers used standardized protocols to acquire structural MRI and high-angular resolution diffusion-weighted MRI (dMRI) with advanced pulse sequences. The current imaging protocols were updated based on understanding gained from the Human Connectome Project study in young adults [Harms *et al.*, 2018; Van Essen *et al.*, 2012]. The MRI scan parameters used in this study are briefly summarized below.

This study used three MRI scans, including (1) a T1-weighted MPRAGE (gradient spin-echo; TR = 2400 ms, TE = 2.14 ms, TI = 1000 ms, flip angle = $8°$, matrix size = 192 x 192, FOV = 224 x 224 mm, 280 slices) with 0.7 mm isometric voxels, (2) a T2-weighted hippocampal high-resolution MRI (TR = 4800 ms, TE = 106 ms, matrix size = 128 x 128, FOV = 150 x 150 mm) with 0.4 x 0.4 x 2 mm voxels, and (3) a multishell dMRI sequence (TR = 3230 ms, TE = 89.20 ms, flip angle = $78°$, refocus flip angle = $160°$, matrix size = 208 x 144, FOV = 210 x 140 mm, slice thickness = 1.50 mm, multiband factor = 4, echo spacing = 0.69 ms, bandwidth = 1700 Hz/Px, phase partial Fourier = 6/8, b-values = 1500 and 3000 s/mm^2) with 1.25 mm isotropic voxels and 92 blip-up and 92 blip-down volumes and a total of 14 b_0 volumes.

Neuroimage Processing

The structural MRI scans were processed using the FreeSurfer (version 7.2.0) and Automatic Segmentation of Hippocampal Subfields (ASHS; version 2.0) software packages. The FreeSurfer pipeline parcellated the brain into regional segments using the subcortical [Fischl *et al.*, 2002; Fischl *et al.*, 2004a], cortical gray matter and white matter parcellations [Desikan *et al.*, 2006; Fischl *et al.*, 2004b], and hippocampal subfields [Iglesias *et al.*, 2015] atlases. The subcortical (**Figure 1.4**) and cortical (**Figure 1.5**) atlases are provided with a list of brain regions.
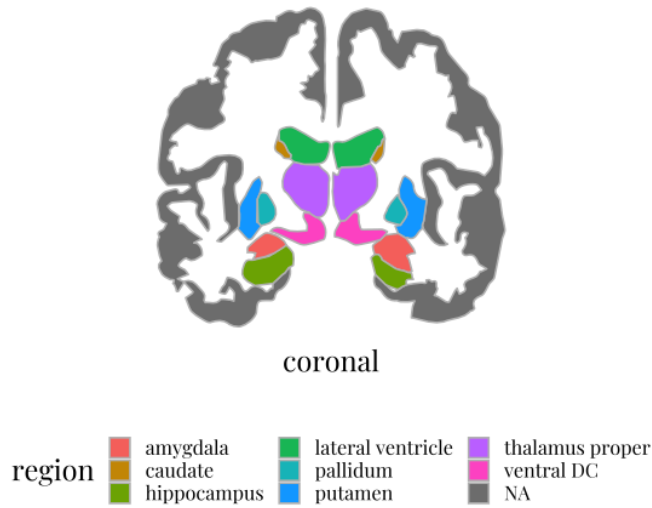
The ASHS pipeline segmented MTL regions using the University of Pennsylvania Memory Center 3-Tesla atlas for T1-weighted MRI [Xie *et al.*, 2016].

Regional volumetric measures were normalized using an estimated total intracranial volume. Only normalized values were used for statistical modeling. The R Studio packages 'ggseg' and 'ggseg3d' were used to visualize brain statistics [Mowinckel & Vidal-Piñeiro, 2019], and the package 'showtext' was used for custom fonts in R Graphs [Qiu, 2022].

Statistical Analyses

Relationships between age, Aβ, APOE ε4, hippocampal volume, and verbal memory scores were assessed using Spearman correlation and Welch two-sample t-test (α level < 0.05). Linear regression models were used to study the relationship between brain/blood biomarkers and cognition. The blood biomarkers were a ratio of plasma-derived Aβ 40,42 and ApoE proteotype, the neuroimaging markers were regional brain volumes, and the model outcomes were domain-specific cognition scores, including total, fluid, and crystallized intelligence. The following regression equation was used: Cognition Score ~ B_{age}Age + $B_{A\beta}$Aβ + B_{APOE}APOE + ϵ

The total words recalled at the short-delay assessment of the RAVLT and age-uncorrected scores for NIH Toolbox Cognition Battery composite measures were used. Statistics (p-values) were False Discovery Rate (FDR)-corrected using the Benjamini-Hochberg procedure. Models were checked for linearity, predictor collinearity, variance homogeneity, residual normality, and heteroskedasticity. No predictor or distributional irregularities were detected. Model estimate coefficients (**B**) values, standard deviation (S.D.), standard error of the mean (S.E.M.), F-values, t-values, and FDR-corrected p-values are provided where appropriate.

coronal

region
amygdala   lateral ventricle   thalamus proper
caudate   pallidum   ventral DC
hippocampus   putamen   NA

Figure 1.4 Automated segmentation of subcortical brain regions.

left   right
hemisphere

region
bankssts   lingual   precuneus
caudal anterior cingulate   medial orbitofrontal   rostral anterior cingulate
caudal middle frontal   middle temporal   rostral middle frontal
corpus callosum   parahippocampal   superior frontal
cuneus   paracentral   superior parietal
entorhinal   pars opercularis   superior temporal
fusiform   pars orbitalis   supramarginal
inferior parietal   pars triangularis   frontal pole
inferior temporal   pericalcarine   temporal pole
isthmus cingulate   postcentral   transverse temporal
lateral occipital   posterior cingulate   insula
lateral orbitofrontal   precentral

Figure 1.5 Cortical gray and white matter brain regions.

1.3 Results

We assessed the relationships between age, Aβ, and APOE on brain structure using multiple ANOVAs to explain differences in regional volume. First, we examined differences in hippocampal volume and then assessed volume differences globally across the whole brain using three neuroanatomical atlases for (1) archicortical/subcortical, (2) cortical gray matter, and (3) cortical white matter parcellations. Next, we conducted complementary analyses using dual segmentation pipelines for hippocampal subfields and MTL volumes to investigate how sub-regional differences contribute to age-related memory decline and assess the consistency of results across approaches with different automated protocols, boundary conditions, and geometric assumptions. Lastly, we model domain-specific cognitive performance.
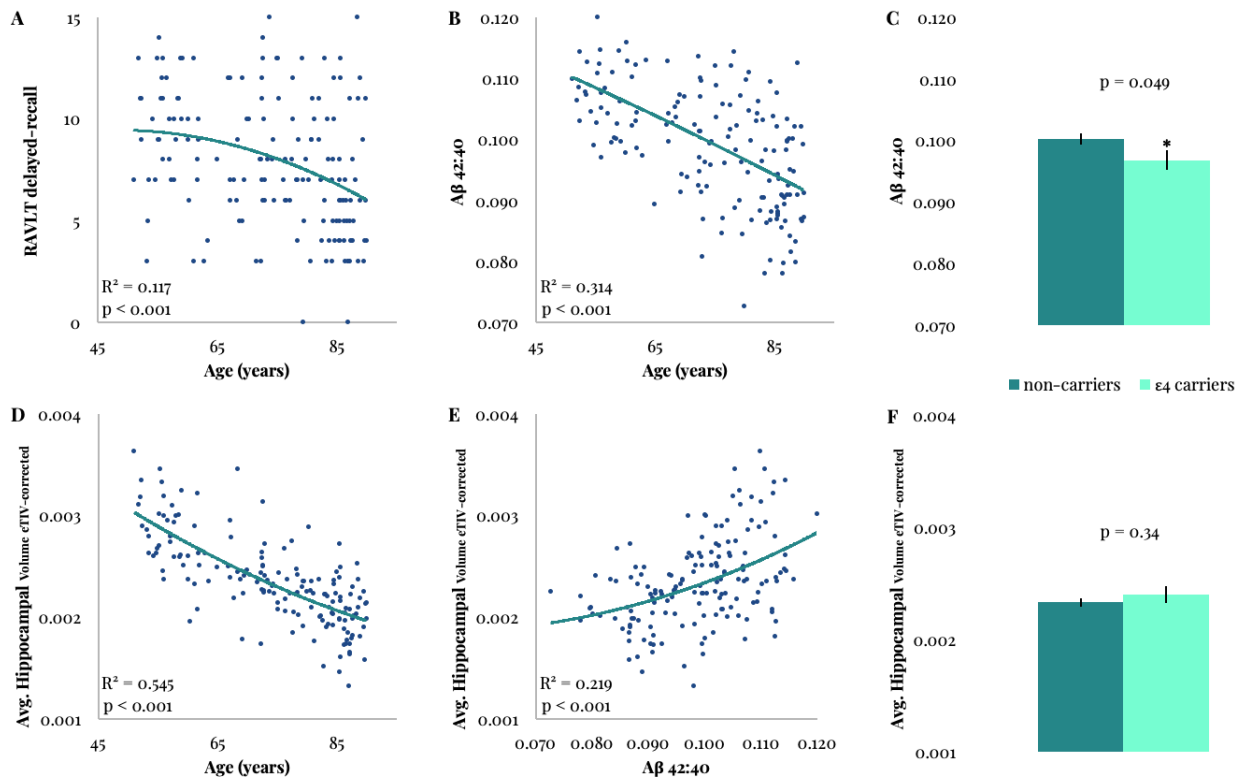
The relationship between age, Aβ, APOE & hippocampal volume

We investigated age-related changes in cognitive function, hippocampal volume, and Aβ ratio, and found significant associations between these three variables. The hippocampal volume and cognition scores decreased with age, whereas the plasma-derived measure of Aβ increased with age. The age-dependent relationships were fit with second-order polynomial equations and summarized using the coefficient of determination provided by R^2 (**Figure 1.6**).

Next, we investigated the relationship between these biomarker variables independent of age-related changes. Aβ was significantly associated with hippocampal volume, where a lower level of Aβ in the blood plasma, indicating a higher Aβ burden in the brain, was related to smaller hippocampal volume (**Figure 1.6 E**). Additionally, APOE ε4 carriers had significantly

different Aβ levels compared to non-carriers, suggesting more Aβ pathology for individuals with at least one copy of the ε4 allele (**Figure 1.6 C**). Nevertheless, we did not find sufficient evidence to support a relationship between the ε4-carriers and hippocampal volume. Curiously, the mean hippocampal volume was slightly elevated for carriers compared to non-carriers (**Figure 1.6 F**), although not significantly different. This may reflect compensatory reserve factors yet to be determined within the sample cohort (*e.g.*, exercise or educational attainment, which are protective lifestyle characteristics against ε4-related neuropathology).

Figure 1.6 The relationships between (**A**) memory scores by age, (**B**) Aβ by age, (**C**) Aβ by APOE ε4 status (non-carriers = 0.100 ± 0.0009, ε4-carriers = 0.097 ± 0.0016), (**D**) hippocampal volume by age, (**E**) hippocampal volume by Aβ, and (**F**) hippocampal volume by APOE ε4 status (non-carriers = 0.0023 ± 0.00004, ε4-carriers = 0.0024 ± 0.00008).

The effects of age, Aβ & APOE on brain volume

We also investigated the extent to which regional volumes across the entire brain varied by age, Aβ, and APOE ε4 carrier status. Using one-way ANOVA, we found many differences across regional volumes using the automated subcortical segmentation atlas, where an impressive number of regions were associated with old age and Aβ pathology and relatively fewer differences related to ε4 carrier status (**Figure 1.7 A**). Overall, we found similar association patterns in the left and right hemispheres. Test statistics are listed in the Appendix and were corrected using the Benjamini Hochberg method (**Table A1**).

In addition, we found similar trends in biomarker relationships using a cortical gray matter atlas (**Figure 1.7 B; Table A2**) or a cortical white matter atlas (**Figure 1.7 C; Table A3**), where smaller cortical volume was age-dependent and lower plasma Aβ, indicating a more significant burden of brain-based amyloid pathology. Again, ε4 carrier status had a marginal effect on cortical gray matter volume but more influence on cortical white matter volume.

The effects of age, Aβ & APOE on MTL structure

To gain a holistic view of MTL structural changes across age, we used dual segmentation protocols for delineating regional boundaries within the hippocampal formation and parahippocampal gyrus. These differences are due to assumptions made by the automated segmentation algorithms [Wisse *et al.*, 2021; Xie *et al.*, 2019; Mueller *et al.*, 2017] and may result in contradictory findings. Using a multi-atlas approach, we demonstrate the consistency and variability of associations in age-related and biomarker-mediated MTL regional volume loss. The test statistics for the analyses described below are listed in the Appendix.
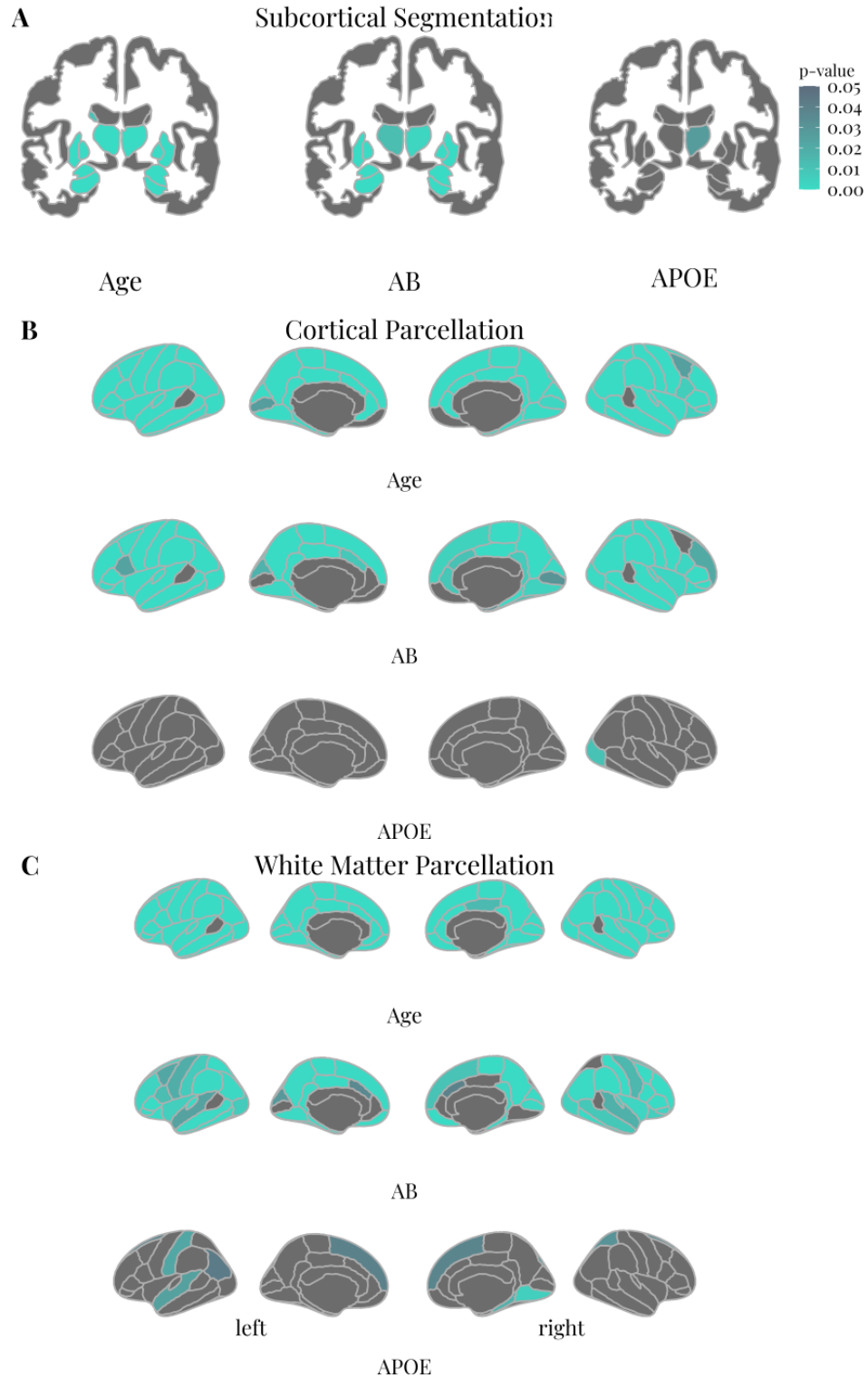
Figure 1.7 Volume differences in (**A**) subcortical, (**B**) cortical gray matter, and (**C**) white matter

brain regions. The legend illustrates FDR–corrected p–values.

The hippocampus comprises distinct subfields, broadly classified by their positioning along the anterior-posterior axis. These categories are often referred to as the hippocampal head-body-tail or, more succinctly, as the anterior and posterior halves of the hippocampus. Regarding head-body-tail distinctions of the hippocampus, we found that bilateral volumes decreased with age. Left hemisphere volumes also decreased with Aβ plasma levels consistent with the amyloid pathology observed in AD (**Table A4**). Volumes did not significantly differ between carriers and non-carriers; however, the overall trend for ε4 carriers was, on average, smaller regional volumes than non-carriers. Similarly, we found anterior-posterior hippocampal volumes decreased bilaterally with age and Aβ, but not in ε4 carriers (**Table A5**).

Next, we explored hippocampal subfield volumes, which generally decreased with age, except for the hippocampal fissure, which increased with age (**Figure 1.8; Table A4**).
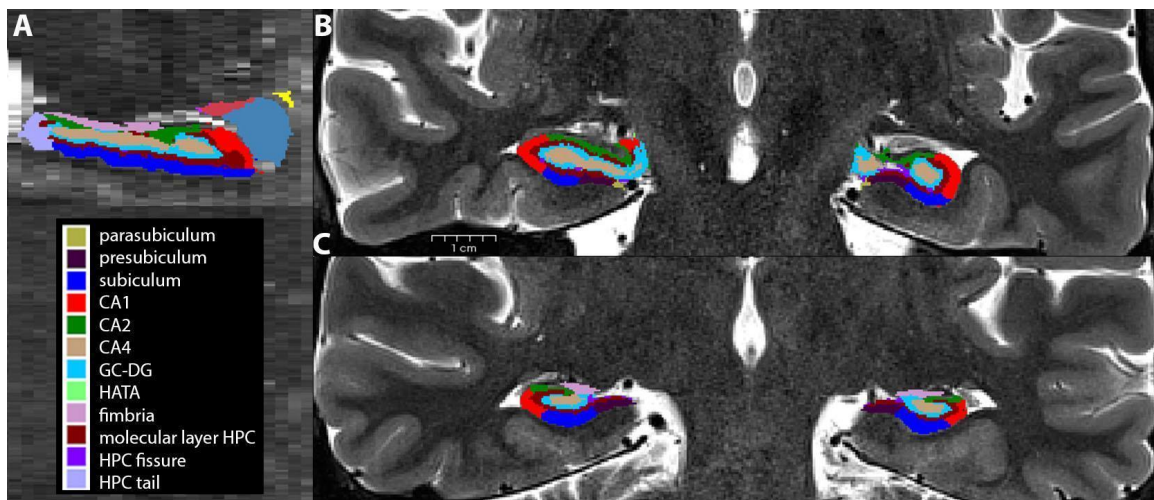
Figure 1.8 Segmentation of hippocampal subfields using FreeSurfer. (**A**) sagittal, (**B**) anterior coronal, and (**C**) posterior coronal view of a high-resolution hippocampal image. The legend designates subfield labels and parcellation color palette—scale bar (1 cm).

Typically, fissure enlargement shows the amount of atrophy within the hippocampus over the lifespan. While most regions showed significant age-dependent volume reductions, the hippocampal fissure size did not differ across the age range studied, which may be due to the unimpaired cognitive profile of study participants. Still, it is remarkable that individuals approaching their mid-to-late 80s showed no significant change in fissure size compared to those in their early 50s. Aβ showed identical relationships with regional volumes as age-related changes, where lower plasma levels were associated with smaller regional volumes. Furthermore, we investigated biomarker-related changes in parahippocampal gyrus volumes, including the entorhinal, perirhinal, and parahippocampal cortices. These regions showed age and Aβ-dependent volume reductions, but not with ε4 carrier status (**Table A5**).

Modeling Cognition

We modeled domain-specific cognition and blood biomarkers using linear regression to explain differences across three composite measures from the NIH Toolbox Cognition Battery for total, fluid, and crystallized intelligence (**Figure 1.9**). The response variable of the three models was cognition score, and the explanatory variables included age, Aβ, and ε4 carrier status. Significant model relationships were found for total cognition ($F_{(3, 129)}$ = 8.34, p < 0.001, R^2-adjusted = 0.35; Residual standard error: 9.99) and fluid intelligence ($F_{(3, 129)}$ = 24.76, p < 0.001, R^2-adjusted = 0.35; Residual standard error: 11.04).

There were main effects of age in both fluid and total cognition models, where older individuals had lower scores (Total: Coefficient = -0.23, Std. Error = 0.090, t-value = -2.6, p-value < 0.05; Fluid: Coefficient = -0.53, Std. Error = 0.099, t-value = -5.3, p-value < 0.001).

Yet, there was only a main effect of Aβ on fluid intelligence, where plasma levels indicating Aβ neuropathology associated with worse performance (Coefficient = 2.88, Std. Error = 1.20, t-value = 2.396, p-value = 0.018). By contrast, we did not find sufficient evidence to support a relationship between the model predictors and performance on the crystalized composite measure ($F_{(3, 129)}$ = 1.127, p = 0.34, R^2-adjusted = 0.0029; Residual standard error: 8.779).
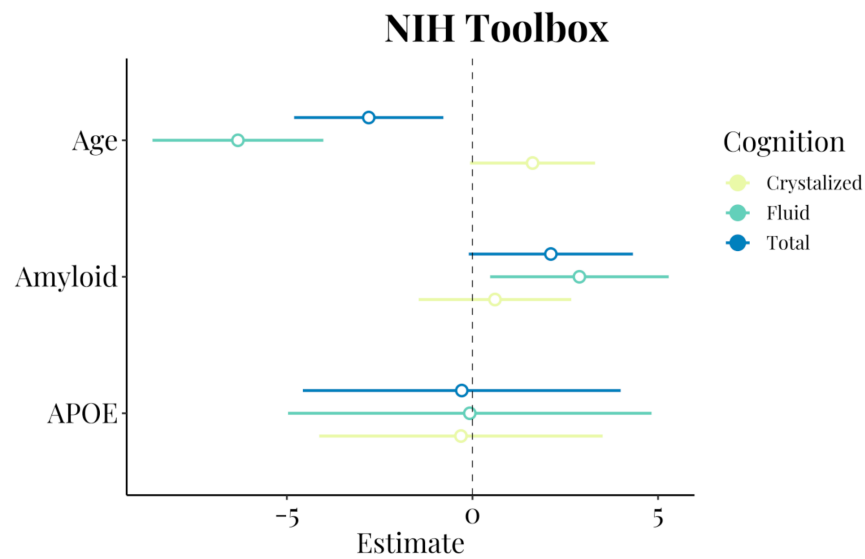
Figure 1.9 NIH Toolbox cognition models and biomarker coefficients.

1.4 Conclusions

In this study, we found that memory performance, hippocampal volume, and biomarkers associated with neurocognitive diseases are intricately related. Principally, verbal memory in typically aging older adults is age-dependent, where older participants had significantly lower scores than mid-life adults. The hippocampal volume and plasma-derived Aβ biomarkers were negatively correlated with age in this group; older participants had smaller hippocampal volumes and more pathogenic levels of Aβ.

Furthermore, we evaluated the relationship between hippocampal volume and two biomarkers associated with neurodegeneration. We found that hippocampal volume is related to the level of Aβ in blood plasma, where smaller hippocampal volumes correspond to a differentiable Aβ burden. In addition, the Aβ burden in individuals with one or two copies of the APOE ε4 allele differed from non-carriers. However, the ε4 carrier status did not relate to hippocampal volume, which may reflect a participant selection bias predicated on individuals needing a non-impaired memory assessment score for study enrollment. Consequently, this may be an intriguing characteristic of the study sample that, when assessed longitudinally, may elucidate cognitive reserve factors contributing to hippocampal preservation despite the increased genetic risk associated with having an APOE ε4 allele. Moreover, since the ApoE protein facilitates the metabolism of lipids throughout the body and nervous system, the metabolic/lipid profiles of older adults who are carriers of the ε4 allele should be explored in future studies. Another area for future investigation is lifestyle factors (*e.g.*, exercise, diet),

which studies have shown benefit body and brain health [Park *et al.*, 2022; Voss *et al.*, 2013; Vaynman & Gomez-Pinilla *et al.*, 2006].

Importantly, we show that biomarkers derived from blood plasma are sensitive to detecting variability in typically aging memory performance. In addition, these blood-based features of declining cognition occur with brain-based biomarkers indicating amyloid accumulation and structural degeneration in key brain regions important for typical memory function. Undeniably, these biomarkers are correlated with each other. The direct causality between Aβ burden, brain structure, and memory impairment requires future investigation to address the temporal sequence of biomarkers apparent for the earliest detection of memory-related pathologies [Luo *et al.*, 2022; Poulakis *et al.*, 2021].

Over the last century, the amyloid hypothesis has emerged as the leading theory contributing to the pathogenesis of AD [Goedert & Spillantini, 2006]; however, this line of inquiry has recently been the subject of intense scrutiny enveloped by the impropriety of some individuals in the scientific community with the fabrication of data in support of this hypothesis [Piller, 2022; Lesné *et al.*, 2006]. While these allegations represent a testimony to the integrity of the scientific process for discovering truth in biological mechanisms, there is still much to be said in support of the relationship between Aβ burden and memory loss [Ashe, 2022; Ashe, 2020; Liu *et al.*, 2015]. Notably, Aβ is not the only biological determinant associated with dementias like AD and works in concert with tau and neurodegeneration, formulating the revised ATN hypothesis [Frisoni *et al.*, 2022]. Studies of Aβ deposition with and without the tau protein, called neurofibrillary tangles, have distinct neuropathological and neuropsychological profiles [Strikwerda-Brown *et al.*, 2022; Thompson *et al.*, 2022; Young *et al.*, 2022].

The field has also begun to investigate the neuroinflammatory and glial contributions to AD-like pathologies suggesting that distinct molecular and biochemical factors are integral to the cognitive resilience/risk of some individuals with marked Aβ and tau pathologies [Ferrari-Souza *et al.*, 2022; Victor *et al.*, 2022; Schindler *et al.*, 2022; Griswold *et al.*, 2021; Kloske *et al.*, 2021; Barroeta-Espar *et al.*, 2019; Shi & Holtzman, 2018; Tao *et al.*, 2018]. Whether Aβ will prove to be the purported causal link between initial neuronal dysfunction and subsequent memory impairment, several nationwide clinical trials are underway to elucidate if the reduction of Aβ prior to clinically relevant impairment will prevent the conversion to AD or reduce the severity of symptomology.

Together these findings represent the first steps toward characterizing age-related cognitive, brain, and physiological markers in cognitively typical older adults. Over the coming years, substantial progress will be made toward understanding the contributions of these markers in delineating typical from atypical aging. A significant feature of the HCP-A study design was to enroll a representative sample of adults from across the U.S. to tease apart the biological, sociocultural, and individual trajectories that predict successful or deleterious effects across the lifespan. The knowledge gained from studies of this kind may then be used to develop directed hypotheses for intervening before the onset of memory loss. We anticipate these findings will illuminate a brighter future for individuals aged 65+ living within and beyond the United States, optimizing the set of healthy life course strategies with potential implications for global health policy and practice [WHO, 2022].

II

HIPPOCAMPAL–NETWORK TARGETED TRANSCRANIAL MAGNETIC STIMULATION

IMPROVES ASSOCIATIVE MEMORY IN OLDER ADULTS.

2.1 Introduction

Memory loss affects 40% of people aged 65 and older, approximately 16 million in the United States [Small, 2002]. Within this age group, one in ten older adults has more severe memory issues referred to as Mild Cognitive Impairment (MCI), of which 15% will advance to a diagnosis of Alzheimer's disease (AD) each year. In addition to the impact on memory, an essential component of AD and dementia-related pathologies is the effect on daily function and independent living. As the proportion of people aged 65 and older in the U.S. grows, and unless interventions are taken to alleviate memory-related disability, these estimates are expected to triple over the next two to three decades [CDC, 2003]. Therefore, a primary goal of learning and memory research has been to explain how brain regions within the medial temporal lobe (MTL) support cognition [Eichenbaum *et al.*, 2007]. Scientists are interested in applying knowledge gained from circuit-level and systems-based studies in combination with neurotechnologies to modulate hippocampal networks and memory performance.

Recent advances in therapeutic drug targets to treat memory impairment have produced a viable yet contentiously debated treatment for reducing amyloid plaques in the brain [Rabinovici *et al.*, 2021]. Still, the prohibitively high treatment cost is criticized for outweighing the clinical benefit (*i.e.*, a significant reduction of Aβ) [Whittington *et al.*, 2022] and contrary to a clear indication of adverse effects (*e.g.*, microhemorrhages occurred in ~35% of patients) [Glymour *et al.*, 2022]. Furthermore, biologically active therapeutic agents can have non-specific metabolic and systemic health effects (*e.g.*, risk of liver and kidney failure) that reduce the patient's quality of life and overall value-based care. Moreover, many therapies only

show moderate efficacy with limited effectiveness [Casey *et al.*, 2010]. Another approach to address memory-related concerns is cognitive-behavioral rehabilitation and training paradigms; however, these dialectical and intervention-based methods have variable benefits with low success for patients with moderate to severe impairments [Hampstead *et al.*, 2013, Greenaway *et al.*, 2013, van Paasschen *et al.*, 2013].

While the diagnostic and therapeutic toolbox available to clinicians has remained fixed, physician-scientists and researchers have focused on developing novel strategies for preserving or restoring memory, which are urgently needed. Neuromodulation technologies offer unparalleled prospects for treating memory impairments by enabling the specific targeting of select brain regions indicated in the pathophysiology of neurologic and psychiatric diseases, and these technologies are broadly grouped by their method of accessing the brain. The invasive type requires surgery to implant electrodes covering the brain's surface or penetrating the tissue to access deeper structures (*e.g.*, intracranial electrocorticography and deep brain stimulation). Studies using invasive neurotechnologies have reported that direct stimulation of the entorhinal area in the MTL facilitated memory [Suthana *et al.*, 2012; Suthana & Fried *et al.*, 2014; Titiz *et al.*, 2017]. These remarkable findings are, however, qualified by the risks involved with implanting intracranial electrodes, which have limited its broad application for use in only specific neurological conditions, hindered further by high procedural costs and inherent ethical concerns [Vedam-Mai *et al.*, 2021; Cinel *et al.*, 2019].

In contrast, non-invasive neuromodulation can stimulate the brain without the risks associated with surgical implantation. In recent years, the variety of technologies utilizing this approach has increased due in part to their versatility in studying and treating brain disease.

The most common methods are transcranial-focused ultrasound, electrical stimulation, and transcranial magnetic stimulation (TMS). While each method has specific technical advantages, the most widely implemented and clinically validated is TMS.

Fundamentally, TMS capitalizes on stimulation protocols that vary the frequency and intensity of magnetic pulses, allowing researchers and clinicians to entrain neural activity patterns for activating or inhibiting targeted brain regions. These protocols can deliver many pulses repetitively in a relatively short period and intermittently to emulate the endogenous firing of neurons. Specifically, a brief, high-frequency burst of stimulation called a tetanus block, or more precisely a 'theta-burst' because of the timing at which stimulation pulses are delivered, has been shown to increase synaptic strength, the connection between neurons, facilitated by long-term potentiation (LTP), the neurobiological substrate of learning and memory. The phenomenon of LTP has enduring neurophysiological effects that have been examined across various memory paradigms and model organisms, ranging from *in vitro* assays of hippocampal neurons to electrophysiological circuit manipulation in animals and humans [Squire & Kandel *et al.*, 2003].

Studies using theta-burst TMS have successfully improved memory for young adults [Freedberg *et al.*, 2021; Hebscher *et al.*, 2021; Freedberg *et al.*, 2020; Hermiller *et al.*, 2019; Nilakantan *et al.*, 2017; Wang *et al.*, 2014], and hold promise for use in older adults, in particular, to preserve or reverse memory deficits in AD and MCI [Chou *et al.*, 2020].
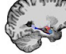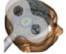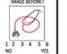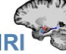
Figure 2.1 Research equipment in the TMS Clinic at the UCLA Semel Institute.

Part II – Study Aims & Objectives

Our study used a randomized, condition-blinded, and placebo-controlled trial design of intermittent theta-burst stimulation (iTBS) TMS to promote memory in older adults (ages 55+). Participants were assessed for baseline memory function. Using an MRI-guided approach informed by resting-state activity, the hippocampal network was targeted by stimulating functionally connected regions in the lateral posterior parietal cortex, a core component of the network [Ciaramelli *et al.*, 2020], consecutively across five days of iTBS. Behavioral changes in memory performance were monitored daily. In addition, task-based functional and structural MRI, as well as electrophysiological scalp recordings, were used to assess the network dynamics mediating the iTBS protocol for memory enhancement (**Figure 2.1**).

2.2 Methods

Figure 2.2 Study design for iTBS in older adults. Before enrolling in this study, participants were screened for eligibility. On visit 1, participants provided informed consent and underwent behavioral and cognitive assessments to determine baseline function. On visit 2, participants had an initial MRI scan with simultaneous memory testing. On visits 3 thru 7, five iTBS sessions occurred Monday through Friday, and memory testing was completed daily. On visits 3 and 7, scalp EEG was collected before, during, and after delivery of iTBS. On visit 7, a follow-up MRI scan was also performed with memory tests. Finally, on visit 8, a final assessment of memory occurred 24-72 hours from the last iTBS session. There were a total of 8 study visits, typically over a 1 to 2-month period. Additionally, the University of California Los Angeles safety and health protocols were implemented to ensure the health and safety of study participants for mitigating the spread of COVID-19 per the Los Angeles Department of Public Health and the U.S. Centers for Disease Control and Prevention recommendations.

<u>Participants</u>

A total of fifty-six healthy older adults (age 60 to 80 years) were screened and provided informed consent by an ABPN-certified Psychiatrist for enrollment in the study. Participants were excluded for past or present diagnosis of neurological disease, major psychiatric illness, or a Mini-Mental State Examination (MMSE) score of 26 or below. Twenty-two participants completed the study protocol (**Figure 2.2**). The study design and protocols were approved by the University of California Los Angeles Institutional Review Board (IRB) [IRB#15-001366].

<u>Behavioral Measures</u>

Enrolled participants underwent a neuropsychological battery to confirm cognitive performance typical for demographic-adjusted norms. The behavioral measures included two scales for Activities of Daily Living [Katz *et al.*, 1963; Lawton & Brody, 1969; Graf, 2008], the MMSE [Folstein *et al.*, 1975], the Wechsler Adult Intelligence Scale-Third Edition (WAIS-III Digit Span & Vocabulary Test of Premorbid Functioning-TOPF) [Wechsler, 1997], the Trail Making Test (Trails A & B), an abbreviated (form 4) Boston Naming Test [Lansing *et al.*, 1999], the California Verbal Learning Test-Second Edition (CVLT-II) and the Wechsler Memory Scale-Third Edition (WMS-III Visual Reproduction and Recognition) [Wechsler, 1997]. Participants were screened for subjective reports of memory complaints using two questionnaires, including prospective and retrospective memory assessments [Crawford *et al.*, 2003; Smith *et al.*, 2000; Gilewski *et al.*, 1990]. In addition, participants that scored ≥ 8 on the Hamilton Depression Scale (Ham-D) were not eligible for study enrollment due to confounds related to a diagnosis of depression and comorbid effects on memory function.

Magnetic resonance imaging (MRI) scans were acquired using a 3-Tesla Siemens PRISMA system. A total of nine imaging sequences were collected at two different study visits, including two structural MRIs, a resting-state functional MRI (rs-fMRI), two runs of task-based fMRI (during object recognition encoding and retrieval), and dual-phase acquisition high-angular resolution diffusion-weighted MRI (dMRI) scans. These were collected before and after iTBS treatment on the third and seventh study visits (**Figure 2.2**), typically within 1-2 months of study enrollment and completion.

The two structural MRI included: (1) T1-weighted MPRAGE (TR = 2400 ms, TE = 2.22 ms, TI = 1000 ms, flip angle = 8°, FOV = 256 x 256 mm, voxel size = 0.8 mm^3, bandwidth = 220 Hz/Px, iPAT acceleration factor PE = 2), and (2) T2-weighted hippocampal high-resolution MRI (TR = 5200 ms, TE = 107 ms, flip angle = 139°, FOV = 200 x 200 mm, voxel size = 0.4 x 0.4 x 2.0 mm, bandwidth = 195 Hz/Px).

The rs-fMRI and task-based functional scans used a gradient EPI sequence (TR = 800 ms, TE = 33.80 ms, flip angle = 52°, FOV = 210 x 210 mm, slice thickness = 1.90 mm, 80 slices, voxel size = 1.9 mm^3, multiband factor = 8, echo spacing = 0.65 ms, bandwidth = 2164 Hz/Px). During the rs-fMRI scan, participants were instructed to fixate on an illuminated crosshair in the center of their visual field. During the task-based fMRI scans, participants completed two rounds of the object recognition task where they learned and recalled images of novel objects. Responses were recorded using a 4 x 1 button box inside the MRI scanner.

The dMRI scans included two runs acquired with opposite phase-encoding using a spin-echo EPI sequence (TR = 3230 ms, TE = 89.20 ms, flip angle = 78°, refocusing flip angle =

160°, FOV = 210 x 140 mm, matrix size = 208 x 144 mm, slice thickness = 1.50 mm, 92 blip-up and 92 blip-down slices, voxel size = 1.5 mm³, multiband factor = 4, echo spacing = 0.69 ms, bandwidth = 1700 Hz/Px, phase partial Fourier = 6/8, b-values = 1500 and 3000 s/mm²).

<u>Neuroimage Processing</u>

The structural MRIs were processed using three segmentation protocols across two software packages for identifying MTL regions: FreeSurfer (version 7.2.0) and Automatic Segmentation of Hippocampal Subfields (ASHS; version 2.0). Two protocols used the ASHS pipeline for hippocampal subfields and adjacent MTL regions (including BA 35 & 36 perirhinal cortex) but used different atlases. The first ASHS protocol used the University of Pennsylvania (UPenn) Memory Center (PMC) 3-Tesla atlas for T2-weighted MRI [Xie *et al.*, 2017; Yushkevich *et al.*, 2015; Adler *et al.*, 2014], and the second ASHS protocol used the UPenn PMC 3-Tesla atlas for T1-weighted MRI [Xie *et al.*, 2016]. The third protocol used the FreeSurfer pipeline to determine hippocampal subfield volumes using the *ex vivo*, ultra-high-resolution atlas [Iglesias *et al.*, 2015].

<u>Hippocampal Network Targeting</u>

To target hippocampal networks, the rs-fMRI scan was processed with the FEAT package from FMRIB's Software Library [Smith *et al.*, 2004; Woolrich *et al.*, 2009; Jenkinson *et al.*, 2012] to produce a high-quality function connectivity analysis. An initial first-level analysis was performed, which included MCFLIRT motion correction [Jenkinson *et al.*, 2002], interleaved slice timing correction, brain extraction, spatial smoothing (FWHM = 3.8 mm), high-pass

filtering (100 s cutoff), and MELODIC ICA data exploration [Beckmann *et al.*, 2005]. FLIRT was applied to the rs-fMRI scan for linear registration to the T1-weighted structural MRI and the Montreal Neurological Institute (MNI) 152 T1-weighted 2 mm brain MRI [Mazziotta *et al.*, 2001; Jenkinson & Smith, 2001; Jenkinson *et al.*, 2002]. Components of the MELODIC ICA determined to be structured noise (or unexpected activation) were filtered from the corrected data.

The left hippocampal-seeded resting-state time series was extracted and used to find functionally connected brain regions. Finally, regions in the left posterior parietal cortex (LPPC) with a high degree of functional connectivity to the left hippocampus were used for identifying a region-of-interest (ROI). The LPPC ROI was used to target the TMS.

Neuronavigation

For localizing the ROI, the visor2™ software (ANT Neuro$^{©}$ 2022) was used for MRI-guided neuronavigation targeting of the LPPC (**Figure 2.3**). The program enabled real-time navigation of the TMS coil guided by the participant's structural MRI and functional target.
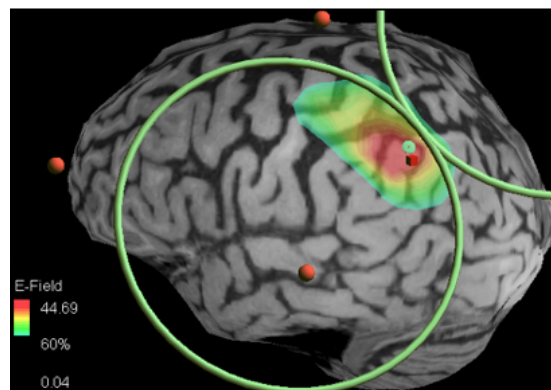
Figure 2.3 MRI-guided neuronavigation of hippocampal network targeting the LPPC.

Motor Threshold

To calibrate the TMS device (Magstim© 2021), the active motor threshold (aMT) was determined. The aMT is the minimum electrical energy required to elicit a motor movement. A board-certified Psychiatrist trained in the clinical use of TMS interrogated the left primary motor cortex (*i.e.*, a region generally referred to as the 'hand knob') with single-pulse TMS to generate a Motor Evoked Potential (MEP), representing a response in the first dorsal interosseous muscle of the right hand. The procedure involved light adduction of the index finger and thumb immediately preceding the TMS pulse. The clinical team gradually increased the intensity of the TMS coil until the characteristic features of the MEP were observed. Electrophysiologically, the MEP was recorded as an increase (≥ 50 μV) with a subsequent decrease in voltage [Bastani & Jaberzadeh, 2012] compared to the baseline muscle activity. Visually, the MEP response was observed as a muscle contraction, or finger twitch, in the participant's right hand.

Stimulation Procedure

Random assortment was used to assign one of two condition-blinded iTBS protocols. The active iTBS protocol (*i.e.*, the 'treatment' condition) was administered at 80% aMT, and the inactive-sham iTBS protocol (*i.e.*, the 'control' condition) was at 10% aMT. Half of the participants received the iTBS protocol for the treatment condition. Both the treatment and control conditions had iTBS delivered to the LPPC [Wang *et al.*, 2014].

In a single (10-minute) iTBS session, a total of 1800 pulses were delivered over 60 cycle repetitions (**Figure 2.4**). High-frequency bursts had 3 pulses delivered at 50 Hz frequency (*i.e.*, a

'triplet burst'), and triplet bursts were delivered at 5 Hz (theta) frequency. Each cycle lasted 10 s with 10 triplet bursts occurring in 2 s (*i.e.*, a total of 30 pulses/cycle) intermittently spaced by an 8 s wait time where no pulses were delivered. Each day participants received a single iTBS session for a total of five days.
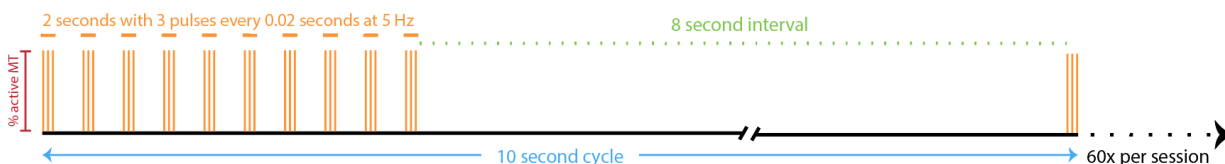
Figure 2.4 Diagram of the protocol for intermittent theta-burst stimulation (iTBS).

Object Recognition Task

For each iteration of the Object Recognition task, participants learned (encoding) and recalled (retrieval) images of everyday objects (**Figure 2.5**). The task consisted of three blocks (including a novel, previously unseen image in each block and session) alternating between encoding and retrieval sessions separated by a baseline distractor condition [Shane & Petersen *et al.*, 2004; Stark & Squire, 2001].

During encoding, a set of 40 images was presented (3 s each) and was proceeded by a fixation dot, which lasted for a jittered interval (at least 2 s, centered on 2.5 s). During the baseline distractor condition (30 s), a series of digits were presented quickly (*i.e.*, ~0.7 s each), prompting participants to identify the numbers as odd or even and press corresponding buttons. This control task promotes hippocampal-dependent memory of object stimuli, and baseline-given tasks performed at rest typically show elevated hippocampal activation [Suthana *et al.*, 2015].

During retrieval, old previously viewed target images were presented in addition to lure images (*i.e.*, similar but not identical images), testing the specificity of memory encoding. The lure and target images were randomly interleaved, during which participants were asked to respond to whether an image was OLD or NEW and assess how confident they were (*i.e.*, 1-Definitely new, 2-Likely new, 3-Maybe new, 4-Maybe old, 5-Likely old, 6-Definitely old). Different images were used in each block and session. Similar versions of this task have separated familiar-based recognition memory from recollection-dependent hippocampal memory and found novel object discrimination impairments in typically aging older adults [Yassa *et al.*, 2011a; Yassa *et al.*, 2011b].
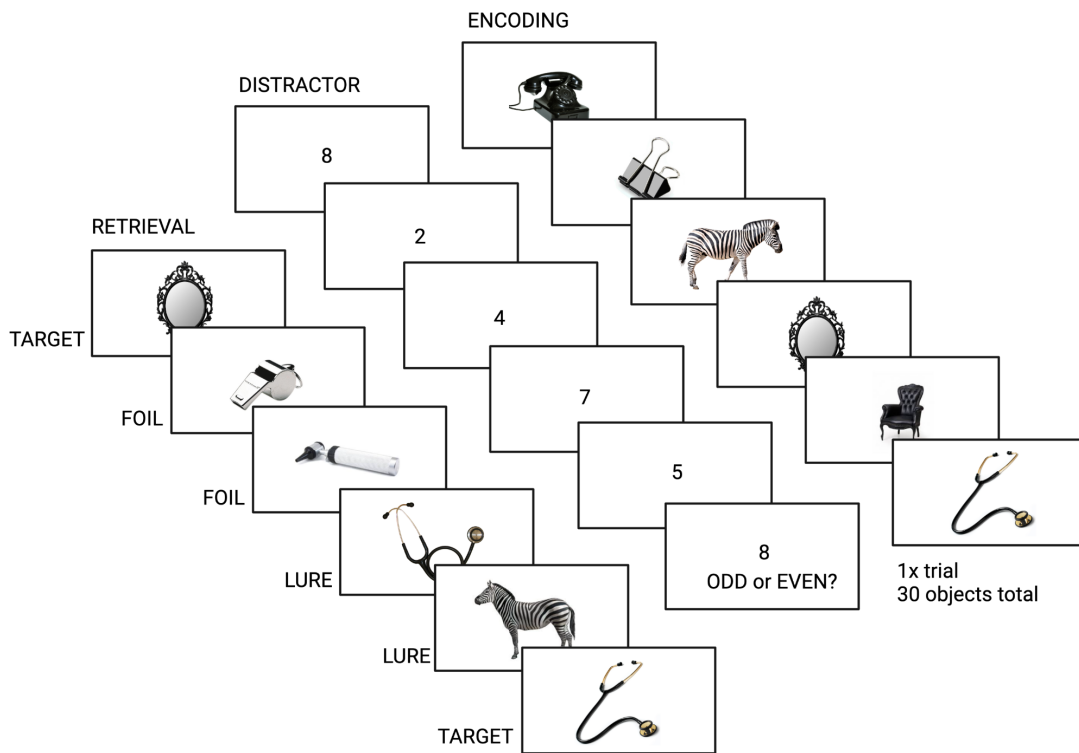
Figure 2.5 Task design for the Object Recognition associative memory assessment.

Behavioral Analysis

Performance ratios on the Object Recognition task were calculated using the percentage (%) of correctly/incorrectly identified stimuli ("New" vs. "Old") over the total number presented. These include six measures of Target, Lure, Foil, Recollected, Familiar, and Missed items. In addition, a discrimination ratio (DR) was determined using the equation [p("New"|Lure) – p("New"|Target)]. Following each of the five iTBS sessions, two assessments of the Object Recognition task were completed (with 40 items per assessment), and an average composite assessment ratio was determined for each iTBS session. The performance ratio is a value between "0" and "1," where a value of "1" on the DR, Target, Lure, Foil, and Recollected measures indicate the maximum performance. Conversely, a value of "0" on the Missed and Familiar measures indicates the optimal performance. We used a linear estimate coefficient (slope) across the five days of consecutive iTBS sessions to assess behavioral performance change and account for individual differences in baseline performance.

Statistical Analysis

A one-way ANOVA was computed using R Studio to determine the effect of behavioral response type ("Old" vs. "New"), iTBS protocol condition (Treatment vs. Control), and outcome (change scores) with the post-hoc Kruskal-Wallis rank sum test (α level < 0.05), where the outcome was performance change (slope), and the predictor was iTBS group condition. Two-way ANOVAs were used to compare continuous variables (neuropsychological scores and age) and chi-square tests for categorical variables (biological sex) between groups.

2.3 Results

A total of twenty-two participants ($n_{control}$ = 11, $n_{treatment}$ = 11) completed the iTBS study protocol (mean age ± S.D. = 68 ± 5.3 years; Female n = 13). Baseline memory assessments confirmed typical neuropsychological and memory-related cognitive function (**Table 2.1**).

Assessment Measure (Test)	Raw score	± S.E.M.	Z score	± S.E.M.
General Cognitive Function (MMSE)	29.45	0.16	–	–
Depression Scale (Ham–D)	1.81	0.43	–	–
Vocabulary (TOPF)	59.00	1.69	1.13	0.12
Psychomotor Processing (Trail A)	39.15	5.06	−0.48	0.26
Executive Functioning (Trail B)	80.43	8.13	−0.13	0.19
Word Retrieval (BNT form 4)	14.59	0.18	0.61	0.15

Table 2.1 Neuropsychological assessments scores.

Associative memory performance

Across five iTBS sessions, stimulation-mediated changes in behavior were monitored using the Object Recognition task performance ratios. In our analyses, we investigated seven metrics, including (1) the specificity of recognition memory (Discrimination Ratio, DR), (2) the proportion of objects correctly identified as "Old" (Target Objects), (3) the proportion of objects correctly identified as "New" (Lure Objects). A higher value indicates better task performance.

The effect of iTBS on memory

First, we examined differences between iTBS condition groups (treatment vs. control) in the DR performance across iTBS sessions. We found that the treatment group receiving active iTBS had a mean slope of 0.4 compared to the control group, which had a mean slope of 0.2

and received an inactive sham iTBS (**Figure 2.6**; Kruskal-Wallis chi-squared = 2.28, df = 1, p-value = 0.13). The mean and standard error (S.E.M.) of group performance across sessions and behavioral change score (slope) are provided (**Table 2.2**).
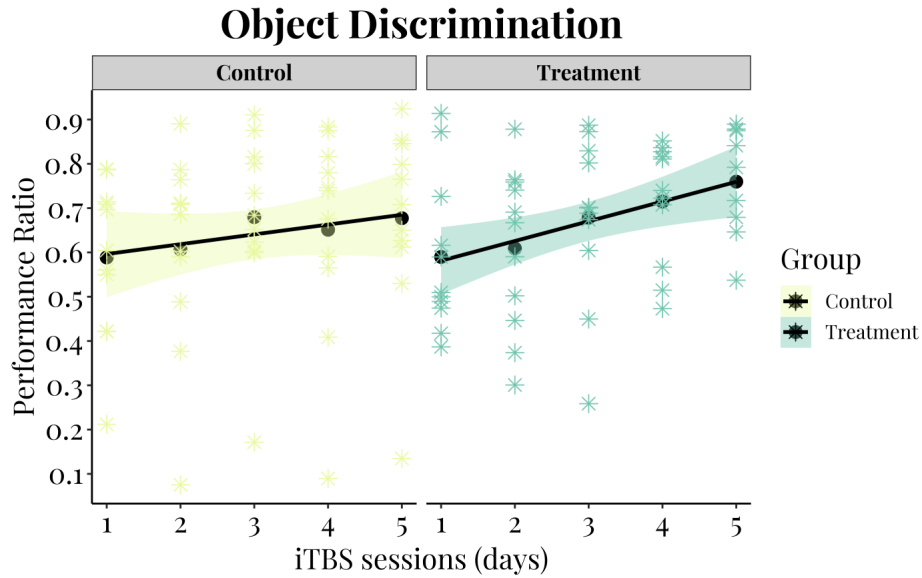
Figure 2.6 Object Recognition discrimination performance ratio across iTBS sessions (days). The plot illustrates the mean performance ratio per session (●) and the linear model across sessions with standard error of the mean (± S.E.M.) as shaded boundaries. Individual participants' performance ratios are also shown (✳).

	Control Condition		Treatment Condition	
	Mean DR	**± S.E.M.**	**Mean DR**	**± S.E.M.**
iTBS day 1	0.59	0.05	0.59	0.05
iTBS day 2	0.61	0.07	0.61	0.05
iTBS day 3	0.68	0.06	0.68	0.06
iTBS day 4	0.65	0.07	0.71	0.04
iTBS day 5	0.68	0.07	0.76	0.04
Slope	0.02	0.00	0.04	0.01

Table 2.2 Group averages across iTBS sessions and slope across days.

In addition, we assessed behavioral change in performance scores using two approaches (**Figure 2.7**). First, we measured change as the difference in DR from baseline (day 1) across sessions (days 2-5). We found no significant between-group change (p = 0.18). Second, we quantified change as the percent increase in DR from baseline and found no significant interaction between iTBS conditions across sessions (p = 0.075).
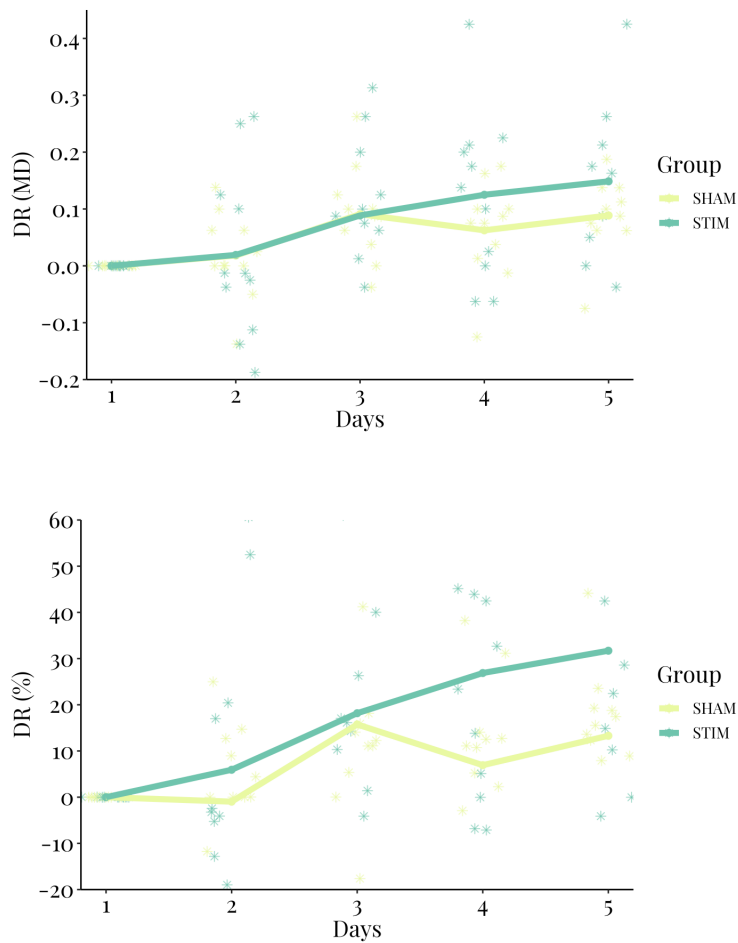
Figure 2.7 Behavioral change in DR performance from baseline. Participant scores for mean difference (MD—top panel) and percent change (%—bottom panel) are shown (✳). The legend identifies marker and group labels.

Then, we performed post-hoc assessments examining combined difference measures from the first approach showing a significant difference in DR for the treatment ($p < 0.05$) and control ($p < 0.05$) groups. However, post-hoc assessments of combined performance from the second approach revealed a significant difference in the treatment group ($p < 0.05$) that was not observed in the control group ($p = 0.25$).

We also investigated whether performance differed for pairwise comparisons of iTBS session and condition. The first method showed the treatment group on the last iTBS session was significantly different compared to the baseline of either group ($p < 0.05$). Although, the second method did not reveal any pairwise differences.

Next, we examined performance as the proportion of objects correctly identified as "Old" or "New" during retrieval, indicating items presented during encoding (*i.e.*, Target) or novel items not shown during encoding (*i.e.*, Lure and Foil), respectively. By analyzing the change (slope) across sessions we found that the results of the Kruskal–Wallis test were significant for target objects, but not for the other measures (**Figure 2.8**; Target: $H = 5.45$, 1 d.f., $p < 0.05$; Lure: $H = 0.18$, 1 d.f., $p = 0.67$; Foil: $H = 0.16$, 1 d.f., $p = 0.69$). On average, the number of correct responses for target objects increased in the treatment condition compared to the control, suggesting that active iTBS improved memory encoding.

In addition, we explore participants' performance ratios for Recollected, Familiar, and Missed items. The results were significant for missed objects, but not for the other two measures (**Figure 2.8**; Recollected: $H = 1.81$, 1 d.f., $p = 0.18$; Familiar: $H = 0.04$, 1 d.f., $p = 0.84$; Missed: $H = 5.15$, 1 d.f., $p < 0.05$).
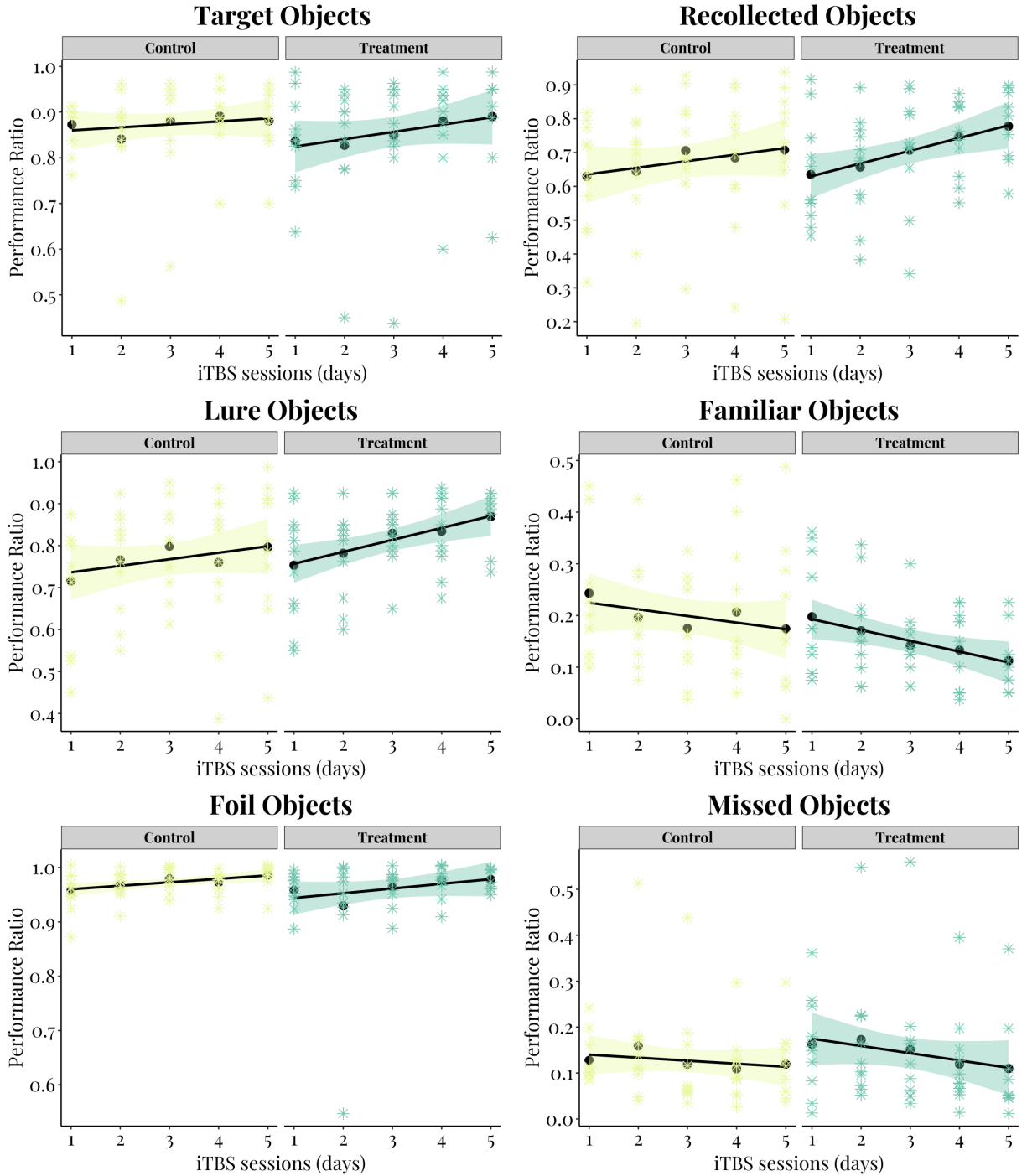
Figure 2.8 Performance ratios for Target, Lure, Foil, Recollected, Familiar, and Missed objects. The plots illustrate the mean performance ratio per session (●) and a linear model with standard error of the mean (± S.E.M.) shaded boundaries across sessions. The individual participant ratios are also shown (✳).

The effect of age & MTL regional volume on memory

Previous studies have shown that an individual's age and MTL regional brain volume are associated with memory capabilities. Therefore, we investigated if these factors were related to the differences in behavioral change between iTBS conditions. We found an age-dependent relationship where older participants had smaller regional volumes in the bilateral CA1, right CA2 subfields, left parahippocampal cortex, dentate gyri, and hippocampal fissures. Furthermore, we did not find evidence to support the assumption that differences in MTL volume were related to better or worse performance on the Object Recognition task.
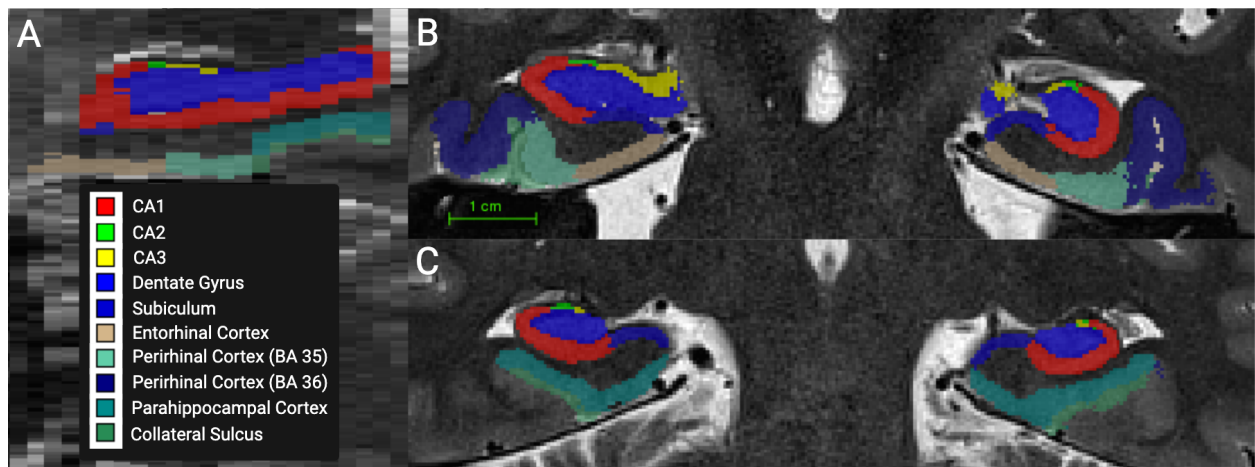
Figure 2.9 Segmentation of hippocampal subfields using the ASHS pipeline [Xie *et al.*, 2017; Yushkevich *et al.*, 2015; Adler *et al.*, 2014]. (**A**) sagittal, (**B**) anterior coronal, and (**C**) posterior coronal view of a high-resolution hippocampal image. The legend designates subfield labels and parcellation color palette—scale bar (1 cm).

2.4 Conclusions

Overall, these results show that iTBS, a short (~10 min.) non-invasive TMS treatment delivered over five days, is safe and feasible in older adults. While our data suggest an improvement in memory-related function for the treatment condition compared to the control condition, at present certain analyses may be statistically underpowered to detect a difference between conditions. Several suggestions that could improve these results include the collection of more data from additional participants, oversampling (*i.e.*, collecting more data from the same participants), denoising methods to remove distant-dependent motion artifacts [Fair *et al.*, 2012], or implementing real-time MRI monitoring software to improve data quality and reduce study costs [Dosenbach *et al.*, 2017]. Moreover, variability in response to the iTBS treatment may be due to differences in the distance from the target location to the TMS coil, where an additional 3% of TMS output is necessary for every millimeter from the stimulating coil to produce an equivalent level of brain activation as the motor threshold (MT) response [Stokes *et al.*, 2005]. Thus, the cortical depth of the LPPC target should be considered in choosing the optimal stimulation parameters. Also, skull thickness, which varies 2.4 ± 0.8 mm depending on skull bone location (*e.g.*, parietal vs. occipital), age, and sex-based differentiation [Lillie *et al.*, 2015], is critical for maximizing the therapeutic effects of TMS. Accordingly, the treating psychiatrist should scale MT by these measures, improving stimulation quality and ensuring equitable treatment delivery in the clinic. These measures can be determined by MRI/CT or demographically-adjusted norms for the specific skull region and target depth [Peterson & Dechow *et al.*, 2002].

Furthermore, there may be ways to improve the efficacy of this intervention in future studies. Specifically, in clinical trials where TMS is FDA-approved for treating Major Depressive Disorder, Obsessive-Compulsive Disorder, and smoking cessation, the treatment duration occurs over six weeks, with multiple days of stimulation sessions each week. Therefore, longer interventions (> 1-week protocols) may yield more potent memory effects. The participants recruited for this study included adults (ages 55+) without clinically apparent memory deficits and who received iTBS treatment over five consecutive days, so it is also plausible that individuals with impairment (*e.g.*, MCI) might be more resistant/sensitive to the intervention [Sundman *et al.*, 2020]. Future research studies are needed to shed light on the treatment duration, the longevity of improvement, the specific target population, and the optimal treatment window for promoting memory. These four components will be essential for the effective clinical implementation of TMS for memory loss.

In this study, we utilized an MRI-guided approach for targeting the iTBS treatment, which capitalized on the functional architecture of cortical areas in the posterior parietal lobe that lay on the surface of the brain and were highly connected to the hippocampus. These deeper and medial regions of the brain are impractical for direct targeting with TMS. Therefore, our approach was designed to maximize hippocampal-cortical connectivity using resting-state brain activity as a marker of the optimal location for treatment delivery. However, various other MRI modalities can be used to investigate hippocampal network connectivity (*e.g.*, arterial spin labeling and diffusion-weighted MRI) and guide the stimulation targeting functionally or structurally connected brain regions.

Arterial spin labeling (ASL) measures tissue perfusion using magnetically tagged blood flow and is more routinely used in clinical practice than resting-state functional MRI. Also, the measurement of cerebral blood flow derived from ASL perfusion MRI protocols is a reliable biomarker for predicting cognitive function in older adults [De Vis *et al.*, 2018]. Therefore, detecting brain regions with perfusion ASL can reveal which brain regions within the hippocampal memory network have sufficient or deficient blood flow. These measures can inform the cortical topography for target selection in combination with TMS. The MRI-guided approach allows targeting of physiologically intact regions considered suitable for modulation. In addition, brain regions identified with insufficient perfusion may indicate dysfunctional brain areas or damaged cortical tissue that ought to be circumvented during target selection. Indeed, this technique has been combined with transcranial electrical stimulation to the prefrontal cortex showing perfusion changes originating in the locus coeruleus and broadly distributed throughout the cortex [Sherwood *et al.*, 2018].

Both the resting-state fMRI and ASL perfusion MRI approaches use blood-based indicators of brain connectivity. An alternative approach for future studies modulating hippocampal network activity would be to use diffusion MRI (dMRI) to estimate the location and structure of axon fiber bundles that form short and long-range connections between cortical and hippocampal brain regions. Arguably, the cell body is the computational center of the neuron that integrates neural signals and determines subsequent activity dependent on the fidelity of its inputs. Yet another neuronal structure, the axon, facilitates the propagation of these signals throughout the brain. Groups of individual axons form fasciculated bundles that relay activity in a particular brain region with proximally and distally connected regions.

Recently, a study investigating TMS to improve memory in older adults with MCI used a dMRI-guided approach for targeting stimulation to specific brain regions [Chen *et al.*, 2022]. The investigators demonstrate how theta-burst stimulation of superficial cortical regions in the parietal lobe is distributed to the hippocampus via the inferior longitudinal fasciculus and produces hippocampal network changes in resting-state functional connectivity related to associative memory improvement previously reported [Hermiller *et al.*, 2020]. Since dMRI measures constitute a statistical approach to understanding brain connectomics, careful attention should be used when interpreting these results; however, these findings may be methodologically improved when well-validated priors are used to constrain analyses to estimate connections that are supported by neuroanatomical ground truth ascertained through direct observation [Jenkinson & Chappell, 2018].

Together our results show that neuroimaging-guided iTBS holds promise for modulating memory in older adults. Future studies should characterize the magnitude of iTBS effects in larger sample sizes, patients with memory impairment (*e.g.*, MCI, AD), on different types of memory changes (*e.g.*, explicit verbal/visuospatial associative functions) and elucidate systems-level (*e.g.*, brain structural) mediators which will reliably predict memory performance changes in response to treatment.

III

MEMORY ENHANCEMENT WITH ENTORHINAL–HIPPOCAMPAL

MICROSTRUCTURAL INTEGRITY & PROXIMITY OF DEEP BRAIN STIMULATION.

3.1 Introduction

Decades of research and clinical observations have established that episodic memory, the ability to remember event-related experiences, is a critical higher-level cognitive function dependent on the hippocampus and the adjacent cortical regions, including the entorhinal cortex and its afferent white matter projections to the hippocampus—the perforant pathway [Squire *et al.*, 2004; Eichenbaum, 2000; Ramón y Cajal, 1904; Ramón y Cajal, 1894].

In animal studies (**Figure 3.1**), electrical stimulation of the entorhinal-hippocampal perforant path can produce long-term potentiation (LTP) [Fain & O'Dell, 2014; Bliss & Cooke, 2011; Vertes, 2005; Williams & Givens *et al.*, 2003; Bliss & Lomo, 1973], and cholinergic input onto the parahippocampal gyrus modulates these connections [Lin *et al.*, 2022; Haam & Yakel, 2017]. Both outcomes are associated with memory improvement [Pastalkova *et al.*, 2006; Ehret *et al.*, 2001; Feuerstein *et al.*, 1997].
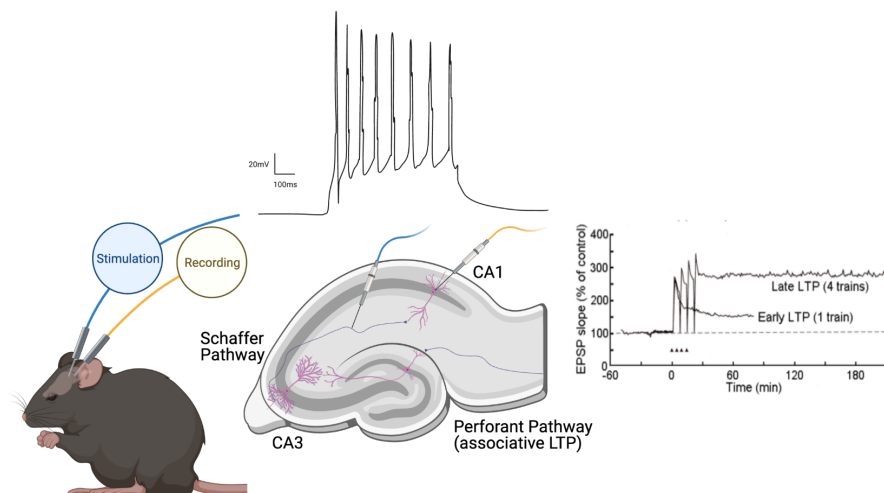
Figure 3.1 Theta-burst stimulation to the hippocampal circuit (*e.g.*, the Schaffer collateral or perforant pathway) elicits LTP in rodent model organisms.
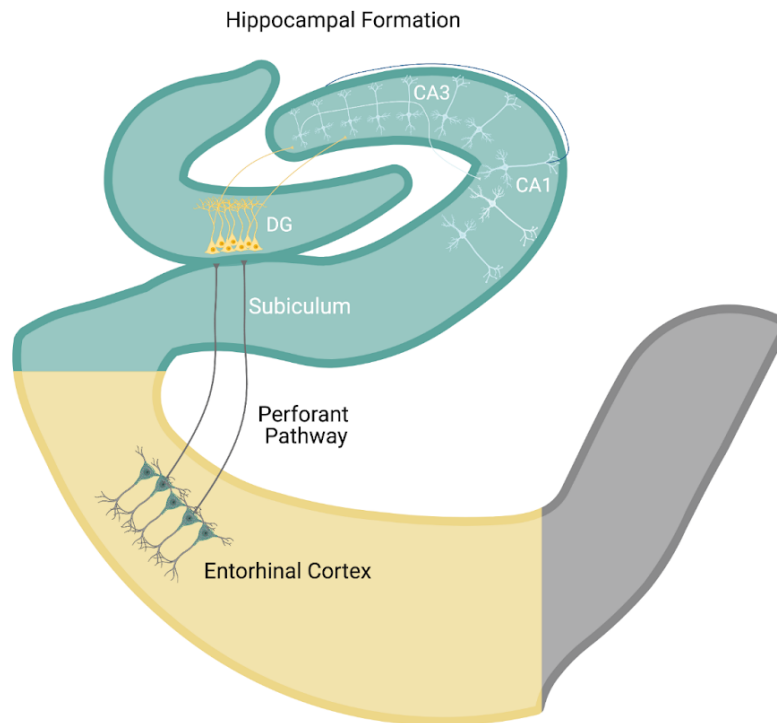
Figure 3.2 The entorhinal–hippocampal memory circuit in humans.

In human participants (**Figure 3.2**), a few studies on the effect of electrical stimulation of the entorhinal white matter region, specifically within the angular bundle, have arrived at contrary findings, with some reporting memory enhancement [Mankin *et al.*, 2021; Titiz *et al.*, 2017; Suthana *et al.*, 2012] and others reporting impairment [Halgren *et al.*, 1985; Jacobs *et al.*, 2016]. The angular bundle consists of several myelinated fiber pathways, and it is unknown which specific tract electrical stimulation worked to facilitate memory [Mankin *et al.*, 2020].

The perforant pathway is one potential candidate tract within the angular bundle and is highly conserved across rodents and primates [Zeineh *et al.*, 2017; Witter *et al.*, 2007]. Within the angular bundle, myelin-stained sections of brains from patients with Alzheimer's disease showed a reduced intensity of staining in the perforant path compared to controls [Hyman *et*

al., 1986], reporting a congruence between the presence of Aβ plaques in the molecular layer of the dentate gyrus at the site of projection fiber termination. This suggests that accumulation of neuropathology in the entorhinal-hippocampal circuit influences the severity of memory impairments in AD. However, postmortem tissue analysis can only reveal certain aspects of the structure-function relationship between perforant pathway fibers and memory. To understand the causality of these associations, the pathway needs to be studied *in vivo* and directly modulated to elicit performance changes in memory.

For instance, diffusion-weighted MRI (dMRI) is used to investigate the microstructural properties of brain tissue [Soares *et al.*, 2013]. By fitting tensors to the dMRI signal, researchers can estimate fiber bundles derived from measurements of the restricted diffusion of water as a molecular probe of brain tissue microstructure. In unrestricted compartments of the brain, such as ventricles filled with CSF, water molecules diffuse freely via a property called Brownian motion. This characteristic reflects the isotropic displacement of water such that any molecule has an equal probability of moving in any direction from its initial position.

Conversely, in restricted compartments, such as white matter with densely packed axon fiber bundles, diffusion of water is constrained perpendicular to the cell membrane and myelin sheath but relatively unconstrained parallel to the axonal process. This quality of unequal diffusion along neuronal axes is called anisotropy. By measuring the direction and magnitude of molecular displacement in three dimensions, a diffusion tensor is determined for every voxel, a unit of brain space (mm^3), in the dMRI. From these measurements, estimates of the microstructural organization of the brain, in particular for regions with a high prevalence and density of axon fiber bundles, are determined [Hua *et al.*, 2008].
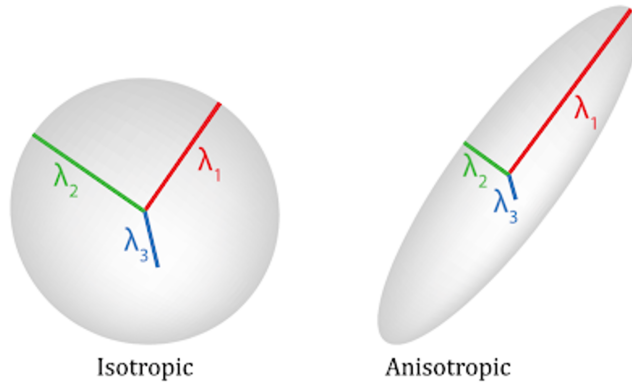
Figure 3.3 Fundamentals of modeling diffusion characteristics for evaluating the microstructure of brain tissue.

Thus, using a tensor, which describes a multilinear relationship, is a concise way of representing molecular displacement in three dimensions. Within each voxel, the diffusion of water molecules is summarized as an eigenvector, the direction molecules move in a given time across three principal directions, illustrated by the red, green, and blue axes (**Figure 3.3**). The distance traveled, or the total molecular displacement along a particular direction, is an eigenvalue, indicated by λ_1, λ_2, and λ_3 terms, ordered by magnitude. In estimating whether the displacement is equal (isotropic) or unequal (anisotropic), fractional anisotropy (FA) is used to relate the proportion of diffusion on the primary axis to the secondary and tertiary axes.

The following equation determines the value of FA:

$$
\textbf{FA} = \sqrt{\frac{1}{2}} \frac{\sqrt{(\lambda_1 - \lambda_2)^2 + (\lambda_1 - \lambda_3)^2 + (\lambda_2 - \lambda_3)^2}}{\sqrt{(\lambda_1^2 + \lambda_2^2 + \lambda_3^2)}}
$$

The value of FA is essentially a ratio describing the degree of anisotropic diffusion (*i.e.*, movement favored along the primary axis) determined for every voxel of the brain. Moreover, in axons, diffusion across the neuronal membrane is restricted but less so along the length of the process, meaning there is less movement along the two radial axes, λ_2 and λ_3, compared to the longitudinal axis, λ_1. A large FA is given by a value of one.

Conversely, a low FA, value of zero, represents diffusion equally distributed across the three directions. It is important to note, however, that similar FA values can result from differences in any of the three eigenvalues. For example, radial diffusion lengths of 0.45 in λ_2 and λ_3 and a longitudinal diffusion length of 0.96 in λ_1 produce an FA of 0.44 (where the diffusion length constant (λ) is in units of 10^{-3} mm^2/s). But a longitudinal diffusion of 1.2 and radial diffusions of 0.57 would give the same value of FA [Johansen-Berg & Behrens *et al.*, 2014]. Therefore, specific microstructural changes in the axon or myelin can be attributed to differences in radial and longitudinal diffusion, respectively.

These interpretations have been experimentally confirmed using a mouse model of retinal ischemia to investigate the biological foundations of diffusion properties, showing that optic nerve degeneration resulted in different longitudinal and radial diffusion changes over time [Song *et al.*, 2002; Song *et al.*, 2003]. Acute changes reduced longitudinal diffusion with radial diffusion unchanged and resulted from axonal degradation with intact myelin sheaths. Whereas chronic changes increased radial diffusion that resulted from myelin degeneration validated with immunohistochemistry. Although myelination contributes to FA, other sources, including the axon structure itself, contribute the greatest difference to FA.

Studies in typically aging adults relating microstructural changes with differences in memory performance have utilized high-resolution dMRI sequences to resolve fiber bundles on the submillimeter scale and found age-dependent decreases in connectivity for older adults compared to young adults [Yassa *et al.*, 2010]. Studies in diseases affecting memory have used a variety of dMRI analytic approaches to discern microstructural and hippocampal degeneration in the prodromal stages of AD [Zhang *et al.*, 2014].

For example, probabilistic tractography using *ex vivo* dMRI has been used to investigate entorhinal-hippocampal connectivity with a dual-step approach (*i.e.*, by assessing these connections in segments from the entorhinal cortex to the subiculum and the subiculum to the dentate gyrus). This approach revealed robust connectivity maps between the subiculum and the anterior hippocampus compared to the posterior hippocampus [Augustinack *et al.*, 2010]. Connectivity maps between the entorhinal cortex and subiculum were feasible; however, restricting the analysis to layer II of the entorhinal cortex, where perforant pathway fibers emanate, was too constrained for proper estimation. In addition, deterministic tractography resolved the perforant pathway and alvear pathway fibers, and has been corroborated by histological studies in animals [Bell *et al.*, 2021; Shukla & Bridges, 2001; Deller *et al.*, 1996]. Pertinently, dMRI tractography methods enable non-invasive assessment of tissue microstructure that can be used to explain differences in clinical populations or applied in combination with neurotechnologies for directly targeting specific brain circuits.

Part III – Study Aims & Objectives

In this study, we investigate connectivity between the entorhinal cortex and hippocampal formation using probabilistic tractography to optimize direct electrical stimulation for memory performance improvement. By examining the location of intracranial electrodes in relation to the perforant pathway, we associate the proximity of stimulation and performance enhancement across four hippocampal-dependent episodic memory tasks. Our findings suggest that the effects of stimulation on behavior are dependent on electrode placement within the entorhinal white matter area, which is consistent with decades of findings that high-frequency theta-burst stimulation applied to the perforant pathway supports LTP of the hippocampal circuit and positively influences episodic memory. Additionally, we suggest that connectomic measures, the integrity of fibers, density, and location, can inform MTL targeting for next-generation personalized neuromodulation of cognitive function.

To date, dMRI is the only available tool for *in vivo* study of neuroanatomical white matter pathways, which we coupled with the direct evaluation of MTL circuit modulation for influencing memory capacity. In sum, we present the role of entorhinal-hippocampal microstructure and electrode proximity in enhancing episodic memory in humans.

3.2 Methods

<u>Participants</u>

The study included nineteen adults (mean age ± S.D. = 34 ± 12.59 years; Range 20-63 years; Female n = 10; right-handed n = 14) with pharmacoresistant epilepsy implanted with intracranial depth electrodes for 7-14 days for clinical evaluation. A total of 33 electrode sites were used to deliver direct current stimulation within the MTL. The locations of fifteen electrodes were in white matter (left n = 4) between the entorhinal cortex and hippocampus, and eight were in MTL gray matter (left n = 10) regions.

Participants volunteered for the study and were informed of the risks and benefits of the study protocols, approved by the University of California Los Angeles Institutional Review Board (IRB) for human biomedical research [IRB#10-000973 & 15-000548].

<u>Neuroimage Acquisition</u>

Magnetic Resonance Images (MRIs) were acquired on a 3-Tesla Siemens PRISMA scanner, including (1) a T2-weighted hippocampal high-resolution MRI (spin echo, TR = 5200 ms, TE = 105 ms, 24 slices, contiguous, matrix size = 512 x 512, voxel size = 0.391 x 0.391 x 3 mm), (2) a T1-weighted whole-brain MPRAGE (TR = 1800 ms, TE = 2.93 s, voxel size = 0.9 x 0.9 x 0.8 mm), and (3) a diffusion-weighted MRI (dMRI; TR = 9900 ms, TE = 81 ms, flip angle = 90, FOV = 256 mm × 256 mm, matrix size = 128 × 128, voxel size = 2.0 × 2.0 × 2.0 mm) with 64 acquisition directions (b = 1000 s/mm^2) and a single b_0 image (b_0 = 0 s/mm^2). The images were acquired preoperatively 1-2 weeks before implantation of the intracranial depth electrodes.

Hippocampal Segmentation

Automatic Segmentation of Hippocampal Subfields (ASHS; version 2.0) software package was used to identify MTL brain regions and obtain volume measures. For tractography, three regions, including the hippocampus, subiculum, and entorhinal cortex, were used.

Electrode Localization

The depth electrodes implanted for clinical epilepsy monitoring [Fried *et al.*, 1999] were localized following implantation with high-quality Spiral Computed Tomography (CT) scans (acquired with 1 s rotation, 1.5 helical pitch, 1 mm slice collimation, and 0.5 mm reconstruction interval). Using a 3-way registration protocol in BrainLab, CTs were registered to T2-weighted hippocampal high-resolution and T1-weighted whole-brain MPRAGE MRIs.

MTL subregions were determined from neuroanatomical boundaries that demarcated regions from atlases correlating MRI visible landmarks with underlying histological features [Duvernoy *et al.*, 2013; Insausti & Amaral, 2003]. These methods have been used to localize microelectrodes in MTL [Suthana *et al.*, 2009; Ekstrom *et al.*, 2008; Zeineh *et al.*, 2003].

Diffusion MRI Processing

The dMRI scans were processed using the FMRIB Software Library (FSL) package [Smith *et al.*, 2004; Jenkinson & Smith, 2001], including eddy current correction [Smith *et al.*, 2002a], brain extraction [Smith *et al.*, 2002b], and fitting of diffusion tensors to the data [Basser *et al.*, 1994; Pierpaoli *et al.*, 1996]. The output of tensor fitting yields voxel-wise maps.

Tract–Based Spatial Statistics

Using Tract–Based Spatial Statistics, a skeleton-wise analysis was performed on the FA image to generate a white matter spleen that identifies the center of tracts [Smith *et al.*, 2006]. The FA skeleton threshold will be set at 2000 (corresponding to FA > 0.2) to remove voxels containing gray matter or cerebrospinal fluid.

To assess crossing fibers, cleaned and corrected dMRI scans were processed using BEDPOSTX (Bayesian Estimation of Diffusion Parameters Obtained using Sampling Techniques for Modeling Crossing Fibers) [Behrens *et al.*, 2007]. The approach provides estimates of the probability density functions across three principal directions using Markov Chain Monte Carlo sampling to determine the number of crossing fibers voxel-wise throughout the brain.

Probabilistic Tractography

The corrected, tensor fit, and diffusion estimated dMRI scans were analyzed using FSL's Diffusion Toolbox (FDT) to obtain probabilistic tractography estimates of global brain connectivity between any two region-of-interests (ROIs) given the likelihood of a connection existing based on the diffusion characteristics and fiber modeling [Behrens *et al.*, 2003]. FSL's FDT repetitively samples the distributions on voxel-wise principal diffusion directions.

To generate a probabilistic connectivity distribution, three (ROIs) identifying the entorhinal cortex (ERC), the hippocampal formation, including the *Cornu Ammonis* (CA) fields 1-3, and *Fascia dentata* (dentate gyrus), together referred to as the hippocampus, and the subiculum, were used to sample the diffusion distributions. The probabilistic tractography analyses were run in Seed Mask Mode, and the parameters are provided (**Table 3.1**).

FDT Probabilistic Tractography	ProbtractX Options
Sample Number	5000
Curvature Threshold	$0.05 (= 89.7^{\circ})$
Max. Step Number	5000
Step Length	0.5 mm
Fiber Volume Fraction	0.01
Loopcheck	✓
Euler Streamlining	✓
Constrained Tracking	✓
Distance Correction	✓
	Waypoint Options
Bidirectional Independence	✓
Ordered Crossing	✓
Condition	and
	Matrix Option
Matrix	Seed x Seed

Table 3.1 FMRIB's Diffusion Toolbox (FDT) version 5.0 probabilistic tractography parameters. The seed space was set to a single mask of the Entorhinal cortex. The targets included waypoint masks of the Subiculum and Hippocampus (crossing in listed order) with termination in the Hippocampus. These masks were registered to native diffusion space for tractography.

In order to accurately measure the perforant pathway fibers and obtain diffusion metrics about their microstructure features, the regions listed above were used as anatomical priors for the analysis. The tracks began from the entorhinal cortex (seed ROI) to generate a local connectivity map ending in the hippocampus. Tracks were confined by a waypoint ROI (subiculum) such that viable tracks must pass through the subicular region as perforant path fibers traverse (or perforate) this brain region. The following track parameters were used: step length = 0.5 mm, total number of steps = 5000, and curvature threshold = 0.05 (~89.7°) [Augustinack *et al.*, 2010]. The connection probability from the seed region was calculated as

the proportion of the total number of samples reaching the target that also passed through the waypoint region. The connectivity maps were used to extract diffusion tensor metrics about the angular bundle tissue microstructure, including the dMRI measures (FA, MD, AD, and RD) previously described.

Electrode Distance Analysis

To estimate the contribution of electrode position in DBS-related memory enhancement, custom scripts in python were used to analyze the distance of the stimulating electrode to the perforant pathway (*i.e.*, the probabilistic connectivity distribution map). Distance (mm) was calculated in two ways from the center of each stimulating electrode to either (1) the center of mass (the average location of the perforant pathway weighted by the density of the crossing fibers), or (2) the location of the highest density of pathway fibers.

Behavioral Tasks

Participants completed at least one of four behavioral tasks, designed to probe hippocampal-dependent episodic memory, with a cognitively engaging distractor task between encoding and retrieval phases, including (1) Person Recognition, (2) Object Recognition, (3) Verbal Free-Recall, and (4) Face-Name Association. Full descriptions of these tasks are published (**Figure 3.4**) [Mankin *et al.*, 2021; Titiz *et al.*, 2017].

The tasks included three parts: (1) a learning (encoding) period, (2) a distraction period (30 s) with an odd/even number task, and (3) a recall (retrieval) period. Participants completed the tasks on a laptop using Mathworks' Matlab with Psychtoolbox extensions [Brainard, 1997].

Using a within-subject design, a randomly selected half of the stimuli presented had electrical stimulation delivered before stimulus presentation. Composite scores were assessed across tasks for performance on stimulated vs. non-stimulated trials.
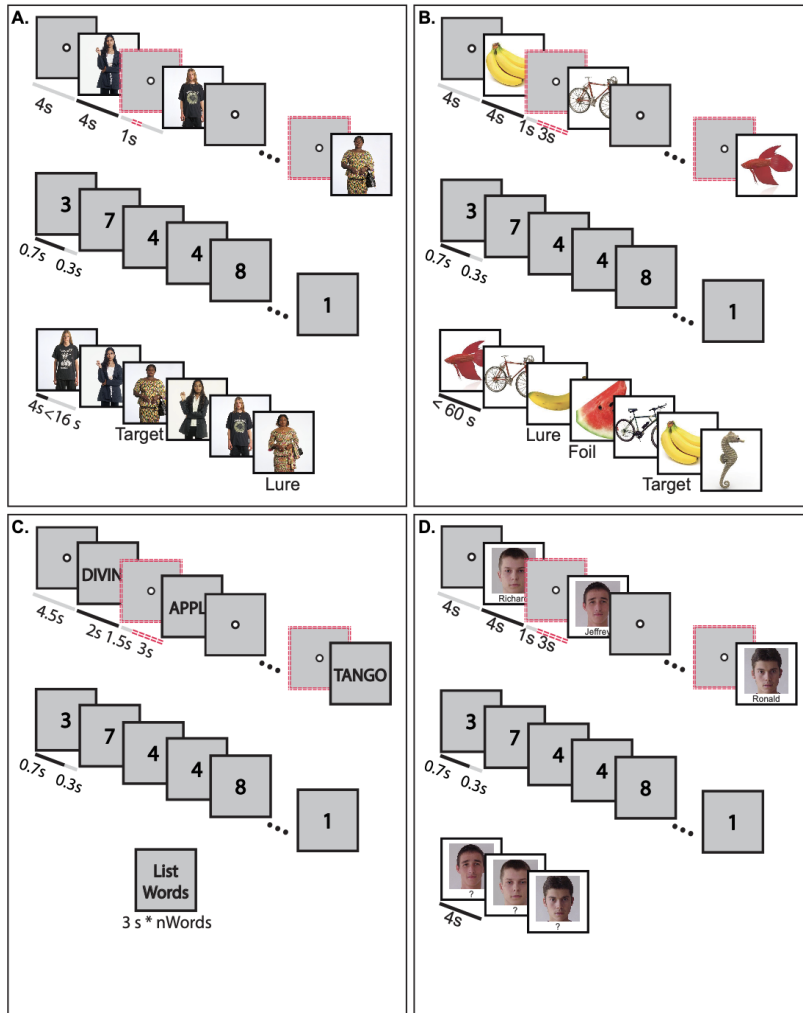
Figure 3.4 Schematized illustration of four hippocampal-dependent episodic memory tasks [Mankin *et al.*, 2021; Titiz *et al.*, 2017] (**A**) Person Recognition. (**B**) Object Recognition. (**C**) Verbal Free-Recall. (**D**) Face-Name Association. The stimulation trials are shown in dotted red, and the trials without stimulation are shown in black. The stimulus delay is shown in gray.

Behavioral Analysis

The 'simulation performance index' was calculated, per electrode, by taking the percentage difference of performance scores across trials grouped by stimulation condition and averaged across behavioral tasks.

Statistical Analysis

The relationships between simulation performance index, electrode proximity, and tissue microstructure were determined using a Generalized Linear Model (GLM) in SPSS (IBM Corporation, Armonk, NY). The GLM approach provides a more flexible form of regression capable of handling non–Gaussian distributions.

3.3 Results

Entorhinal white matter stimulation enhances memory

We used a meta-analytic approach to ascertain the key variables predicting stimulation-related memory improvement (**Figure 3.5**). We found significant differences in stimulation performance index for stimulated trials compared to non-stimulated trials, meaning that participants accurately recalled more task stimuli on trials that received stimulation, demonstrating a positive or enhancing effect on episodic memory encoding.

Visualization of entorhinal-hippocampal perforant pathway

Connectivity distributions (**Figure 3.6**), generated by probabilistic tractography, were used to visualize entorhinal-hippocampal perforant path inputs onto the hippocampus originating from the entorhinal cortex and traversing through the subicular region of the hippocampal formation. The tractography analyses were informed by neuroanatomical priors supported by findings from cytohistological and lipid staining techniques of perforant path connectivity. Path accuracy was improved by requiring tracts to cross through both the subiculum and hippocampus constrained by crossing order such that a path from the entorhinal cortex was viable if it first passed through the subiculum and then the hippocampus.

Tensor maps were skeletonized to extract microstructural estimates, and an FA threshold greater than 0.2 was applied, ensuring estimates were within a range typically observed for white matter regions.

Using a Generalized Linear Model in SPSS, we evaluated Fractional Anisotropy (FA), a probabilistic tractography measure of structural organization, in the perforant pathway and the contribution of electrode proximity to the perforant path for DBS–related behavioral improvement ($n_{electrodes}$ = 9).
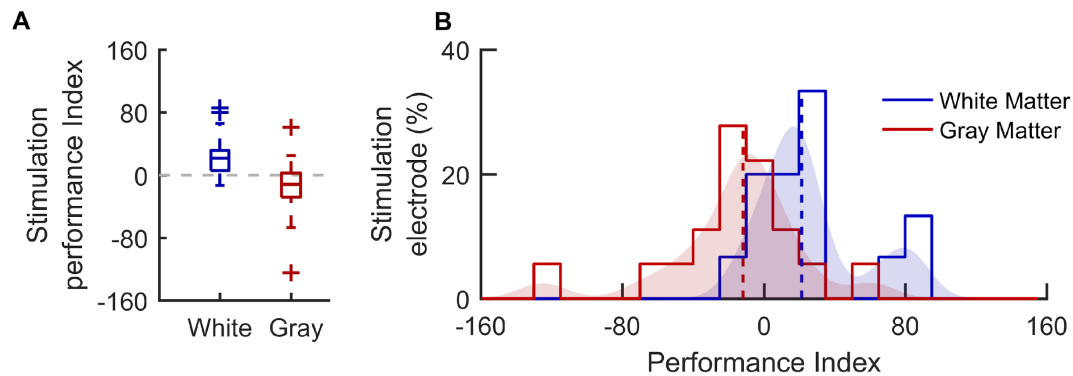
Figure 3.5 The stimulation performance index by electrode location in gray or white matter. (**A**) Entorhinal white matter (blue) simulation that immediately preceded the presentation of task stimuli (*i.e.*, encoding period) resulted in, on average, better performance. In contrast, nearby MTL gray matter (red) stimulation showed no significant effect. (**B**) The stimulation performance index was significantly different across white versus gray matter stimulation conditions ($p < 0.001$, two–sided non–parametric Wilcoxon Rank–sum test), with white matter exhibiting memory improvement (blue curve; median, [25th, 75th percentile] = 21.51, [5.73, 31.35]; $p < 0.001$, Wilcoxon Signed–rank test, n_{white} = 15) and gray matter showing a trend towards memory impairment (red curve; median, [25th, 75th percentile] = –11.82, [–28.27, 2.53]; $p = 0.053$, Wilcoxon Signed–rank test, n_{gray} = 18). The stimulation electrode (%) represents the proportion of electrodes positioned in each region. The vertical dashed lines indicate median values.
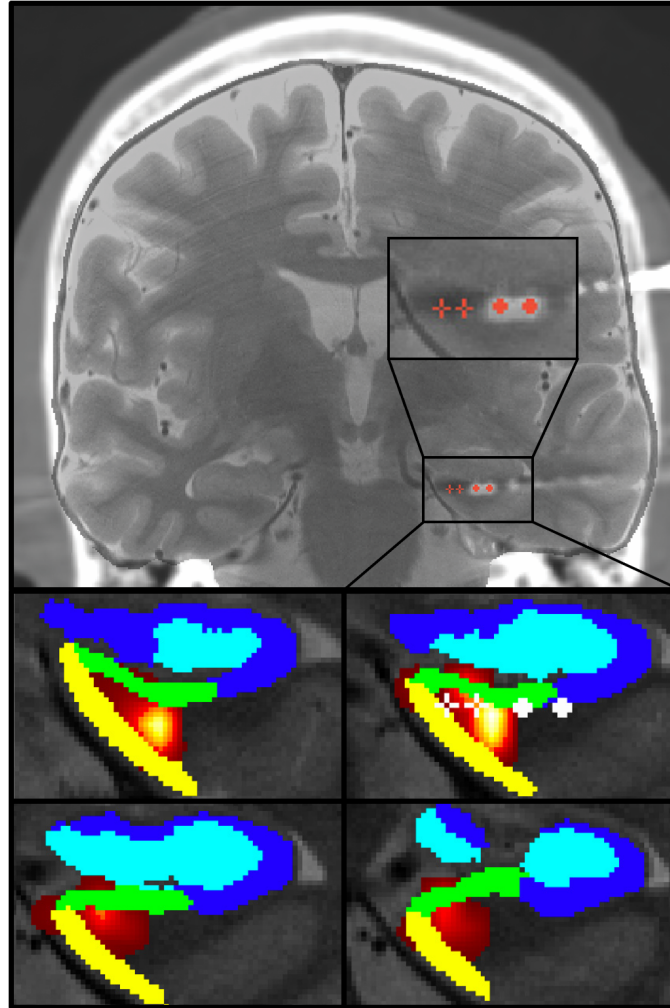
Figure 3.6 Visualization of an example electrode localization, MTL regions, and probabilistic tractography. Top panel, electrode contacts were localized by co-registration of CT and MRI scans. Bipolar (✚ symbols) and micro-wire contacts (✛ symbols), with the left-most reference for recording and the second left for micro-stimulation. Bottom panel, the left hippocampus CA fields 1-3 (dark blue), dentate gyrus (light blue), subiculum (green), entorhinal cortex (yellow), and contacts (white) are overlaid on a high-resolution hippocampal MRI. The heat map (red-yellow) illustrates the entorhinal-hippocampal connectivity distribution, indicating low (red) to high (yellow) connectivity. Slices are anterior (top left) to posterior (bottom right).
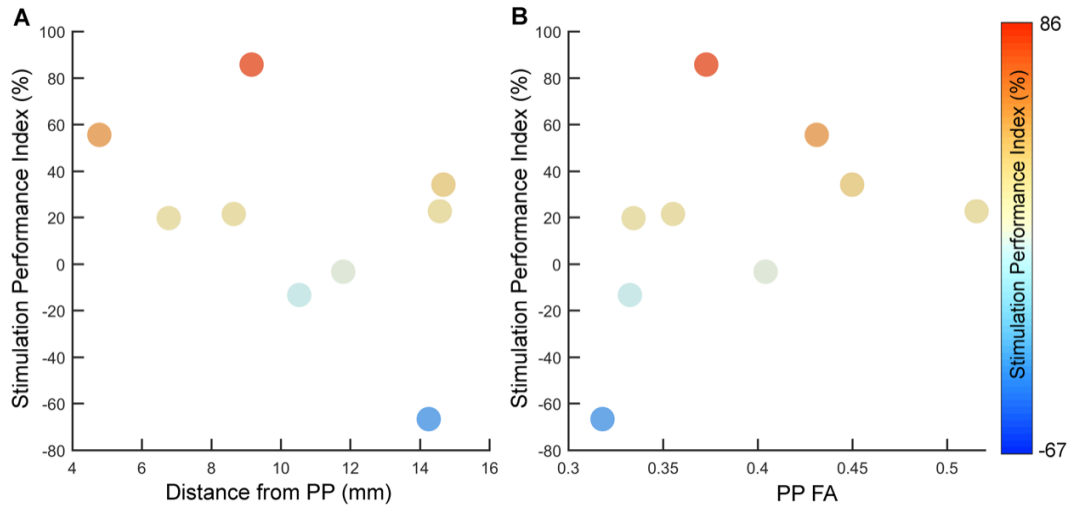
Figure 3.7 The relationship between stimulation performance index and (**A**) electrode distance from the perforant pathway (PP), and (**B**) fractional anisotropy (FA) of the PP. Positive (negative) stimulation performance index values indicate an improved (impaired) memory performance with stimulated trials compared to non-stimulated trials. The plot shows negative (blue) and positive (red) changes in the simulation performance index, where the marker color corresponds to the index value. Electrode distance was measured two ways from the location of the highest fiber density and the global average of the path. Both measures were significant and negatively correlated with the stimulation performance index (*i.e.*, the farther stimulation occurred from the entorhinal-hippocampal connections, the less memory was facilitated). Global average distance results are not shown.

Electrode location & microstructural integrity influence memory

Of the 19 subjects, 9 had dMRI scans, which were distortion corrected, processed using FSL, and diffusion tensor fitted. Probabilistic connectivity distributions were used to measure electrode distance from the entorhinal-hippocampal connections of the perforant pathway.

The distance of the electrode was assessed using two approaches. Either from the maximal density of crossing fibers or the path's center of gravity.

Then, we used a linear regression model to investigate the relationship between FA and electrode proximity to stimulation performance index, a composite of the four hippocampal-dependent memory tasks. FA and distance were significantly associated with the simulation performance index. FA was positively related (β = 402.36, Wald ^{2} = 6.9, p < 0.05), where a higher FA value (representing greater path integrity) conferred a performance enhancement (**Figure 3.7**). Distance, measured as the electrode proximity to the perforant pathway, was negatively related (β = –7.93, Wald ^{2} = 7.95, p < 0.05), where the closer stimulation occurred to the path's center of mass facilitated performance (**Figure 3.8**).
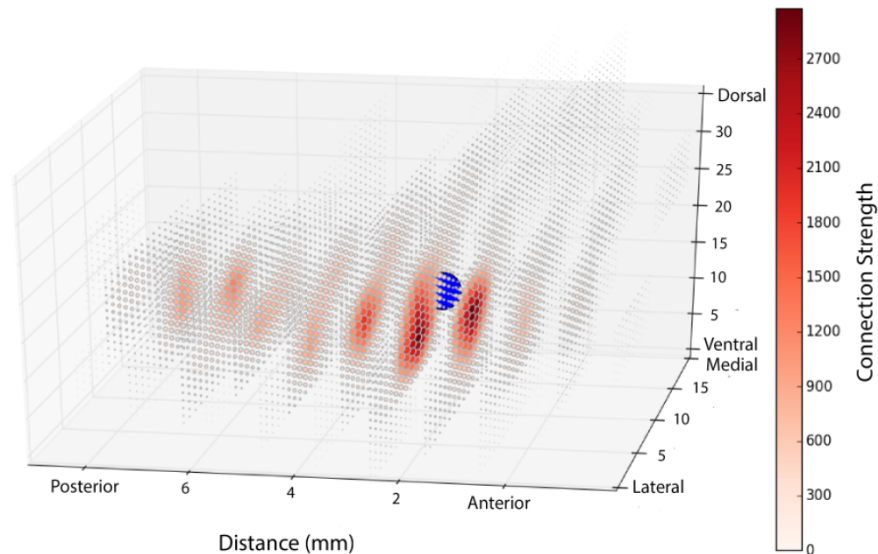
Figure 3.8 The distribution of connectivity strength (shaded red) and electrode contact (blue). The connection heat map represents the total number of paths per voxel and is a measure of the maximum number of samples taken during the tractography analyses of 5000 possible connections. For visibility, the electrode is shown as larger than the actual size.

3.4 Conclusions

These results suggest that microstructural properties of the perforant pathway modulate the stimulation performance index and that electrical stimulation in close proximity to this crucial pathway is important for episodic memory enhancement in these participants. These principal modulating factors determine the optimal DBS site that may be essential for developing therapeutic memory treatments in humans.

Furthermore, although the results are promising, it is necessary to acknowledge that they were carried out in patients with epilepsy, which may limit the extent to which these findings can be generalized to other clinical populations. Future research studies are needed to shed light on additional features to be considered in target placement and should investigate the duration of improvement. These components will be essential for the effective clinical implementation of invasive neurotechnologies for severe memory loss. However, given the focal delivery of this approach and advances in the implantation of intracranial electrodes, the application of DBS in earlier stages of the AD continuum (*e.g.*, MCI) could have profound effects on the quality of life and improvements to memory faculties and is known to be the case for early treatment of Parkinson's disease. Indeed, the concept of circuit-level and systems-based neuromodulation approaches has broad and potentially far-reaching clinical applications for a myriad of neurological and psychiatric diseases, when applied with scientific and medical integrity [Pham *et al.*, 2022; Macrina, 2015].

For instance, alternative targets for modulating memory functions include a series of gray matter regions and white matter connections that comprise the Papez circuit, which has been

implicated in AD pathophysiology [Forno *et al.*, 2021]. Our experiments explored hippocampal input stimulation to improve memory function. Yet, the entorhinal–hippocampal connections are only one aspect, albeit a central component, of the Papez circuit. Downstream from these apical fibers, the network extends brain-wide connecting sensory input in the thalamus with frontoparietal regions and then looping back into the parahippocampal gyrus in the MTL via cingulum projections. These connections, when damaged, can disrupt typical memory functioning and thus may also be viable targets for alleviating cognitive impairments, especially for individuals where entorhinal–hippocampal targeting may not be practical or if the microstructural properties indicate a suboptimal effect. Therefore, understanding how modulation at specific nodes influences differential aspects of episodic memory performance will be pivotal for addressing a spectrum of intellectual disabilities.

In conclusion, our results suggest that the location and microstructural integrity of the entorhinal–hippocampal perforant pathway contribute to stimulation-mediated episodic memory improvement. In addition, these findings may inform future approaches that aim to modulate MTL brain regions by selecting targets relative to this pathway. The opportunity to study the direct effects of electrical stimulation in the entorhinal–hippocampal circuit is not currently possible under alternative circumstances. It, therefore, constitutes the application of a fundamental understanding of hippocampal-mediated memory and its neurobiological constituents. Overall, this study is a testament to decades of scientific research using high-frequency electrical stimulation to modulate learning and memory, incorporating state-of-the-art neurotechnological approaches with *in vivo* assessment of brain connectivity.

Summary & Significance

In Part I, we show that cognition and memory scores are related to biomarkers obtained from the blood and the brain. The level of Aβ derived from blood plasma was correlated with domain-specific cognitive scores across several neuropsychological assessments. Since it is known that memory relies on the hippocampus, we also assessed the relationship between verbal memory scores and total hippocampal volume. We found that participants with smaller hippocampal volumes had lower assessment performance. Also, that APOE ε4 carriers, known to be at higher risk for developing late-onset AD, had more pathogenic levels of Aβ. Smaller hippocampal volume was related to the levels of Aβ. Together these factors (Aβ, cognition, hippocampal volume) were associated with age such that older participants had more progressed biomarker phenotypes. Since the hippocampus changes with age and is associated with age-related memory decline, we wanted to apply these findings in combination with brain stimulation to improve cognition in older adults.

In Part II, we used non-invasive Transcranial Magnetic Stimulation (TMS) to target hippocampal networks to improve associative memory function. We found that an intermittent theta-burst stimulation protocol is feasible in adults (aged 55+), and our results represent hopeful progress toward developing novel approaches for mitigating age-related memory decline. Studies like this, and others ongoing, will determine if TMS for modulating brain networks important for memory will be effective in those with more advanced impairments.

In Part III, we explored how Deep Brain Stimulation (DBS) of entorhinal-hippocampal circuits could be used to improve memory. DBS techniques have only been used in a few memory studies finding variable effects. We found the microstructural integrity of the hippocampal input pathway from the entorhinal cortex was associated with performance enhancement for stimulated compared to non-stimulated trials. In addition, the effect was most evident when the stimulation occurred at electrodes closer to the locus of the entorhinal-hippocampal connection density. Our results provide insights into how hippocampal inputs might preferentially be used to develop novel therapeutic targets for treating severe deficits in memory and cognitive function.

In summary, this dissertation reflects the work of a team of neuroscientists and clinical professionals working to understand age-dependent changes in the brain and body that contribute to benign senescence or constitute the initial pathological hallmarks of progressive brain changes resulting in cognitive impairment. We believe that the neurotechnologies presented in this manuscript will pioneer a new era of therapeutics, informed by and in conjunction with molecular and neurobiological approaches, for treating brain disease.

Appendix

Tables with test statistics for regional brain volumes assessed in the HCP-A study (Part I). P-values, significance, F-values, and FDR-corrected p-values (p-correct), using the Benjamini Hochberg method, are shown.

Table A1

Factor	Region Label	Left Hemisphere				Right Hemisphere			
		p-value	significant	F-value	p-correct	p-value	significant	F-value	p-correct
Age	thalamus	0.000	significant	36.1	0.000	0.000	significant	43.2	0.000
	caudate	0.010	significant	6.9	0.010	0.069	–	3.4	0.070
	putamen	0.000	significant	65.7	0.000	0.000	significant	65.7	0.000
	pallidum	0.000	significant	99.4	0.000	0.000	significant	76.6	0.000
	hippocampus	0.000	significant	123.4	0.000	0.000	significant	152.6	0.000
	amygdala	0.000	significant	121.3	0.000	0.000	significant	109.0	0.000
Aβ	thalamus	0.012	significant	6.5	0.013	0.003	significant	9.5	0.003
	caudate	0.417	–	0.7	0.422	0.501	–	0.5	0.504
	putamen	0.000	significant	14.7	0.000	0.000	significant	19.1	0.000
	pallidum	0.000	significant	21.3	0.000	0.000	significant	19.0	0.000
	hippocampus	0.000	significant	33.6	0.000	0.000	significant	33.5	0.000
	amygdala	0.000	significant	29.6	0.000	0.000	significant	31.2	0.000
APOE	thalamus	0.049	significant	3.1	0.065	0.020	significant	4.0	0.027
	caudate	0.080	–	2.6	0.104	0.193	–	1.7	0.233
	putamen	0.703	–	0.4	0.747	0.715	–	0.3	0.755
	pallidum	0.294	–	1.2	0.343	0.296	–	1.2	0.345
	hippocampus	0.301	–	1.2	0.349	0.418	–	0.9	0.466
	amygdala	0.629	–	0.5	0.676	0.570	–	0.6	0.619

Table A1. Subcortical brain regional volumes using the FreeSurfer pipeline (version 7.2.0) from the 'aseg' atlas [Fischl *et al.*, 2002; Fischl *et al.*, 2004a].

Table A2

Factor	Region Label	Left Hemisphere				Right Hemisphere			
		p-value	significant	F-value	p-correct	p-value	significant	F-value	p-correct
Age	caudalanteriorcingulate	0.000	significant	29.6	0.000	0.000	significant	18.8	0.000
	caudalmiddlefrontal	0.000	significant	27.2	0.000	0.025	significant	5.1	0.026
	cuneus	0.000	significant	27.9	0.000	0.000	significant	22.9	0.000
	entorhinal	0.000	significant	15.1	0.000	0.000	significant	18.5	0.000
	fusiform	0.000	significant	48.1	0.000	0.000	significant	44.4	0.000
	inferiorparietal	0.000	significant	51.1	0.000	0.000	significant	57.8	0.000
	inferiortemporal	0.000	significant	33.6	0.000	0.000	significant	41.8	0.000
	isthmuscingulate	0.000	significant	25.8	0.000	0.000	significant	18.7	0.000
	lateraloccipital	0.000	significant	42.1	0.000	0.000	significant	35.7	0.000
	lateralorbitofrontal	0.000	significant	50.4	0.000	0.005	significant	8.3	0.005
	lingual	0.000	significant	38.1	0.000	0.000	significant	35.1	0.000
	medialorbitofrontal	0.297	–	1.1	0.298	0.917	–	0.0	0.917
	middletemporal	0.000	significant	86.3	0.000	0.000	significant	52.0	0.000
	parahippocampal	0.000	significant	46.8	0.000	0.000	significant	67.0	0.000
	paracentral	0.000	significant	56.1	0.000	0.000	significant	44.2	0.000
	parsopercularis	0.000	significant	14.9	0.000	0.006	significant	7.9	0.006
	parsorbitalis	0.000	significant	43.7	0.000	0.000	significant	38.0	0.000
	parstriangularis	0.000	significant	43.6	0.000	0.000	significant	34.4	0.000
	pericalcarine	0.027	significant	5.0	0.027	0.002	significant	10.2	0.002

	postcentral	0.000	significant	56.0	0.000	0.000	significant	84.9	0.000
	posteriorcingulate	0.000	significant	35.9	0.000	0.000	significant	48.8	0.000
	precentral	0.000	significant	67.2	0.000	0.000	significant	64.7	0.000
	precuneus	0.000	significant	56.1	0.000	0.000	significant	68.2	0.000
	rostralanteriorcingulate	0.000	significant	14.5	0.000	0.000	significant	15.9	0.000
	rostralmiddlefrontal	0.000	significant	73.5	0.000	0.000	significant	20.3	0.000
	superiorfrontal	0.000	significant	70.3	0.000	0.000	significant	31.1	0.000
	superiorparietal	0.000	significant	47.1	0.000	0.000	significant	45.4	0.000
	superiortemporal	0.000	significant	60.0	0.000	0.000	significant	62.2	0.000
	supramarginal	0.000	significant	33.0	0.000	0.000	significant	51.0	0.000
	transversetemporal	0.000	significant	53.3	0.000	0.000	significant	17.9	0.000
	insula	0.000	significant	26.7	0.000	0.000	significant	23.7	0.000
Aβ	caudalanteriorcingulate	0.008	significant	7.3	0.008	0.010	significant	6.9	0.011
	caudalmiddlefrontal	0.001	significant	11.3	0.001	0.122	–	2.4	0.124
	cuneus	0.016	significant	6.0	0.017	0.001	significant	12.1	0.001
	entorhinal	0.071	–	3.3	0.073	0.032	significant	4.7	0.033
	fusiform	0.000	significant	19.2	0.000	0.011	significant	6.7	0.011
	inferiorparietal	0.000	significant	21.2	0.000	0.000	significant	23.8	0.000
	inferiortemporal	0.000	significant	15.3	0.000	0.000	significant	16.8	0.000
	isthmuscingulate	0.000	significant	13.2	0.000	0.006	significant	7.7	0.007
	lateraloccipital	0.000	significant	16.8	0.000	0.001	significant	11.3	0.001
	lateralorbitofrontal	0.000	significant	25.3	0.000	0.000	significant	13.8	0.000
	lingual	0.001	significant	10.9	0.001	0.004	significant	8.7	0.004
	medialorbitofrontal	0.983	–	0.0	0.983	0.280	–	1.2	0.284
	middletemporal	0.000	significant	25.3	0.000	0.000	significant	21.9	0.000
	parahippocampal	0.000	significant	20.8	0.000	0.000	significant	28.5	0.000
	paracentral	0.000	significant	25.2	0.000	0.000	significant	22.5	0.000
	parsopercularis	0.023	significant	5.3	0.024	0.002	significant	10.2	0.002
	parsorbitalis	0.000	significant	23.8	0.000	0.000	significant	19.6	0.000
	parstriangularis	0.000	significant	15.3	0.000	0.000	significant	17.6	0.000
	pericalcarine	0.331	–	1.0	0.335	0.030	significant	4.8	0.031
	postcentral	0.000	significant	33.3	0.000	0.000	significant	29.3	0.000
	posteriorcingulate	0.000	significant	14.8	0.000	0.000	significant	14.8	0.000
	precentral	0.000	significant	31.3	0.000	0.000	significant	24.3	0.000
	precuneus	0.000	significant	33.1	0.000	0.000	significant	37.6	0.000
	rostralanteriorcingulate	0.066	–	3.4	0.067	0.008	significant	7.2	0.009
	rostralmiddlefrontal	0.000	significant	15.0	0.000	0.020	significant	5.5	0.021
	superiorfrontal	0.000	significant	26.3	0.000	0.004	significant	8.6	0.004
	superiorparietal	0.000	significant	28.8	0.000	0.000	significant	32.1	0.000
	superiortemporal	0.000	significant	23.2	0.000	0.000	significant	29.6	0.000
	supramarginal	0.000	significant	20.2	0.000	0.000	significant	19.3	0.000
	transversetemporal	0.000	significant	25.3	0.000	0.000	significant	14.9	0.000
	insula	0.000	significant	16.4	0.000	0.002	significant	10.0	0.002
APOE	caudalanteriorcingulate	0.175	–	1.8	0.215	0.827	–	0.2	0.849
	caudalmiddlefrontal	0.308	–	1.2	0.355	0.560	–	0.6	0.611
	cuneus	0.730	–	0.3	0.765	0.743	–	0.3	0.775
	entorhinal	0.365	–	1.0	0.416	0.943	–	0.1	0.947
	fusiform	0.370	–	1.0	0.419	0.187	–	1.7	0.228
	inferiorparietal	0.178	–	1.7	0.219	0.291	–	1.2	0.341
	inferiortemporal	0.759	–	0.3	0.787	0.957	–	0.0	0.957
	isthmuscingulate	0.305	–	1.2	0.352	0.866	–	0.1	0.882
	lateraloccipital	0.092	–	2.4	0.119	0.008	significant	5.0	0.011
	lateralorbitofrontal	0.278	–	1.3	0.327	0.169	–	1.8	0.210
	lingual	0.944	–	0.1	0.947	0.947	–	0.1	0.949
	medialorbitofrontal	0.237	–	1.5	0.283	0.370	–	1.0	0.419
	middletemporal	0.104	–	2.3	0.133	0.235	–	1.5	0.282

Region Label	p-value	significant	F-value	p-correct	p-value	significant	F-value	p-correct
parahippocampal	0.559	–	0.6	0.611	0.415	–	0.9	0.464
paracentral	0.077	–	2.6	0.100	0.171	–	1.8	0.211
parsopercularis	0.315	–	1.2	0.362	0.810	–	0.2	0.835
parsorbitalis	0.707	–	0.3	0.749	0.375	–	1.0	0.423
parstriangularis	0.095	–	2.4	0.123	0.606	–	0.5	0.653
pericalcarine	0.472	–	0.8	0.520	0.831	–	0.2	0.849
postcentral	0.280	–	1.3	0.330	0.727	–	0.3	0.765
posteriorcingulate	0.914	–	0.1	0.929	0.605	–	0.5	0.653
precentral	0.419	–	0.9	0.466	0.563	–	0.6	0.613
precuneus	0.922	–	0.1	0.935	0.924	–	0.1	0.935
rostralanteriorcingulate	0.678	–	0.4	0.726	0.588	–	0.5	0.638
rostralmiddlefrontal	0.498	–	0.7	0.548	0.139	–	2.0	0.176
superiorfrontal	0.374	–	1.0	0.422	0.160	–	1.9	0.200
superiorparietal	0.683	–	0.4	0.728	0.145	–	2.0	0.183
superiortemporal	0.079	–	2.6	0.103	0.169	–	1.8	0.210
supramarginal	0.334	–	1.1	0.383	0.148	–	1.9	0.187
transversetemporal	0.103	–	2.3	0.133	0.366	–	1.0	0.416
insula	0.236	–	1.5	0.282	0.291	–	1.2	0.341

Table A2. Cortical gray matter parcellation using the FreeSurfer pipeline (version 7.2.0) from the Desikan-Killiany atlas [Desikan *et al.*, 2006].

Table A3		Left Hemisphere				Right Hemisphere			
Factor	Region Label	p-value	significant	F-value	p-correct	p-value	significant	F-value	p-correct
Age	caudalanteriorcingulate	0.000	significant	37.7	0.000	0.000	significant	55.4	0.000
	caudalmiddlefrontal	0.000	significant	17.3	0.000	0.090	–	2.9	0.090
	cuneus	0.000	significant	32.4	0.000	0.000	significant	17.0	0.000
	entorhinal	0.000	significant	42.3	0.000	0.000	significant	42.8	0.000
	fusiform	0.000	significant	87.2	0.000	0.000	significant	65.8	0.000
	inferiorparietal	0.000	significant	36.9	0.000	0.000	significant	21.3	0.000
	inferiortemporal	0.000	significant	55.1	0.000	0.000	significant	51.5	0.000
	isthmuscingulate	0.000	significant	32.3	0.000	0.000	significant	17.3	0.000
	lateraloccipital	0.000	significant	23.5	0.000	0.000	significant	22.4	0.000
	lateralorbitofrontal	0.000	significant	103.2	0.000	0.000	significant	81.0	0.000
	lingual	0.000	significant	77.0	0.000	0.000	significant	44.0	0.000
	medialorbitofrontal	0.000	significant	54.4	0.000	0.000	significant	48.7	0.000
	middletemporal	0.000	significant	70.6	0.000	0.000	significant	76.3	0.000
	parahippocampal	0.000	significant	120.0	0.000	0.000	significant	121.8	0.000
	paracentral	0.000	significant	56.4	0.000	0.000	significant	33.2	0.000
	parsopercularis	0.000	significant	20.2	0.000	0.000	significant	29.2	0.000
	parsorbitalis	0.000	significant	49.4	0.000	0.000	significant	60.3	0.000
	parstriangularis	0.000	significant	59.8	0.000	0.000	significant	54.9	0.000
	pericalcarine	0.001	significant	12.3	0.001	0.014	significant	6.2	0.014
	postcentral	0.000	significant	23.4	0.000	0.000	significant	30.5	0.000
	posteriorcingulate	0.000	significant	55.3	0.000	0.000	significant	69.2	0.000
	precentral	0.000	significant	27.5	0.000	0.000	significant	17.3	0.000
	precuneus	0.000	significant	45.0	0.000	0.000	significant	59.1	0.000
	rostralanteriorcingulate	0.000	significant	21.9	0.000	0.000	significant	22.7	0.000
	rostralmiddlefrontal	0.000	significant	56.7	0.000	0.000	significant	19.3	0.000
	superiorfrontal	0.000	significant	75.0	0.000	0.000	significant	50.5	0.000
	superiorparietal	0.000	significant	40.3	0.000	0.000	significant	35.8	0.000
	superiortemporal	0.000	significant	31.8	0.000	0.000	significant	37.0	0.000
	supramarginal	0.000	significant	19.8	0.000	0.000	significant	30.4	0.000
	frontalpole	0.000	significant	23.9	0.000	0.048	significant	4.0	0.048
	temporalpole	0.000	significant	26.2	0.000	0.000	significant	18.0	0.000
	transversetemporal	0.000	significant	25.8	0.000	0.000	significant	14.0	0.000

Aβ	insula	0.000	significant	55.2	0.000	0.000	significant	48.4	0.000
	caudalanteriorcingulate	0.035	significant	4.5	0.036	0.000	significant	13.3	0.000
	caudalmiddlefrontal	0.021	significant	5.5	0.022	0.498	–	0.5	0.502
	cuneus	0.028	significant	5.0	0.029	0.052	–	3.8	0.054
	entorhinal	0.000	significant	18.0	0.000	0.000	significant	14.2	0.000
	fusiform	0.000	significant	21.4	0.000	0.000	significant	13.2	0.000
	inferiorparietal	0.001	significant	11.0	0.001	0.002	significant	9.7	0.003
	inferiortemporal	0.000	significant	14.9	0.000	0.004	significant	8.7	0.004
	isthmuscingulate	0.000	significant	12.8	0.001	0.005	significant	8.1	0.006
	lateraloccipital	0.006	significant	7.7	0.007	0.072	–	3.3	0.074
	lateralorbitofrontal	0.000	significant	19.7	0.000	0.000	significant	26.4	0.000
	lingual	0.001	significant	11.5	0.001	0.008	significant	7.4	0.008
	medialorbitofrontal	0.000	significant	23.2	0.000	0.002	significant	10.4	0.002
	middletemporal	0.001	significant	11.5	0.001	0.000	significant	18.8	0.000
	parahippocampal	0.000	significant	27.1	0.000	0.000	significant	24.6	0.000
	paracentral	0.000	significant	15.6	0.000	0.003	significant	9.2	0.003
	parsopercularis	0.012	significant	6.5	0.013	0.000	significant	16.3	0.000
	parsorbitalis	0.001	significant	11.5	0.001	0.001	significant	10.6	0.002
	parstriangularis	0.000	significant	15.2	0.000	0.000	significant	19.0	0.000
	pericalcarine	0.582	–	0.3	0.584	0.635	–	0.2	0.636
	postcentral	0.006	significant	7.7	0.007	0.015	significant	6.1	0.016
	posteriorcingulate	0.000	significant	16.1	0.000	0.000	significant	14.4	0.000
	precentral	0.018	significant	5.7	0.019	0.115	–	2.5	0.117
	precuneus	0.001	significant	11.4	0.001	0.000	significant	23.7	0.000
	rostralanteriorcingulate	0.255	–	1.3	0.259	0.009	significant	7.0	0.010
	rostralmiddlefrontal	0.003	significant	9.4	0.003	0.065	–	3.5	0.067
	superiorfrontal	0.001	significant	12.1	0.001	0.017	significant	5.8	0.018
	superiorparietal	0.000	significant	14.0	0.000	0.000	significant	20.5	0.000
	superiortemporal	0.024	significant	5.2	0.025	0.005	significant	8.3	0.005
	supramarginal	0.001	significant	12.1	0.001	0.002	significant	9.9	0.002
	frontalpole	0.000	significant	20.2	0.000	0.040	significant	4.3	0.041
	temporalpole	0.005	significant	8.1	0.006	0.014	significant	6.2	0.015
	transversetemporal	0.038	significant	4.4	0.040	0.154	–	2.1	0.157
APOE	insula	0.000	significant	15.5	0.000	0.000	significant	14.5	0.000
	caudalanteriorcingulate	0.448	–	0.8	0.495	0.746	–	0.3	0.776
	caudalmiddlefrontal	0.124	–	2.1	0.158	0.160	–	1.9	0.200
	cuneus	0.813	–	0.2	0.836	0.267	–	1.3	0.316
	entorhinal	0.858	–	0.2	0.875	0.428	–	0.9	0.475
	fusiform	0.642	–	0.4	0.689	0.183	–	1.7	0.223
	inferiorparietal	0.031	significant	3.6	0.042	0.345	–	1.1	0.395
	inferiortemporal	0.765	–	0.3	0.790	0.220	–	1.5	0.264
	isthmuscingulate	0.348	–	1.1	0.397	0.722	–	0.3	0.762
	lateraloccipital	0.066	–	2.8	0.087	0.004	significant	5.8	0.005
	lateralorbitofrontal	0.038	significant	3.3	0.052	0.175	–	1.8	0.216
	lingual	0.736	–	0.3	0.770	0.683	–	0.4	0.728
	medialorbitofrontal	0.295	–	1.2	0.343	0.013	significant	4.5	0.017
	middletemporal	0.080	–	2.6	0.104	0.200	–	1.6	0.241
	parahippocampal	0.744	–	0.3	0.775	0.124	–	2.1	0.158
	paracentral	0.156	–	1.9	0.196	0.144	–	2.0	0.183
	parsopercularis	0.194	–	1.7	0.234	0.697	–	0.4	0.741
	parsorbitalis	0.066	–	2.8	0.087	0.070	–	2.7	0.093
	parstriangularis	0.254	–	1.4	0.302	0.252	–	1.4	0.299
	pericalcarine	0.763	–	0.3	0.790	0.929	–	0.1	0.938
	postcentral	0.016	significant	4.3	0.022	0.589	–	0.5	0.638
	posteriorcingulate	0.420	–	0.9	0.466	0.560	–	0.6	0.611
	precentral	0.050	–	3.1	0.067	0.190	–	1.7	0.230

Region Label	p-value	significant	F-value	p-correct	p-value	significant	F-value	p-correct
precuneus	0.729	–	0.3	0.765	0.937	–	0.1	0.945
rostralanteriorcingulate	0.440	–	0.8	0.486	0.028	significant	3.7	0.038
rostralmiddlefrontal	0.166	–	1.8	0.206	0.023	significant	3.9	0.031
superiorfrontal	0.029	significant	3.6	0.040	0.057	–	2.9	0.076
superiorparietal	0.114	–	2.2	0.146	0.091	–	2.4	0.119
superiortemporal	0.018	significant	4.1	0.025	0.039	significant	3.3	0.053
supramarginal	0.395	–	0.9	0.442	0.166	–	1.8	0.206
frontalpole	0.180	–	1.7	0.220	0.051	–	3.0	0.069
temporalpole	0.054	–	3.0	0.072	0.303	–	1.2	0.350
transversetemporal	0.386	–	1.0	0.433	0.830	–	0.2	0.849
insula	0.276	–	1.3	0.326	0.160	–	1.9	0.200

Table A3. Cortical white matter parcellation using the FreeSurfer pipeline (version 7.2.0) from the Desikan-Killiany atlas [Desikan *et al.*, 2006; Fischl *et al.*, 2004b].

Table A4			Left Hemisphere			Right Hemisphere		
Factor	**Region Label**	**p-value**	**significant**	**F-value**	**p-correct**	**p-value**	**significant**	**F-value**	**p-correct**
Age	hippocampal.body	0.000	significant	119.0	0.000	0.000	significant	68.8	0.000
	hippocampal.head	0.000	significant	69.0	0.000	0.000	significant	20.1	0.000
	hippocampal.tail	0.000	significant	130.1	0.000	0.000	significant	68.4	0.000
	parasubiculum	0.171	–	1.9	0.171	0.530	–	0.4	0.530
	presubiculum.head	0.000	significant	19.5	0.000	0.000	significant	38.0	0.000
	presubiculum.body	0.010	significant	6.8	0.010	0.000	significant	23.9	0.000
	subiculum.head	0.000	significant	50.8	0.000	0.000	significant	68.3	0.000
	subiculum.body	0.000	significant	114.7	0.000	0.000	significant	136.7	0.000
	hippocampal.fissure	0.081	–	3.1	0.081	0.057	–	3.7	0.057
	molecular.layer.HP.head	0.000	significant	57.8	0.000	0.000	significant	55.3	0.000
	molecular.layer.HP.body	0.000	significant	62.2	0.000	0.000	significant	75.0	0.000
	GC.ML.DG.head	0.000	significant	81.8	0.000	0.000	significant	108.3	0.000
	GC.ML.DG.body	0.000	significant	123.2	0.000	0.000	significant	119.6	0.000
	CA1.head	0.000	significant	71.5	0.000	0.000	significant	105.1	0.000
	CA1.body	0.000	significant	77.2	0.000	0.000	significant	105.5	0.000
	CA2.3.head	0.000	significant	53.0	0.000	0.000	significant	60.2	0.000
	CA2.3.body	0.000	significant	32.2	0.000	0.000	significant	48.0	0.000
	CA4.head	0.000	significant	79.1	0.000	0.000	significant	99.7	0.000
	CA4.body	0.000	significant	100.6	0.000	0.000	significant	95.8	0.000
	fimbria	0.000	significant	101.5	0.000	0.000	significant	78.5	0.000
Aβ	hippocampal.body	0.000	significant	32.0	0.000	0.003	significant	9.3	0.003
	hippocampal.head	0.000	significant	24.2	0.000	0.062	–	3.5	0.063
	hippocampal.tail	0.000	significant	27.0	0.000	0.018	significant	5.7	0.018
	parasubiculum	0.477	–	0.5	0.478	0.430	–	0.6	0.430
	presubiculum.head	0.001	significant	11.1	0.001	0.000	significant	17.0	0.000
	presubiculum.body	0.044	significant	4.1	0.044	0.011	significant	6.6	0.011
	subiculum.head	0.000	significant	23.6	0.000	0.000	significant	25.2	0.000
	subiculum.body	0.000	significant	28.7	0.000	0.000	significant	35.2	0.000
	hippocampal.fissure	0.378	–	0.8	0.379	0.501	–	0.5	0.501
	molecular.layer.HP.head	0.000	significant	20.4	0.000	0.000	significant	20.9	0.000
	molecular.layer.HP.body	0.000	significant	22.9	0.000	0.000	significant	16.7	0.000
	GC.ML.DG.head	0.000	significant	24.0	0.000	0.000	significant	24.8	0.000
	GC.ML.DG.body	0.000	significant	31.8	0.000	0.000	significant	26.4	0.000
	CA1.head	0.000	significant	25.4	0.000	0.000	significant	29.2	0.000
	CA1.body	0.000	significant	19.6	0.000	0.000	significant	31.3	0.000
	CA2.3.head	0.000	significant	13.6	0.000	0.000	significant	15.9	0.000
	CA2.3.body	0.003	significant	9.2	0.003	0.000	significant	23.6	0.000
	CA4.head	0.000	significant	24.4	0.000	0.000	significant	25.3	0.000
	CA4.body	0.000	significant	23.9	0.000	0.000	significant	24.4	0.000

| Factor	Region Label	p-value	significant	F-value	p-correct	p-value	significant	F-value	p-correct
	fimbria	0.000	significant	35.8	0.000	0.000	significant	21.6	0.000
APOE	hippocampal.body	0.180	–	1.7	0.185	0.781	–	0.2	0.783
	hippocampal.head	0.203	–	1.6	0.207	0.784	–	0.2	0.786
	hippocampal.tail	0.410	–	0.9	0.416	0.822	–	0.2	0.824
	parasubiculum	0.555	–	0.6	0.560	0.932	–	0.1	0.932
	presubiculum.head	0.320	–	1.1	0.326	0.558	–	0.6	0.562
	presubiculum.body	0.356	–	1.0	0.361	0.260	–	1.4	0.265
	subiculum.head	0.567	–	0.6	0.571	0.786	–	0.2	0.788
	subiculum.body	0.199	–	1.6	0.203	0.523	–	0.7	0.528
	hippocampal.fissure	0.083	–	2.5	0.085	0.602	–	0.5	0.606
	molecular.layer.HP.head	0.220	–	1.5	0.225	0.240	–	1.4	0.245
	molecular.layer.HP.body	0.146	–	2.0	0.150	0.346	–	1.1	0.352
	GC.ML.DG.head	0.183	–	1.7	0.187	0.419	–	0.9	0.425
	GC.ML.DG.body	0.240	–	1.4	0.245	0.105	–	2.3	0.108
	CA1.head	0.194	–	1.7	0.199	0.647	–	0.4	0.650
	CA1.body	0.238	–	1.5	0.243	0.613	–	0.5	0.617
	CA2.3.head	0.185	–	1.7	0.189	0.346	–	1.1	0.351
	CA2.3.body	0.499	–	0.7	0.504	0.427	–	0.9	0.432
	CA4.head	0.333	–	1.1	0.339	0.505	–	0.7	0.510
	CA4.body	0.342	–	1.1	0.348	0.178	–	1.7	0.183
	fimbria	0.650	–	0.4	0.653	0.482	–	0.7	0.487

Table A4. Hippocampal subfields using the FreeSurfer pipeline (version 7.2.0) from the *ex vivo*, ultra-high-resolution atlas [Iglesias *et al.*, 2015].

Table A5		Left Hemisphere				Right Hemisphere			
Factor	Region Label	p-value	significant	F-value	p-correct	p-value	significant	F-value	p-correct
Age	anterior hippocampus	0.000	significant	60.5	0.000	0.000	significant	64.2	0.000
	posterior hippocampus	0.000	significant	99.8	0.000	0.000	significant	98.4	0.000
	entorhinal cortex	0.000	significant	32.2	0.000	0.000	significant	23.4	0.000
	perirhinal cortex (BA 35)	0.000	significant	93.3	0.000	0.000	significant	79.7	0.000
	perirhinal cortex (BA 36)	0.000	significant	44.7	0.000	0.000	significant	34.1	0.000
	parahippocampal cortex	0.000	significant	100.9	0.000	0.000	significant	95.1	0.000
Aβ	anterior hippocampus	0.000	significant	18.0	0.000	0.000	significant	20.8	0.000
	posterior hippocampus	0.000	significant	29.5	0.000	0.000	significant	29.1	0.000
	entorhinal cortex	0.000	significant	16.0	0.000	0.000	significant	18.1	0.000
	perirhinal cortex (BA 35)	0.000	significant	28.7	0.000	0.000	significant	33.7	0.000
	perirhinal cortex (BA 36)	0.000	significant	18.6	0.000	0.002	significant	10.2	0.002
	parahippocampal cortex	0.000	significant	26.9	0.000	0.000	significant	30.8	0.000
APOE	anterior hippocampus	0.923	–	0.1	0.923	0.878	–	0.1	0.879
	posterior hippocampus	0.245	–	1.4	0.250	0.209	–	1.6	0.214
	entorhinal cortex	0.679	–	0.4	0.682	0.556	–	0.6	0.560
	perirhinal cortex (BA 35)	0.439	–	0.8	0.444	0.274	–	1.3	0.279
	perirhinal cortex (BA 36)	0.467	–	0.8	0.473	0.138	–	2.0	0.142
	parahippocampal cortex	0.591	–	0.5	0.595	0.151	–	1.9	0.155

Table A5. Hippocampal and MTL brain regions using the ASHS pipeline (version 2.0) from the University of Pennsylvania Memory Center 3-Tesla atlas for T1-weighted MRI [Xie *et al.*, 2016].

Diversity Statement

Recent work in several fields of science has identified a bias in citation practices such that papers from women and other minority scholars are under-cited relative to the number of such papers in the field [Mitchell *et al.*, 2013; Dion *et al.*, 2018; Caplar *et al.*, 2017; Maliniak *et al.*, 2013; Dworkin *et al.*, 2020; Bertolero *et al.*, 2020; Wang *et al.*, 2021; Chatterjee & Werner, 2021; Fulvio *et al.*, 2021]. Here we sought to proactively consider choosing references that reflect the diversity of the field in thought, form of contribution, gender, race, ethnicity, and other factors. First, we obtained the predicted gender of the first and last author of each reference by using databases that store the probability of a first name being carried by a woman [Dworkin *et al.*, 2020; Zhou *et al.*, 2020]. By this measure, our references contain 13.6% woman(first)/woman(last), 11.1% man(first)/woman(last), 19.8% woman(first)/man(last), and 56.1% man(last)/man(last). For the top 5 neuroscience journals, the expected gender proportions are 6.7% for woman(first)/woman(last), 9.4% for man(first)/woman(last), 25.5% for woman(first)/man(last), and 58.4% for man(first)/man(last) [Dworkin *et al.*, 2020].
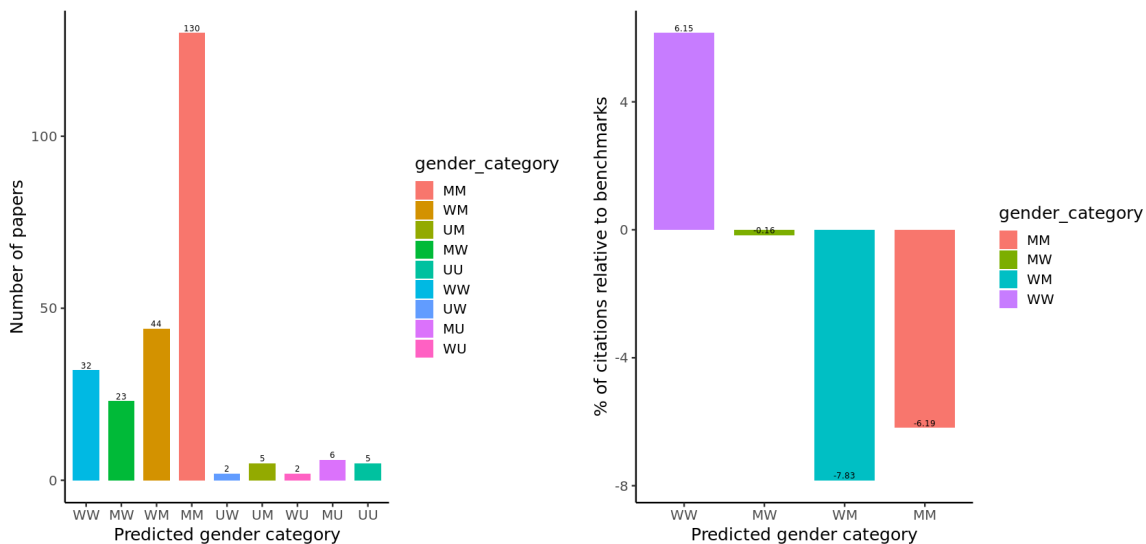
This method is limited in that a) names, pronouns, and social media profiles used to construct the databases may not, in every case, be indicative of gender identity, and b) it cannot account for intersex, non-binary, or transgender people.

Second, we obtained the predicted racial/ethnic category of the first and last author of each reference by databases that store the probability of a first and last name being carried by an author of color [Ambekar *et al.*, 2009; Sood & Laohaprapanon, 2018]. By this measure, our references contain 10.8% author of color(first)/author of color(last), 13.4% white(first)/author of color(last), 18.7% author of color(first)/white(last), and 57.2% white(first)/white(last). Using a similar random draw model regressing for relevant variables, the expected race proportions were 11.9% for author of color/author of color, 12.8% for white(first)/author of color, 23.5% for author of color(first)/white(last), and 51.8% for white(first)/white(last) [Bertolero *et al.*, 2020].

This method is limited in that a) names and Florida Voter Data to make the predictions may not be indicative of racial/ethnic identity, and b) it cannot account for Indigenous and mixed-race authors or those who may face differential biases due to the ambiguous racialization or ethnicization of their names. We look forward to future work that could help us to better understand how to support equitable practices in science.
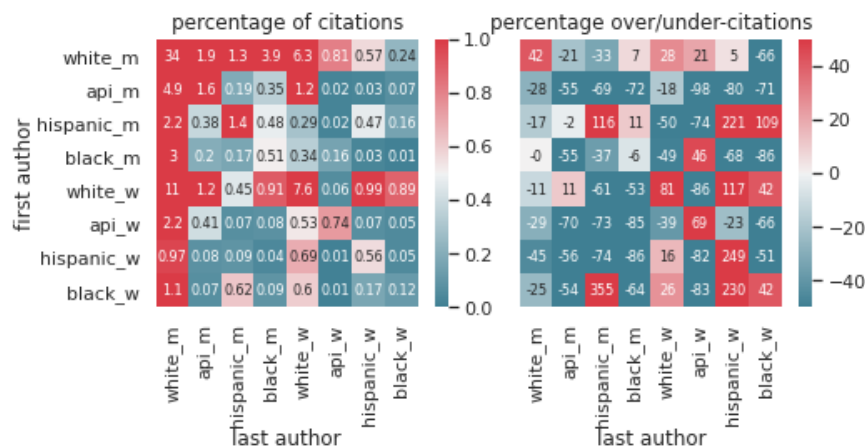
Bibliography

ACL. (2020) *Profile of Older Americans*. Annual Summary. U.S. Department of Health and Human Services, p. 26.

Adler, D.H. *et al.* (2014) 'Histology-derived volumetric annotation of the human hippocampal subfields in postmortem MRI', *NeuroImage*, 84, pp. 505–523.

Alzforum. (2020) 'Plasma Aβ Test Wins Approval—Are p-Tau Tests Far Behind?'

Ambekar, A. *et al.* (2009) 'Name-ethnicity classification from open sources', in *Proceedings of the 15th ACM SIGKDD international conference on Knowledge discovery and data mining*. Paris, France: ACM Press, p. 49.

Apostolova, L. (2022) *Longitudinal Early-onset Alzheimer's Disease Study Protocol*. Clinical trial registration NCT03507257. clinicaltrials.gov.

Arboleda-Velasquez, J.F. *et al.* (2019) 'Resistance to autosomal dominant Alzheimer's disease in an APOE3 Christchurch homozygote: a case report', *Nature Medicine*, 25(11), pp. 1680–1683.

Arfanakis, K. *et al.* (2016) 'Cognitive activity, cognitive function, and brain diffusion characteristics in old age', *Brain Imaging and Behavior*, 10(2), pp. 455–463.

Ashe, K.H. (2020) 'The biogenesis and biology of amyloid β oligomers in the brain', *Alzheimer's & Dementia*, 16(11), pp. 1561–1567.

Ashe, K.H. (2022) 'Alzheimer's target still viable but untested', *Science*, 377(6609), pp. 935–935.

Augustinack, J. *et al.* (2010) 'Direct visualization of the perforant pathway in the human brain with ex vivo diffusion tensor imaging', *Frontiers in Human Neuroscience*, 4.

Barnes, L.L. & Bennett, D.A. (2015) 'Cognitive resilience in APOE*ε4 carriers—is race important?', *Nature reviews. Neurology*, 11(4), pp. 190–191.

Barroeta-Espar, I. *et al.* (2019) 'Distinct cytokine profiles in human brains resilient to Alzheimer's pathology', *Neurobiology of Disease*, 121, pp. 327–337.

Basser, P.J., Mattiello, J. & LeBihan, D. (1994) 'Estimation of the effective self-diffusion tensor from the NMR spin echo', *Journal of Magnetic Resonance. Series B*, 103(3), pp. 247–254.

Bastani, A. & Jaberzadeh, S. (2012) 'A Higher Number of TMS-Elicited MEP from a Combined Hotspot Improves Intra- and Inter-Session Reliability of the Upper Limb Muscles in Healthy Individuals', *PLOS ONE*, 7(10), p. e47582.

Battaglia, F.P. *et al.* (2011) 'The hippocampus: hub of brain network communication for memory', *Trends in Cognitive Sciences*, 15(7), pp. 310–318.

Bauer, P.J. *et al.* (2013) 'III. NIH Toolbox Cognition Battery (CB): measuring episodic memory', *Monographs of the Society for Research in Child Development*, 78(4), pp. 34–48.

Baum, G.L. *et al.* (2022) 'Graded Variation in T1w/T2w Ratio during Adolescence: Measurement, Caveats, and Implications for Development of Cortical Myelin', *Journal of Neuroscience*, 42(29), pp. 5681–5694.

Beckmann, C.F. *et al.* (2005) 'Investigations into resting-state connectivity using independent component analysis', *Philosophical Transactions of the Royal Society of London. Series B, Biological Sciences*, 360(1457), pp. 1001–1013.

Behrens, T.E.J. *et al.* (2003) 'Characterization and propagation of uncertainty in diffusion-weighted MR imaging', *Magnetic Resonance in Medicine*, 50(5), pp. 1077–1088.

Behrens, T.E.J. *et al.* (2007) 'Probabilistic diffusion tractography with multiple fibre orientations: What can we gain?', *NeuroImage*, 34(1), pp. 144–155.

Bell, K.A. *et al.* (2020) 'The Entorhinal Cortical Alvear Pathway Differentially Excites Pyramidal Cells and Interneuron Subtypes in Hippocampal CA1', *Cerebral Cortex (New York, NY)*, 31(5), pp. 2382–2401.

Bertolero, M.A. *et al.* (2020) 'Racial and ethnic imbalance in neuroscience reference lists and intersections with gender'. bioRxiv, p. 2020.10.12.336230.

Bethlehem, R.A.I. *et al.* (2022) 'Brain charts for the human lifespan', *Nature*, 604(7906), pp. 525–533.

Blennow, K. *et al.* (2010) 'Cerebrospinal fluid and plasma biomarkers in Alzheimer disease', *Nature Reviews. Neurology*, 6(3), pp. 131–144.

Bliss, T.V.P. & Cooke, S.F. (2011) 'Long-term potentiation and long-term depression: a clinical perspective', *Clinics*, 66, pp. 3–17.

Bliss, T.V.P. & Lomo, T. (1973) 'Long-lasting potentiation of synaptic transmission in the dentate area of the anaesthetized rabbit following stimulation of the perforant path', *The Journal of Physiology*, 232(2), pp. 331–356.

Blue, E.E. *et al.* (2019) 'Local ancestry at APOE modifies Alzheimer's disease risk in Caribbean Hispanics', *Alzheimer's & Dementia : the journal of the Alzheimer's Association*, 15(12), pp. 1524–1532.

Bookheimer, S. & Burggren, A. (2009) 'APOE-4 Genotype and Neurophysiological Vulnerability to Alzheimer's and Cognitive Aging', *Annual review of clinical psychology*, 5, pp. 343–362.

Bookheimer, S.Y. *et al.* (2019) 'The Lifespan Human Connectome Project in Aging: An overview', *NeuroImage*, 185, pp. 335–348.

Bourgeat, P. *et al.* (2022) 'β-amyloid PET harmonisation across longitudinal studies: Application to AIBL, ADNI and OASIS3', *NeuroImage*, 262, p. 119527.

Brady, T.F. *et al.* (2008) 'Visual long-term memory has a massive storage capacity for object details', *Proceedings of the National Academy of Sciences*, 105(38), pp. 14325–14329.

Brainard, D.H. (1997) 'The Psychophysics Toolbox', *Spatial Vision*, 10(4), pp. 433–436.

Brier, M.R. *et al.* (2016) 'Tau and Aβ imaging, CSF measures, and cognition in Alzheimer's disease', *Science Translational Medicine*, 8(338), pp. 338ra66-338ra66.

Campbell, N.A. *et al.* (2009) *Biology*. Pearson, Benjamin Cummings.

Cantero, J.L. *et al.* (2016) 'Regional Hippocampal Atrophy and Higher Levels of Plasma Amyloid-Beta Are Associated with Subjective Memory Complaints in Nondemented Elderly Subjects', *The Journals of Gerontology Series A: Biological Sciences and Medical Sciences*, 71(9), pp. 1210–1215.

Caplar, N., Tacchella, S. & Birrer, S. (2017) 'Quantitative evaluation of gender bias in astronomical publications from citation counts', *Nature Astronomy*, 1(6), pp. 1–5.

Carlozzi, N.E. *et al.* (2013) 'VI. NIH Toolbox Cognition Battery (CB): measuring processing speed', *Monographs of the Society for Research in Child Development*, 78(4), pp. 88–102.

Casey, D.A., Antimisiaris, D. & O'Brien, J. (2010) 'Drugs for Alzheimer's Disease: Are They Effective?', *Pharmacy and Therapeutics*, 35(4), pp. 208–211.

Chatterjee, P. & Werner, R.M. (2021) 'Gender Disparity in Citations in High-Impact Journal Articles', *JAMA Network Open*, 4(7), p. e2114509.

Chen, H. *et al.* (2016) 'Statistical Approaches for the Study of Cognitive and Brain Aging', *Frontiers in Aging Neuroscience*, 8.

Chen, Y.-C. *et al.* (2022) 'Diffusion MRI-guided theta burst stimulation enhances memory and functional connectivity along the inferior longitudinal fasciculus in mild cognitive impairment', *Proceedings of the National Academy of Sciences of the United States of America*, 119(21), p. e2113778119.

Chernecky, C.C. & Berger, B.J. (2012) *Laboratory Tests and Diagnostic Procedures*. 6th ed. Elsevier Inc.

Chou, Y., That, V.T. & Sundman, M. (2020) 'A Systematic Review and Meta-Analysis of rTMS Effects on Cognitive Enhancement in Mild Cognitive Impairment and Alzheimer's Disease', *Neurobiology of aging*, 86, pp. 1–10.

Chung, S.J. *et al.* (2013) 'Association of GWAS Top Hits with Late-onset Alzheimer Disease in Korean Population', *Alzheimer Disease & Associated Disorders*, 27(3), pp. 250–257.

Ciaramelli, E. *et al.* (2020) 'Functional Interplay Between Posterior Parietal Cortex and Hippocampus During Detection of Memory Targets and Non-targets', *Frontiers in Neuroscience*, 14.

Cinel, C., Valeriani, D. & Poli, R. (2019) 'Neurotechnologies for Human Cognitive Augmentation: Current State of the Art and Future Prospects', *Frontiers in Human Neuroscience*, 13, p. 13.

Corder, E.H. *et al.* (1993) 'Gene dose of apolipoprotein E type 4 allele and the risk of Alzheimer's disease in late onset families', *Science (New York, N.Y.)*, 261(5123), pp. 921–923.

Corwin, J. & Bylsma, F.W. (1993) 'Psychological examination of traumatic encephalopathy', *Clinical Neuropsychologist*, 7(1), pp. 3–21.

Crawford, J.R. *et al.* (2003) 'The Prospective and Retrospective Memory Questionnaire (PRMQ): Normative data and latent structure in a large non-clinical sample', *Memory (Hove, England)*, 11(3), pp. 261–275.

De Vis, J.B. *et al.* (2018) 'Arterial-spin-labeling (ASL) perfusion MRI predicts cognitive function in elderly individuals: A 4-year longitudinal study', *Journal of magnetic resonance imaging: JMRI*, 48(2), pp. 449–458.

Deller, T. *et al.* (1996) 'The alvear pathway of the rat hippocampus', *Cell and Tissue Research*, 286(3), pp. 293–303.

Desikan, R.S. *et al.* (2006) 'An automated labeling system for subdividing the human cerebral cortex on MRI scans into gyral based regions of interest', *NeuroImage*, 31(3), pp. 968–980.

Dhana, A. *et al.* (2022) 'Association of Subjective Memory Complaints with White Matter Hyperintensities and Cognitive Decline Among Older Adults in Chicago, Illinois', *JAMA Network Open*, 5(4), p. e227512.

Dion, M.L., Sumner, J.L. & Mitchell, S.M. (2018) 'Gendered Citation Patterns across Political Science and Social Science Methodology Fields', *Political Analysis*, 26(3), pp. 312–327.

Dosenbach, N.U.F. *et al.* (2017) 'Real-time motion analytics during brain MRI improve data quality and reduce costs', *NeuroImage*, 161, pp. 80–93.

Duvernoy, H.M., Cattin, F. & Risold, P.-Y. (2013) *The Human Hippocampus: Functional Anatomy, Vascularization and Serial Sections with MRI*. Springer Science & Business Media.

Dworkin, J.D. *et al.* (2020) 'The extent and drivers of gender imbalance in neuroscience reference lists', *Nature Neuroscience*, 23(8), pp. 918–926.

Ehret, A. *et al.* (2001) 'Modulation of electrically evoked acetylcholine release in cultured rat septal neurones', *Journal of Neurochemistry*, 76(2), pp. 555–564.

Eichenbaum, H. (2000) 'A cortical-hippocampal system for declarative memory', *Nature Reviews. Neuroscience*, 1(1), pp. 41–50.

Eichenbaum, H., Yonelinas, A.P. & Ranganath, C. (2007) 'The medial temporal lobe and recognition memory', *Annual Review of Neuroscience*, 30, pp. 123–152.

Eisai. (2020) 'AHEAD 3-45 Study: A Study to Evaluate Efficacy and Safety of Treatment with Lecanemab in Participants with Preclinical Alzheimer's Disease and Elevated Amyloid and Also in Participants With Early Preclinical Alzheimer's Disease and Intermediate Amyloid', *Clinical trial registration*, NCT04468659.

Ekstrom, A. *et al.* (2008) 'High-resolution depth electrode localization and imaging in patients with pharmacologically intractable epilepsy', *Journal of Neurosurgery*, 108(4), pp. 812–815.

Everding, G. (2022) 'Blood test for Alzheimer's highly accurate in large, international study', *Washington University School of Medicine in St. Louis*, 22 February.

Fagan, A.M. *et al.* (2014) 'Longitudinal Change in CSF Biomarkers in Autosomal-Dominant Alzheimer's Disease', *Science Translational Medicine*, 6(226), pp. 226ra30-226ra30.

Fain, G.L. & O'Dell, T. (2014) *Molecular and Cellular Physiology of Neurons, Second Edition*. Second Edition. Harvard University Press.

Fair, D.A. *et al.* (2013) 'Distinct neural signatures detected for ADHD subtypes after controlling for micro-movements in resting state functional connectivity MRI data', *Frontiers in Systems Neuroscience*, 6, p. 80.

Farrer, L.A. *et al.* (1997) 'Effects of Age, Sex, and Ethnicity on the Association Between Apolipoprotein E Genotype and Alzheimer Disease: A Meta-analysis', *JAMA*, 278(16), pp. 1349–1356.

Ferrari-Souza, J.P. *et al.* (2022) 'Astrocyte biomarker signatures of amyloid-β and tau pathologies in Alzheimer's disease', *Molecular Psychiatry*, pp. 1–9.

Feuerstein, T.J. & Seeger, W. (1997) 'Modulation of acetylcholine release in human cortical slices: possible implications for Alzheimer's disease', *Pharmacology & Therapeutics*, 74(3), pp. 333–347.

Fischl, B. *et al.* (2002) 'Whole brain segmentation: automated labeling of neuroanatomical structures in the human brain', *Neuron*, 33(3), pp. 341–355.

Fischl, B., van der Kouwe, A., *et al.* (2004a) 'Automatically parcellating the human cerebral cortex', *Cerebral Cortex (New York, N.Y.: 1991)*, 14(1), pp. 11–22.

Fischl, B., Salat, D.H., *et al.* (2004b) 'Sequence-independent segmentation of magnetic resonance images', *NeuroImage*, 23 Suppl 1, pp. S69-84.

Fleischman, D. *et al.* (2013) 'Faster cognitive decline in the years prior to MR imaging is associated with smaller hippocampal volumes in cognitively healthy older persons', *Frontiers in Aging Neuroscience*, 5.

Folstein, M.F., Folstein, S.E. & McHugh, P.R. (1975) '"Mini-mental state": A practical method for grading the cognitive state of patients for the clinician', *Journal of Psychiatric Research*, 12(3), pp. 189–198.

Forno, G., Lladó, A. & Hornberger, M. (2021) 'Going round in circles—The Papez circuit in Alzheimer's disease', *European Journal of Neuroscience*, 54(10), pp. 7668–7687.

Freedberg, M. *et al.* (2019) 'Persistent Enhancement of Hippocampal Network Connectivity by Parietal rTMS Is Reproducible', *eNeuro*, 6(5), p. ENEURO.0129-19.2019.

Freedberg, M. *et al.* (2021) 'Multiple parietal pathways are associated with rTMS-induced hippocampal network enhancement and episodic memory changes', *NeuroImage*, 237, pp. 118-199.

Fried, I. *et al.* (1999) 'Cerebral microdialysis combined with single-neuron and electroencephalographic recording in neurosurgical patients. Technical note', *Journal of Neurosurgery*, 91(4), pp. 697–705.

Frisoni, G.B. *et al.* (2022) 'The probabilistic model of Alzheimer disease: the amyloid hypothesis revised', *Nature Reviews Neuroscience*, 23(1), pp. 53–66.

Fulvio, J.M., Akinnola, I. & Postle, B.R. (2021) 'Gender (Im)balance in Citation Practices in Cognitive Neuroscience', *Journal of Cognitive Neuroscience*, 33(1), pp. 3–7.

Gabelle, A. *et al.* (2013) 'Plasma amyloid-β levels and prognosis in incident dementia cases of the 3-City Study', *Journal of Alzheimer's Disease*, 33(2), pp. 381–391.

Gershon, R.C. *et al.* (2013) 'NIH Toolbox for Assessment of Neurological and Behavioral Function', *Neurology*, 80(11 Suppl 3), pp. S2–S6.

Gershon, R.C. *et al.* (2014) 'Language measures of the NIH Toolbox Cognition Battery', *Journal of the International Neuropsychological Society: JINS*, 20(6), pp. 642–651.

Gilewski, M.J., Zelinski, E.M. & Schaie, K.W. (1990) 'The Memory Functioning Questionnaire for assessment of memory complaints in adulthood and old age', *Psychology and Aging*, 5(4), pp. 482–490.

Glymour, M.M. *et al.* (2022) 'Aduhelm, the newly approved medication for Alzheimer's disease: what epidemiologists can learn and what epidemiology can offer', *American Journal of Epidemiology*, p. kwac063.

Goedert, M. & Spillantini, M.G. (2006) 'A Century of Alzheimer's Disease', *Science*, 314(5800), pp. 777–781.

Graf, C. (2008) 'The Lawton instrumental activities of daily living scale', *The American Journal of Nursing*, 108(4), pp. 52–62; quiz 62–63.

Graff-Radford, N.R. *et al.* (2007) 'Association of Low Plasma Aβ42/Aβ40 Ratios with Increased Imminent Risk for Mild Cognitive Impairment and Alzheimer Disease', *Archives of Neurology*, 64(3), pp. 354–362.

Greenaway, M.C., Duncan, N.L. & Smith, G.E. (2013) 'The memory support system for mild cognitive impairment: randomized trial of a cognitive rehabilitation intervention', *International Journal of Geriatric Psychiatry*, 28(4), pp. 402–409.

Griswold, A.J. *et al.* (2021) 'Increased APOE ε4 expression is associated with the difference in Alzheimer's disease risk from diverse ancestral backgrounds', *Alzheimer's & Dementia*, 17(7), pp. 1179–1188.

Gullett, J.M. *et al.* (2020) 'The association of white matter free water with cognition in older adults', *NeuroImage*, 219, p. 117040.

Haam, J. & Yakel, J.L. (2017) 'Cholinergic modulation of the hippocampal region and memory function', *Journal of neurochemistry*, 142(Suppl 2), pp. 111–121.

Halgren, E., Wilson, C.L. & Stapleton, J.M. (1985) 'Human medial temporal-lobe stimulation disrupts both formation and retrieval of recent memories', *Brain and Cognition*, 4(3), pp. 287–295.

Hampstead, B.M., Gillis, M.M. & Stringer, A.Y. (2014) 'Cognitive rehabilitation of memory for mild cognitive impairment: a methodological review and model for future research', *Journal of the International Neuropsychological Society: JINS*, 20(2), pp. 135–151.

Hansson, O. *et al.* (2022) 'The Alzheimer's Association appropriate use recommendations for blood biomarkers in Alzheimer's disease', *Alzheimer's & Dementia*.

Hardcastle, C. *et al.* (2020) 'Contributions of Hippocampal Volume to Cognition in Healthy Older Adults', *Frontiers in Aging Neuroscience*, 12, pp. 593-833.

Harms, M.P. *et al.* (2018) 'Extending the Human Connectome Project across ages: Imaging protocols for the Lifespan Development and Aging projects', *NeuroImage*, 183, pp. 972–984.

Hebscher, M. *et al.* (2021) 'Enhanced reinstatement of naturalistic event memories due to hippocampal-network-targeted stimulation', *Current biology: CB*, 31(7), pp. 1428-1437.e5.

Hermiller, M.S. *et al.* (2019) 'Frequency-specific noninvasive modulation of memory retrieval and its relationship with hippocampal network connectivity', *Hippocampus*, 29(7), pp. 595–609.

Holdnack, J.A. *et al.* (2017) 'Interpreting Patterns of Low Scores on the NIH Toolbox Cognition Battery', *Archives of Clinical Neuropsychology: The Official Journal of the National Academy of Neuropsychologists*, 32(5), pp. 574–584.

Hu, Y. *et al.* (2022) 'Assessment of a Plasma Amyloid Probability Score to Estimate Amyloid Positron Emission Tomography Findings Among Adults with Cognitive Impairment', *JAMA Network Open*, 5(4), p. e228392.

Hua, K. *et al.* (2008) 'Tract probability maps in stereotaxic spaces: analyses of white matter anatomy and tract-specific quantification', *NeuroImage*, 39(1), pp. 336–347.

Huang, Y. & Mahley, R.W. (2014) 'Apolipoprotein E: Structure and Function in Lipid Metabolism, Neurobiology, and Alzheimer's Diseases', *Neurobiology of disease*, 72PA, pp. 3–12.

Hyman, B.T. *et al.* (1986) 'Perforant pathway changes and the memory impairment of Alzheimer's disease', *Annals of Neurology*, 20(4), pp. 472–481.

Iglesias, J.E. *et al.* (2015) 'A computational atlas of the hippocampal formation using ex vivo, ultra-high resolution MRI: Application to adaptive segmentation of in vivo MRI', *NeuroImage*, 115, pp. 117–137.

Insausti, R. & Amaral, D.G. (2003) 'Hippocampal Formation', in *The Human Nervous System: Second Edition*. Elsevier Inc., pp. 871–914.

Iriondo, J. & Jordan, J. (2018) 'Older People Projected to Outnumber Children for First Time in U.S. History', *2017 National Population Projections*, 13 March.

Jacobs, J. *et al.* (2016) 'Direct Electrical Stimulation of the Human Entorhinal Region and Hippocampus Impairs Memory', *Neuron*, 92(5), pp. 983–990.

Jagust, W.J. *et al.* (2008) 'Neuropathological basis of magnetic resonance images in aging and dementia', *Annals of Neurology*, 63(1), pp. 72–80.

Janelidze, S. *et al.* (2021) 'Head-to-Head Comparison of 8 Plasma Amyloid-β 42/40 Assays in Alzheimer Disease', *JAMA Neurology*, 78(11), pp. 1375–1382.

Jenkinson, M. *et al.* (2002) 'Improved optimization for the robust and accurate linear registration and motion correction of brain images', *NeuroImage*, 17(2), pp. 825–841.

Jenkinson, M. *et al.* (2012) 'FSL', *NeuroImage*, 62(2), pp. 782–790.

Jenkinson, M. & Chappell, M. (2018) *Introduction to Neuroimaging Analysis*. Oxford, United Kingdom: Oxford University Press.

Jenkinson, M. & Smith, S. (2001) 'A global optimisation method for robust affine registration of brain images', *Medical Image Analysis*, 5(2), pp. 143–156.

Johansen-Berg, H. & Behrens, T.E.J. (eds) (2014) 'Diffusion MRI: From Quantitative Measurement to In vivo Neuroanatomy', in *Diffusion MRI*. (Second Edition). San Diego: Academic Press, Elsevier Inc.

Katz, S. *et al.* (1963) 'Studies of Illness in the Aged: The Index of ADL: A Standardized Measure of Biological and Psychosocial Function', *JAMA*, 185(12), pp. 914–919.

Kaup, A.R. *et al.* (2015) 'Cognitive Resilience to Apolipoprotein E ε4: Contributing Factors in Black and White Older Adults', *JAMA Neurology*, 72(3), pp. 340–348.

Kirmess, K.M. *et al.* (2021) 'The PrecivityAD™ test: Accurate and reliable LC-MS/MS assays for quantifying plasma amyloid beta 40 and 42 and apolipoprotein E proteotype for the assessment of brain amyloidosis', *Clinica Chimica Acta*, 519, pp. 267–275.

Kloske, C.M. *et al.* (2021) 'Inflammatory Pathways Are Impaired in Alzheimer Disease and Differentially Associated with Apolipoprotein E Status', *Journal of Neuropathology and Experimental Neurology*, 80(10), pp. 922–932.

Kozlov, M. (2022) 'Your brain expands and shrinks over time — these charts show how', *Nature*, 604(7905), pp. 230–231.

Kunkle, B.W. *et al.* (2021) 'Novel Alzheimer Disease Risk Loci and Pathways in African American Individuals Using the African Genome Resources Panel: A Meta-analysis', *JAMA neurology*, 78(1), pp. 102–113.

Lanfranco, M.F., Ng, C.A. & Rebeck, G.W. (2020) 'ApoE Lipidation as a Therapeutic Target in Alzheimer's Disease', *International Journal of Molecular Sciences*, 21(17), p. 6336.

Lansing, A. *et al.* (1999) 'An empirically derived short form of the Boston naming test', *Archives of Clinical Neuropsychology: The Official Journal of the National Academy of Neuropsychologists*, 14(6), pp. 481–487.

Lawton, M.P. & Brody, E.M. (1969) 'Assessment of older people: self-maintaining and instrumental activities of daily living', *The Gerontologist*, 9(3), pp. 179–186.

Leal, S.L. & Yassa, M.A. (2013) 'Perturbations of neural circuitry in aging, mild cognitive impairment, and Alzheimer's disease', *Ageing Research Reviews*, 12(3), pp. 823–831.

Lesné, S. *et al.* (2006) 'A specific amyloid-beta protein assembly in the brain impairs memory', *Nature*, 440(7082), pp. 352–357.

Li, Y. *et al.* (2022) 'Validation of Plasma Amyloid-β 42/40 for Detecting Alzheimer Disease Amyloid Plaques', *Neurology*, 98(7), pp. e688–e699.

Lillie, E.M. *et al.* (2016) 'Evaluation of Skull Cortical Thickness Changes with Age and Sex From Computed Tomography Scans', *Journal of Bone and Mineral Research*, 31(2), pp. 299–307.

Lim, Y.Y. *et al.* (2017) 'Effect of APOE Genotype on Amyloid Deposition, Brain Volume, and Memory in Cognitively Normal Older Individuals', *Journal of Alzheimer's disease: JAD*, 58(4), pp. 1293–1302.

Lin, C.-P. *et al.* (2022) 'Structural (dys)connectivity associates with cholinergic cell density in Alzheimer's disease', *Brain: A Journal of Neurology*, p. awac093.

Liu, P. *et al.* (2015) 'Quaternary Structure Defines a Large Class of Amyloid-β Oligomers Neutralized by Sequestration', *Cell Reports*, 11(11), pp. 1760–1771.

Llibre-Guerra, J.J. *et al.* (2022) 'Apolipoprotein E (APOE) genotype, dementia, and memory performance among Caribbean Hispanic versus US populations', *Alzheimer's & Dementia*.

Logue, M.W. *et al.* (2011) 'A Comprehensive Genetic Association Study of Alzheimer Disease in African Americans', *Archives of Neurology*, 68(12), pp. 1569–1579.

Lucey, B.P. (2016) 'Biomarker changes in early Alzheimer's disease', *Science Translational Medicine*, 8(350), pp. 350ec123-350ec123.

Luo, J. *et al.* (2022) 'Accelerated longitudinal changes and ordering of Alzheimer disease biomarkers across the adult lifespan', *Brain*, p. awac238.

MacAulay, R.K., Boeve, A. & Halpin, A. (2021) 'Comparing Psychometric Properties of the NIH Toolbox Cognition Battery to Gold-Standard Measures in Socioeconomically Diverse Older Adults', *Archives of Clinical Neuropsychology: The Official Journal of the National Academy of Neuropsychologists*, p. acab018.

Macrina, F.L. (2005) *Scientific Integrity: Texts and Cases in Responsible Conduct of Research*. 3rd Edition. Washington, D.C.: American Society for Microbiology Press.

Maliniak, D., Powers, R. & Walter, B.E. (2013) 'The Gender Citation Gap in International Relations', *International Organization*, 67(4), pp. 889–922.

Mankin, E.A. *et al.* (2021) 'Stimulation of the right entorhinal white matter enhances visual memory encoding in humans', *Brain Stimulation*, 14(1), pp. 131–140.

Mankin, E.A. & Fried, I. (2020) 'Modulation of Human Memory by Deep Brain Stimulation of the Entorhinal-Hippocampal Circuitry', *Neuron*, 106(2), pp. 218–235.

Marca-Ysabel, M.V. *et al.* (2021) 'Dissecting the role of Amerindian genetic ancestry and the ApoE ε4 allele on Alzheimer disease in an admixed Peruvian population', *Neurobiology of Aging*, 101, p. 298.e11-298.e15.

Marek, S. *et al.* (2022) 'Reproducible brain-wide association studies require thousands of individuals', *Nature*, 603(7902), pp. 654–660.

Mayeux, R. *et al.* (2003) 'Plasma Aβ40 and Aβ42 and Alzheimer's disease: Relation to age, mortality, and risk', *Neurology*, 61(9), pp. 1185–1190.

Mazziotta, J. *et al.* (2001) 'A probabilistic atlas and reference system for the human brain: International Consortium for Brain Mapping (ICBM).', *Philosophical Transactions of the Royal Society of London. Series B*, 356(1412), pp. 1293–1322.

Mervis, J. (2022) 'Census agency aims for a better statistical snapshot of the U.S.', *Science (New York, N.Y.)*, 3 May.

Milner, B. (1954) 'Intellectual function of the temporal lobes', *Psychological Bulletin*, 51(1), pp. 42–62.

Mitchell, S.M., Lange, S. & Brus, H. (2013) 'Gendered Citation Patterns in International Relations Journals1', *International Studies Perspectives*, 14(4), pp. 485–492.

Miyashita, A. *et al.* (2022) 'Genetics of Alzheimer's disease: an East Asian perspective', *Journal of Human Genetics*, pp. 1–10.

Morar, U. *et al.* (2022) 'A study of the longitudinal changes in multiple cerebrospinal fluid and volumetric magnetic resonance imaging biomarkers on converter and non-converter Alzheimer's disease subjects with consideration for their amyloid beta status', *Alzheimer's & Dementia: Diagnosis, Assessment & Disease Monitoring*, 14(1), p. e12258.

Mowinckel, A.M. & Vidal-Piñeiro, D. (2020) 'Visualization of Brain Statistics with R Packages ggseg and ggseg3d', *Advances in Methods and Practices in Psychological Science*, 3(4), pp. 466–483.

Mueller, S.G. *et al.* (2017) 'Systematic comparison of different techniques to measure hippocampal subfield volumes in ADNI2', *NeuroImage : Clinical*, 17, pp. 1006–1018.

Murray, M.E. & Dickson, D.W. (2014) 'Is pathological aging a successful resistance against amyloid-beta or preclinical Alzheimer's disease?', *Alzheimer's Research & Therapy*, 6(3), p. 24.

Nasreddine, Z.S. *et al.* (2005) 'The Montreal Cognitive Assessment, MoCA: a brief screening tool for mild cognitive impairment', *Journal of the American Geriatrics Society*, 53(4), pp. 695–699.

National Institutes of Health & Northwestern University. (2021) 'NIH Toolbox® Scoring and Interpretation Guide for the iPad'.

Nebel, R.A. *et al.* (2018) 'Understanding the impact of sex and gender in Alzheimer's disease: A call to action', *Alzheimer's & dementia : the journal of the Alzheimer's Association*, 14(9), pp. 1171–1183.

Nilakantan, A.S. *et al.* (2017) 'Stimulation of the Posterior Cortical-Hippocampal Network Enhances Precision of Memory Recollection', *Current biology: CB*, 27(3), pp. 465–470.

Nolte, J. (2013) *The Human Brain in Photographs and Diagrams*. 3rd Edition. Elsevier Health Sciences.

van Oijen, M. *et al.* (2006) 'Plasma Aβ1–40 and Aβ1–42 and the risk of dementia: a prospective case-cohort study', *The Lancet Neurology*, 5(8), pp. 655–660.

O'Shea, A. *et al.* (2016) 'Cognitive Aging and the Hippocampus in Older Adults', *Frontiers in Aging Neuroscience*, 8.

Ovod, V. *et al.* (2017) 'Amyloid β concentrations and stable isotope labeling kinetics of human plasma specific to central nervous system amyloidosis', *Alzheimer's & Dementia: The Journal of the Alzheimer's Association*, 13(8), pp. 841–849.

van Paasschen, J. *et al.* (2013) 'Cognitive rehabilitation changes memory-related brain activity in people with Alzheimer disease', *Neurorehabilitation and Neural Repair*, 27(5), pp. 448–459.

Paquola, C. *et al.* (2019) 'Microstructural and functional gradients are increasingly dissociated in transmodal cortices', *PLOS Biology*, 17(5), p. e3000284.

Park, S.-Y. *et al.* (2022) 'Modifying effects of race and ethnicity and APOE on the association of physical activity with risk of Alzheimer's disease and related dementias', *Alzheimer's & Dementia*.

Parsey, C.M. *et al.* (2021) 'Utility of the iPad NIH Toolbox Cognition Battery in a clinical trial of older adults', *Journal of the American Geriatrics Society*, 69(12), pp. 3519–3528.

Pastalkova, E. *et al.* (2006) 'Storage of spatial information by the maintenance mechanism of LTP', *Science (New York, N.Y.)*, 313(5790), pp. 1141–1144.

Patel, A., Biso, G.M.N.R. & Fowler, J.B. (2022) 'Neuroanatomy, Temporal Lobe', in *StatPearls*. Treasure Island (FL): StatPearls Publishing.

Penfield, W. & Milner, B. (1958) 'Memory deficit produced by bilateral lesions in the hippocampal zone', *A.M.A. Archives of Neurology and Psychiatry*, 79(5), pp. 475–497.

Peterson, J. & Dechow, P.C. (2002) 'Material properties of the inner and outer cortical tables of the human parietal bone', *The Anatomical Record*, 268(1), pp. 7–15.

Pham, M.T., Pouratian, N. & Feinsinger, A. (2022) 'Engagement, Exploitation, and Human Intracranial Electrophysiology Research', *Neuroethics*, 15(25).

Phillips, M.C. (2014) 'Apolipoprotein E isoforms and lipoprotein metabolism', *IUBMB Life*, 66(9), pp. 616–623.

Pierpaoli, C. *et al.* (1996) 'Diffusion tensor MR imaging of the human brain', *Radiology*, 201(3), pp. 637–648.

Piller, C. (2022) 'Potential fabrication in research images threatens key theory of Alzheimer's disease', *Science (New York, N.Y.)*, July.

Pomara, N. *et al.* (2005) 'Selective Reductions in Plasma Aβ 1-42 in Healthy Elderly Subjects During Longitudinal Follow-Up: A Preliminary Report', *The American Journal of Geriatric Psychiatry*, 13(10), pp. 914–917.

Poulakis, K. *et al.* (2022) 'Multi-cohort and longitudinal Bayesian clustering study of stage and subtype in Alzheimer's disease', *Nature Communications*, 13(1), pp. 1–15.

Qiu, Y. (2022) 'showtext: Using Fonts More Easily in R Graphs'.

Rabin, J.S. *et al.* (2022) 'Association of β-Amyloid and Vascular Risk on Longitudinal Patterns of Brain Atrophy', *Neurology* [Preprint].

Rabinovici, G.D. (2021) 'Controversy and Progress in Alzheimer's Disease — FDA Approval of Aducanumab', *New England Journal of Medicine*, 385(9), pp. 771–774.

Ramón y Cajal, S. (1894) *Les nouvelles idées sur la structure du système nerveux : chez l'homme et chez les vertébrés (New Ideas on the structure of the nervous system in humans and in vertebrates)*. Edition Française revue et augmentée par l'auteur. Translated by L. Azoulay. Paris: C. Reinwald & Cie, pp. 1–232.

Ramón y Cajal, S. (1904) *Textura del sistema nervioso del hombre y de los vertebrados : estudios sobre el plan estructural y composición histológica de los centros nerviosos adicionados de consideraciones fisiológicas fundadas en los nuevos descubrimientos. (Texture of the nervous system of man and vertebrates : studies on the structural plan and histological composition of the nervous centers added with physiological considerations founded on the new discoveries.)*. Madrid, España: Universidad de Granada.

Reiman, E.M. *et al.* (2020) 'Exceptionally low likelihood of Alzheimer's dementia in APOE2 homozygotes from a 5,000-person neuropathological study', *Nature Communications*, 11(1), p. 667.

Rey, A. (1941) 'L'examen psychologique dans les cas d'encéphalopathie traumatique. (Les problems.). [The psychological examination in cases of traumatic encepholopathy. Problems.]', *Archives de Psychologie*, 28, pp. 215–285.

Risacher, S.L. *et al.* (2019) 'Plasma amyloid beta levels are associated with cerebral amyloid and tau deposition', *Alzheimer's & Dementia : Diagnosis, Assessment & Disease Monitoring*, 11, pp. 510–519.

Sala, A., Nordberg, A. & Rodriguez-Vieitez, E. (2021) 'Longitudinal pathways of cerebrospinal fluid and positron emission tomography biomarkers of amyloid-β positivity', *Molecular Psychiatry*, 26(10), pp. 5864–5874.

Saunders, A.M. *et al.* (1993) 'Association of apolipoprotein E allele epsilon 4 with late-onset familial and sporadic Alzheimer's disease', *Neurology*, 43(8), pp. 1467–1472.

Schindler, S.E. *et al.* (2019) 'High-precision plasma β-amyloid 42/40 predicts current and future brain amyloidosis', *Neurology*, 93(17), pp. e1647–e1659.

Schindler, S.E. *et al.* (2022) 'Effect of Race on Prediction of Brain Amyloidosis by Plasma Aβ42/Aβ40, Phosphorylated Tau, and Neurofilament Light', *Neurology*, 99(3), pp. e245–e257.

Scott, E.P., Sorrell, A. & Benitez, A. (2019) 'Psychometric Properties of the NIH Toolbox Cognition Battery in Healthy Older Adults: Reliability, Validity, and Agreement with Standard Neuropsychological Tests', *Journal of the International Neuropsychological Society: JINS*, 25(8), pp. 857–867.

Scoville, W.B. & Milner, B. (1957) 'Loss of recent memory after bilateral hippocampal lesions', *Journal of Neurology, Neurosurgery, and Psychiatry*, 20(1), pp. 11–21.

Sepulveda-Falla, D. *et al.* (2022) 'Distinct tau neuropathology and cellular profiles of an APOE3 Christchurch homozygote protected against autosomal dominant Alzheimer's dementia', *Acta Neuropathologica* [Preprint].

Shane, M.S. & Peterson, J.B. (2004) 'Self-induced memory distortions and the allocation of processing resources at encoding and retrieval', *Cognition and Emotion*, 18(4), pp. 533–558.

Shapiro, A. (2020) 'PrecivityAD™ Blood Test's Reach Expands to Europe and California Following Initial Launch; Test Detects Alzheimer's Disease Pathology', 8 December.

Sherwood, M.S. *et al.* (2018) 'Repetitive Transcranial Electrical Stimulation Induces Quantified Changes in Resting Cerebral Perfusion Measured from Arterial Spin Labeling', *Neural Plasticity*, 2018, p. e5769861.

Shi, Y. & Holtzman, D.M. (2018) 'Interplay between innate immunity and Alzheimer's disease: APOE and TREM2 in the spotlight', *Nature reviews. Immunology*, 18(12), pp. 759–772.

Shigemizu, D. *et al.* (2021) 'Ethnic and trans-ethnic genome-wide association studies identify new loci influencing Japanese Alzheimer's disease risk', *Translational Psychiatry*, 11(1), pp. 1–10.

Shukla, C. & Bridges, L.R. (2001) 'Tau, beta-amyloid and beta-amyloid precursor protein distribution in the entorhinal-hippocampal alvear and perforant pathways in the Alzheimer's brain', *Neuroscience Letters*, 303(3), pp. 193–197.

Sienski, G. *et al.* (2021) 'APOE4 disrupts intracellular lipid homeostasis in human iPSC-derived glia', *Science Translational Medicine*, 13(583), p. eaaz4564.

Silverthorn, D.U., Ober, W.C. & Garrison, C.W. (2006) *Human Physiology: An Integrated Approach*. Pearson/Benjamin Cummings.

Small, G.W. (2002) 'What we need to know about age-related memory loss', *BMJ : British Medical Journal*, 324(7352), pp. 1502–1505.

Smith, G. *et al.* (2000) 'Prospective and retrospective memory in normal ageing and dementia: a questionnaaire study', *Memory (Hove, England)*, 8(5), pp. 311–321.

Smith, S.M. *et al.* (2002a) 'Accurate, robust, and automated longitudinal and cross-sectional brain change analysis', *NeuroImage*, 17(1), pp. 479–489.

Smith, S.M. (2002b) 'Fast robust automated brain extraction', *Human Brain Mapping*, 17(3), pp. 143–155.

Smith, S.M. *et al.* (2004) 'Advances in functional and structural MR image analysis and implementation as FSL', *NeuroImage*, 23 Suppl 1, pp. S208-219.

Smith, S.M. *et al.* (2006) 'Tract-based spatial statistics: voxelwise analysis of multi-subject diffusion data', *NeuroImage*, 31(4), pp. 1487–1505.

Soares, J. *et al.* (2013) 'A hitchhiker's guide to diffusion tensor imaging', *Frontiers in Neuroscience*, 7.

Song, S.-K. *et al.* (2002) 'Dysmyelination revealed through MRI as increased radial (but unchanged axial) diffusion of water', *NeuroImage*, 17(3), pp. 1429–1436.

Song, S.-K. *et al.* (2003) 'Diffusion tensor imaging detects and differentiates axon and myelin degeneration in mouse optic nerve after retinal ischemia', *NeuroImage*, 20(3), pp. 1714–1722.

Sood, G. & Laohaprapanon, S. (2018) 'Predicting Race and Ethnicity from the Sequence of Characters in a Name'. arXiv.

Squire, L.R. & Kandel, E.R. (2003) *Memory: From Mind to Molecules*. Macmillan.

Squire, L.R., Stark, C.E.L. & Clark, R.E. (2004) 'The medial temporal lobe', *Annual Review of Neuroscience*, 27, pp. 279–306.

Stark, C.E. & Squire, L.R. (2001) 'When zero is not zero: the problem of ambiguous baseline conditions in fMRI', *Proceedings of the National Academy of Sciences of the United States of America*, 98(22), pp. 12760–12766.

Stokes, M.G. *et al.* (2005) 'Simple metric for scaling motor threshold based on scalp-cortex distance: application to studies using transcranial magnetic stimulation', *Journal of Neurophysiology*, 94(6), pp. 4520–4527.

Strikwerda-Brown, C. *et al.* (2022) 'Association of Elevated Amyloid and Tau Positron Emission Tomography Signal with Near-Term Development of Alzheimer Disease Symptoms in Older Adults Without Cognitive Impairment', *JAMA Neurology* [Preprint].

Strittmatter, W.J. *et al.* (1993) 'Apolipoprotein E: high-avidity binding to beta-amyloid and increased frequency of type 4 allele in late-onset familial Alzheimer disease.', *Proceedings of the National Academy of Sciences*, 90(5), pp. 1977–1981.

Suchy-Dicey, A. *et al.* (2022) 'APOE genotype, hippocampus, and cognitive markers of Alzheimer's disease in American Indians: Data from the Strong Heart Study', *Alzheimer's & Dementia: The Journal of the Alzheimer's Association* [Preprint].

Sundman, M.H. *et al.* (2020) 'Transcranial magnetic stimulation reveals diminished homoeostatic metaplasticity in cognitively impaired adults', *Brain Communications*, 2(2), p. fcaa203.

Suthana, N. *et al.* (2012) 'Memory Enhancement and Deep-Brain Stimulation of the Entorhinal Area', *New England Journal of Medicine*, 366(6), pp. 502–510.

Suthana, N. & Fried, I. (2014) 'Deep brain stimulation for enhancement of learning and memory', *NeuroImage*, 85 Pt 3, pp. 996–1002.

Suthana, N.A. *et al.* (2009) 'Human hippocampal CA1 involvement during allocentric encoding of spatial information', *The Journal of Neuroscience: The Official Journal of the Society for Neuroscience*, 29(34), pp. 10512–10519.

Suthana, N.A. *et al.* (2015) 'Specific responses of human hippocampal neurons are associated with better memory', *Proceedings of the National Academy of Sciences*, 112(33), pp. 10503–10508.

Tang, M.-X. *et al.* (1998) 'The APOE ε4 Allele and the Risk of Alzheimer Disease Among African Americans, Whites, and Hispanics', *JAMA*, 279(10), pp. 751–755.

Tao, Q. *et al.* (2018) 'Association of Chronic Low-grade Inflammation with Risk of Alzheimer Disease in ApoE4 Carriers', *JAMA Network Open*, 1(6), p. e183597.

Thompson, K.I. *et al.* (2021) 'APOE ε4 as a predictor of tauopathies independent of β-amyloid', *Alzheimer's & Dementia*, 17(S4), p. e054748.

Titiz, A.S. *et al.* (2017) 'Theta-burst microstimulation in the human entorhinal area improves memory specificity', *eLife*. Edited by I. Slutsky, 6, p. e29515.

Toglia, M.P. (1978) *Handbook of semantic word norms*. Hillsdale, N.J.: Lawrence Erlbaum Associates ; New York : Distributed by the Halsted Press Division of John Wiley.

Tosun, D. *et al.* (2021) 'Detection of β-amyloid positivity in Alzheimer's Disease Neuroimaging Initiative participants with demographics, cognition, MRI and plasma biomarkers', *Brain Communications*, 3(2), p. fcab008.

Van Essen, D.C. *et al.* (2012) 'The Human Connectome Project: a data acquisition perspective', *NeuroImage*, 62(4), pp. 2222–2231.

Vaynman, S. & Gomez-Pinilla, F. (2006) 'Revenge of the "Sit": How lifestyle impacts neuronal and cognitive health through molecular systems that interface energy metabolism with neuronal plasticity', *Journal of Neuroscience Research*, 84(4), pp. 699–715.

Vedam-Mai, V. *et al.* (2021) 'Proceedings of the Eighth Annual Deep Brain Stimulation Think Tank: Advances in Optogenetics, Ethical Issues Affecting DBS Research,

Neuromodulatory Approaches for Depression, Adaptive Neurostimulation, and Emerging DBS Technologies', *Frontiers in Human Neuroscience*, 15, p. 644593.

Veldsman, M. *et al.* (2020) 'Cerebrovascular risk factors impact frontoparietal network integrity and executive function in healthy ageing', *Nature Communications*, 11(1), p. 4340.

Versluis, A. & Uyttenbroek, E. (2002) *Exactitudes: Arie Versluis and Ellie Uyttenbroek*. 010 Publishers.

Vertes, R.P. (2005) 'Hippocampal theta rhythm: a tag for short-term memory', *Hippocampus*, 15(7), pp. 923–935.

Victor, M.B. *et al.* (2022) 'Lipid accumulation induced by APOE4 impairs microglial surveillance of neuronal-network activity', *Cell Stem Cell*, 29(8), pp. 1197-1212.e8.

Vlassenko, A.G. *et al.* (2016) 'Imaging and cerebrospinal fluid biomarkers in early preclinical alzheimer disease', *Annals of Neurology*, 80(3), pp. 379–387.

Voss, M.W. *et al.* (2014) 'Revenge of the "sit" II: Does lifestyle impact neuronal and cognitive health through distinct mechanisms associated with sedentary behavior and physical activity?', *Mental Health and Physical Activity*, 7(1), pp. 9–24.

Wang, J.X. *et al.* (2014) 'Targeted enhancement of cortical-hippocampal brain networks and associative memory', *Science (New York, N.Y.)*, 345(6200), pp. 1054–1057.

Wang, X. *et al.* (2021) 'Gendered Citation Practices in the Field of Communication', *Annals of the International Communication Association*, 45(2), pp. 134–153.

Wechsler, D. (1997) *Wechsler Adult Intelligence Scale | Third Edition*.

Weintraub, S. *et al.* (2014) 'The Cognition Battery of the NIH Toolbox for Assessment of Neurological and Behavioral Function: Validation in an Adult Sample', *Journal of the International Neuropsychological Society : JINS*, 20(6), pp. 567–578.

West, T. *et al.* (2021) 'A blood-based diagnostic test incorporating plasma Aβ42/40 ratio, ApoE proteotype, and age accurately identifies brain amyloid status: findings from a multi-cohort validity analysis', *Molecular Neurodegeneration*, 16, p. 30.

Whittington, M.D. *et al.* (2022) 'Cost-Effectiveness and Value-Based Pricing of Aducanumab for Patients with Early Alzheimer Disease', *Neurology*, 98(9), pp. e968–e977.

WHO. (2017) *Global action plan on the public health response to dementia*. Geneva: World Health Organization.

WHO. (2021) *Global status report on the public health response to dementia*. Geneva: World Health Organization.

WHO. (2022) *Optimizing brain health across the life course: WHO position paper*. Geneva: World Health Organization.

Williams, J.M. & Givens, B. (2003) 'Stimulation-induced reset of hippocampal theta in the freely performing rat', *Hippocampus*, 13(1), pp. 109–116.

Wisse, L.E.M. *et al.* (2021) 'Hippocampal subfield volumetry from structural isotropic 1mm3 MRI scans: A note of caution', *Human Brain Mapping*, 42(2), pp. 539–550.

Witter, M.P. (2007) 'The perforant path: projections from the entorhinal cortex to the dentate gyrus', *Progress in Brain Research*, 163, pp. 43–61.

Woolrich, M.W. *et al.* (2009) 'Bayesian analysis of neuroimaging data in FSL', *NeuroImage*, 45(1 Suppl), pp. S173-186.

Wu, C.C. *et al.* (2002) 'Brain structure and cognition in a community sample of elderly Latinos', *Neurology*, 59(3), pp. 383–391.

Xie, L. *et al.* (2016) 'Accounting for the Confound of Meninges in Segmenting Entorhinal and Perirhinal Cortices in T1-Weighted MRI', *Medical image computing and computer-assisted intervention : MICCAI ... International Conference on Medical Image Computing and Computer-Assisted Intervention*, 9901, pp. 564–571.

Xie, L. *et al.* (2017) 'Multi-template analysis of human perirhinal cortex in brain MRI: Explicitly accounting for anatomical variability', *NeuroImage*, 144, pp. 183–202.

Xie, L. *et al.* (2019) 'Automated segmentation of medial temporal lobe subregions on in vivo T1-weighted MRI in early stages of Alzheimer's disease', *Human Brain Mapping*, 40(12), pp. 3431–3451.

Yamazaki, Y. *et al.* (2019) 'Apolipoprotein E and Alzheimer disease: pathobiology and targeting strategies', *Nature Reviews Neurology*, 15(9), pp. 501–518.

Yassa, M.A., Mattfeld, A.T., *et al.* (2011a) 'Age-related memory deficits linked to circuit-specific disruptions in the hippocampus', *Proceedings of the National Academy of Sciences*, 108(21), pp. 8873–8878.

Yassa, M.A., Lacy, J.W., *et al.* (2011b) 'Pattern separation deficits associated with increased hippocampal CA3 and dentate gyrus activity in nondemented older adults', *Hippocampus*, 21(9), pp. 968–979.

Yassa, M.A., Muftuler, L.T. & Stark, C.E.L. (2010) 'Ultrahigh-resolution microstructural diffusion tensor imaging reveals perforant path degradation in aged humans in vivo', *Proceedings of the National Academy of Sciences*, 107(28), pp. 12687–12691.

Yin, Y. & Wang, Z. (2018) 'ApoE and Neurodegenerative Diseases in Aging', in Z. Wang (ed.) *Aging and Aging-Related Diseases: Mechanisms and Interventions*. Singapore: Springer (Advances in Experimental Medicine and Biology), pp. 77–92.

Young, C.B. *et al.* (2022) 'Divergent Cortical Tau Positron Emission Tomography Patterns Among Patients with Preclinical Alzheimer Disease', *JAMA Neurology*, 79(6), pp. 592–603.

Yushkevich, P.A. *et al.* (2015) 'Automated volumetry and regional thickness analysis of hippocampal subfields and medial temporal cortical structures in mild cognitive impairment', *Human Brain Mapping*, 36(1), pp. 258–287.

Zeineh, M.M. *et al.* (2003) 'Dynamics of the hippocampus during encoding and retrieval of face-name pairs', *Science (New York, N.Y.)*, 299(5606), pp. 577–580.

Zeineh, M.M. *et al.* (2017) 'Direct Visualization and Mapping of the Spatial Course of Fiber Tracts at Microscopic Resolution in the Human Hippocampus', *Cerebral Cortex*, 27(3), pp. 1779–1794.

Zetterberg, H. & Karikari, T.K. (2021) 'CSF and blood biomarkers: How strongly do they reflect Alzheimer's pathophysiology and are they dynamic?', *Alzheimer's & Dementia*, 17(S5), p. e054096.

Zhang, B. *et al.* (2014) 'The Role of Diffusion Tensor Imaging in Detecting Microstructural Changes in Prodromal Alzheimer's Disease', *CNS Neuroscience & Therapeutics*, 20(1), pp. 3–9.

Zhou, D. *et al.* (2020) 'Gender Diversity Statement and Code Notebook v1.0'. Zenodo.

Zicha, S. *et al.* (2021) 'Comparative analytical performance of multiple plasma amyloid-beta assays and their relationship to amyloid PET', *Alzheimer's & Dementia*, 17(S5), p. e055504.